LABORATORY STUDIES OF STABLE CARBON ISOTOPE RATIO OF SECONDARY PARTICULATE ORGANIC MATTER IN THE GAS-PHASE

SATOSHI IREI

A DISSERTATION SUBMITTED TO THE FACULTY OF GRADUATE STUDIES
IN PARTIAL FULFILMENT OF THE REQUIREMENTS FOR
THE DEGREE OF

DOCTOR OF PHILOSOPHY

GRADUATE PROGRAM IN CHEMISTRY
YORK UNIVERSITY
TORONTO, ONTARIO

SEPTEMBER, 2008

1. Introduction

Airborne particulate matter (PM) has been studied intensively in the last two decades due to its correlation with adverse health effects (Dockery et al., 1993; Thurston et al., 1994; Crüts et al., 2008) and also the planetary budget of radiative forcing (IPCC, 2001; Ramanathan et al., 2001; Anderson et al., 2003). Particularly in the latter case, the role of airborne PM for cloud formation, also known as an indirect effect of airborne PM on radiative forcing, is the most uncertain. Such effects are expected to depend strongly on its chemical composition including organic material.

Several recent ambient studies have demonstrated that the fraction of the organic component in airborne PM is significant (Lee et al., 2003; Na et al., 2004). The organic fraction of airborne PM, or airborne particulate organic matter (POM), can be categorized into two groups: Primary POM, which is introduced into the atmosphere from emission sources directly, and secondary POM, which is formed from low-volatility oxidation products produced after reactions of volatile organic compounds (VOCs) in the atmosphere.

In contrast to the relatively well-understood origin of primary POM, the understanding of formation of secondary POM is very limited. The main issues are the limited understanding of chemical and physical mechanisms and the ubiquity of photo-oxidation products. For example, the oxidation products of toluene, the most abundant aromatic VOC in the atmosphere, are believed to substantially contribute to secondary POM (Seinfeld and Pandis, 1998). However, due to that both photo-oxidation in the

atmosphere and combustion in vehicular engines are oxidation, many oxidized compounds are formed both as primary and as secondary POM. One of the distinctive differences between these processes is the temperature at which the processes occur: photo-oxidation in the atmosphere is at ambient temperature, while combustion in technical processes occurs typically at high temperature. The history of products originating from such different processes is potentially stored as differences in stable isotope abundances.

Isotope studies are a powerful tool to gain insight into complex chemical and physical mechanisms that cannot be ascertained by concentration measurements only. For example, isotope fractionation in ambient VOCs provides information for degree of chemical reaction, which is difficult to be distinguished from the atmospheric dilution by measuring concentration alone. Stable isotopes can also allow for the identification of sources. Recent developments in stable isotope measurement techniques have made possible the compound specific analyses of stable isotopes at natural abundance levels. Thus, the application of stable isotope studies is well suited toward studies of atmospheric chemistry. There are reports of ambient studies where the measurement of stable isotopes yields useful information about atmospheric photochemistry (Sakugawa and Kaplan, 1995; Rudolph et al., 1997; Narukawa et al., 1999; Fang et al., 2002). It has been demonstrated with VOC studies that, with fundamental understanding of photo-oxidation constructed by laboratory studies, stable isotope measurements give better understanding of photo-oxidation occurring in the atmosphere (Rudolph et al., 2000). Such results can reveal long range transport of VOCs and the location of their sources

(Rudolph and Czuba, 2000; Saito et al., 2002; Thompson et al., 2003; Nara et al., 2007). Very recently, it was demonstrated that photo-oxidation product studies of precursor VOCs improve resolution of the photochemical processing in the atmosphere, and potentially provide better understanding of atmospheric life time and source location of the precursors (Iannone, R., 2008). To date, however, there exists no report on the use of stable isotope techniques for laboratory studies of secondary POM.

Nitro and nitrohydroxy aromatic compounds are known to be primary pollutants in the atmosphere (Kawamura and Kaplan, 1983; Leuenberger et al., 1988; Richartz, et al., 1990; Tremp et al., 1993). These compounds have also have been detected in laboratory studies of the reaction of toluene with OH radical (toluene+OH reaction) in the gas-phase (Atkinson, 1989; Klotz et al., 1998) as well as in secondary POM (Forstner et al., 1997; Jang and Kamens, 2001; Sato et al., 2007). Their amount is often found to be significant, thus, stable carbon isotope measurements of these compounds are probably the most feasible in terms of detection. In contrast to the feasibility of the detection, quantitative analysis for these compounds has to be done very carefully since the compounds are reactive and thermally unstable. One of the analytical methods that minimize their thermal decomposition/unfavorable reactions is derivatization. Alkylsilyl derivatization is one of the common derivatization techniques for the analysis of these compounds, and N-(*tert*-butyldimethylsilyl)-N-methyl-trifluoroacetoamide (MTBSTFA) and N, O-*bis*(trimethylsilyl)trifluoroacetoamide (BSTFA) are the reagents often used for the alkylsilyl derivatization. *tert*-butyldimethylsilyl derivatives made by MTBSTFA are generally more stable than trimethylsilyl (TMS) derivatives made by BSTFA, therefore,

MTBSTFA is often preferred for analysis of phenolic compounds (Heberer and Stan, 1997). MTBSTFA has been tested for the compound specific stable carbon isotope analysis of amino acids (Shinebarger et al., 2002). On the analysis for stable carbon isotope ratios, however, use of BSTFA is more preferable than MTBSTFA since less artificial carbons are added to the targeted compounds. To the best of our knowledge, there has been no report to date for the compound specific stable carbon isotope measurements using the BSTFA derivatization. Therefore, a new method for compound-specific stable carbon isotope ratio of nitro and nitrohydroxy aromatic compounds with BSTFA needed to be developed.

The objective here is to evaluate the usefulness of stable carbon isotope studies for secondary POM by conducting laboratory studies: Stable carbon isotope measurements of secondary POM formed by the reaction of toluene (C_7H_8) with OH radical in a flow reactor and a smog chamber. Compound-specific stable carbon isotope analysis was also made in order to limit interferences from other unrelated organic substances existing in ambient samples. The results presented here will contribute toward the continuing progress in elucidating the formation processes of secondary POM and provide useful information on stable isotope ratio measurements recently emerging in studies of organic compounds in the atmosphere.

2. Theory

2.1. Isotope Fractionation

Stable carbon isotope composition ($\delta^{13}C$) is generally noted as delta value:

$$\delta^{13}C = \left[\frac{R_{sample}}{R_{reference}} - 1 \right] \quad (1)$$

where R_{sample} and $R_{reference}$ are the ratios of ^{13}C abundance to ^{12}C abundance for sample and reference, respectively. Vienna Pee Dee Belemnite (VPDB), an international reference standard, is generally used as the reference. Note that all $\delta^{13}C$ values presented here are relative to VPDB in permil (‰), unless otherwise noted.

Isotope fractionation is a discrimination of isotopologues (i.e., molecules that have the same chemical structure, but different masses) during a physical or chemical process. Isotope fractionation occurs as molecules undergo diffusion, effusion, evaporation, condensation, and chemical reaction. Such isotope fractionation results in different isotope compositions for the reactant and for the products. The isotope compositions of a reactant and its accumulated product at any time during the reaction process can be predicted if certain information is known: the extent of processing, the initial isotope composition of the reactant, and the isotope fractionation factor, α (i.e. $\alpha=k_{13}/k_{12}$ where k_{13} and k_{12} are the rate constants for a specific reaction of the reactant that labeled with ^{13}C and ^{12}C, respectively., when the fractionation is with respect to

stable carbon isotope). For example, for a closed system a general relationship is established for reactant processing during a forward reaction:

$$\frac{R}{{}^{0}R} = f^{\alpha-1} \tag{2}$$

where R, ^{0}R, f and α are the isotope ratio ($^{13}C/^{12}C$) of the reactant at time t, the initial isotope ratio of the reactant, the fraction of the reactant remaining, and the fractionation factor, respectively. Equation 2 is known as the Rayleigh fractionation, a relationship originally developed for the isotope fractionation of water vapor during condensation. Equation 2 can be expressed using epsilon notation (ε) for the kinetic isotope effect (KIE, the reciprocal of the fractionation factor α) and delta notation for the isotope ratio:

$$\frac{\delta+1}{{}^{0}\delta+1} = f^{\frac{-\varepsilon}{\varepsilon+1}} \tag{3}$$

where $\varepsilon = (1/\alpha)-1 = (k_{12}/k_{13})-1$ and $\delta = (R_{sample}/R_{reference})-1$. The superscript zero indicates the initial value. Note that δ and ε here is not in ‰.When the reactant is converted into a product without loss and keeps being accumulated as the process goes on, the following mass balance can be established:

$${}^{0}\delta = f \cdot \delta + (1-f) \cdot \delta_{All\,\mathrm{Pr}od} \tag{4}$$

where $\delta_{AllProd}$ is the isotope ratio for the products accumulated and f is the fraction of the concentration of the residual reactant relative to the initial concentration of the reactant.

By re-arranging Equation 4 with respect to δ and substituting it for δ in Equation 3, the following equation is obtained:

$$\frac{\delta_{All\,\mathrm{Pr}od}+1}{{}^{0}\delta+1}=\frac{1-f^{\frac{1}{\varepsilon+1}}}{1-f} \qquad (5).$$

Equation 5 can be used to predict $\delta_{AllProd}$ if values for ${}^{0}\delta$, ε, and f are known. It is important to note that the calculation is based on the assumption that the reaction produces only one product. However, large or small, any single chemical reaction should exhibit a kinetic isotope effect. Therefore, all distinct products, which must have undergone different reaction pathways, will have different δ values compared to the $\delta_{AllProd}$ value.

2.2. Novel Concept for Secondary POM Study

Stable isotope ratio measurements make possible to link laboratory studies to ambient studies. For example, secondary POM carbon from photo-oxidation of toluene (C_7H_8) is discussed here. The yield of secondary POM carbon (Y_C), which is POM carbon mass (or concentration) over the carbon mass (or concentration) of toluene consumed, can be expressed using the stable carbon isotope ratio, and the expression is derived by the following way. First of all, the carbon mass balance, the carbon isotope balance, as well as the Y_C are expressed as follows:

$${}^{0}C_{C7H8}=C_{C7H8}+C_{All\,\mathrm{Pr}od} \qquad (6)$$

$$ {}^{0}C_{C7H8} \cdot {}^{0}\delta^{13}C_{C7H8} = C_{C7H8} \cdot \delta^{13}C_{C7H8} + C_{All\,\mathrm{Pr}od} \cdot \delta^{13}C_{All\,\mathrm{Pr}od} \quad (7) $$

$$ Y_C = \frac{C_{POM}}{C_{All\,\mathrm{Pr}od}} = \frac{C_{POM}}{{}^{0}C_{C7H8} - C_{C7H8}} \quad (8) $$

where $^{0}C_{C7H8}$ is the initial carbon mass of toluene, C_{C7H8} is the carbon mass of toluene at time t, $C_{AllProd}$ is the carbon mass of the sum of all the products, C_{POM} is the carbon mass of secondary POM formed from the toluene+OH reaction, $^{0}\delta^{13}C_{C7H8}$ is the initial stable carbon isotope ratio of toluene, $\delta^{13}C_{C7H8}$ is the stable carbon isotope ratio of toluene at time t, and $\delta^{13}C_{AllProd}$ is the stable carbon isotope ratio of the sum of all the products. By solving Equation 6 for $C_{AllProd}$ and substituting Equation 6 with respect to $C_{AllProd}$ for the $C_{AllProd}$ in Equation 7, the following equation is obtained:

$$ {}^{0}C_{C7H8} = \frac{\delta^{13}C_{C7H8} - \delta^{13}C_{All\,\mathrm{Pr}od}}{{}^{0}\delta^{13}C_{C7H8} - \delta^{13}C_{All\,\mathrm{Pr}od}} \cdot C_{C7H8} \quad (9) $$

This derivation is based on mass balance principle only. In Equation 8, substitution of Equation 9 for $^{0}C_{C7H8}$ gives:

$$ Y_C = \frac{{}^{0}\delta^{13}C_{C7H8} - \delta^{13}C_{All\,\mathrm{Pr}od}}{\delta^{13}C_{C7H8} - {}^{0}\delta^{13}C_{C7H8}} \cdot \frac{C_{POM}}{C_{C7H8}} \quad (10). $$

Replacing the parameters for the sum of all the products and for the total POM with those for a specific compound ($\delta^{13}C_{AllProd} = F_1 \times \delta^{13}C_{SpecProd}$ and $C_{POM} = F_2 \times C_{SpecProd}$), F_1 and F_2 are specific factors for isotope ratio and carbon mass for the specific product) Equation (10) can be expressed as:

$$Y_C = \frac{{}^0\delta^{13}C_{C7H8} - F_1 \times \delta^{13}C_{Spec\,\mathrm{Pr}\,od}}{\delta^{13}C_{C7H8} - {}^0\delta^{13}C_{C7H8}} \times \frac{F_2 \times C_{Spec\,\mathrm{Pr}\,od}}{C_{C7H8}} \quad (11)$$

Here F_1 is the isotope fractionation of the specific product relative to the sum of all products and F_2 the fraction of the specific product relative to the total secondary POM carbon. Compared to Equation 10, Equation 11 will have a better chance to be successfully applied to ambient studies since the substitution substantially reduces chances of interferences from other organic compounds in atmospheric PM. Note that all parameters on the right side of Equation (11) can be measured and F_1 and F_2 can be found by conducting laboratory studies. Similar to other values in Equation (11) F_1 and F_2 may depend on the reaction conditions.

3. Experiment

3.1. Laboratory Experiment for Generation of Secondary POM

Two types of apparatus were used to create artificial airborne secondary POM from the toluene+OH reaction: a flow reactor and a smog chamber. The flow reactor consisted of a glass tube with quartz windows at opposite ends, which allowed for the transmission of UV light through the length of the tube. Reactive gases were continuously introduced at one end of the reactor cell and they continuously exited from the other end. Photochemical reactions took place when the gases inside the cell were irradiated with UV light. An advantage of this technique was that POM was produced continuously in a steady state, allowing collection of POM over long time periods. A distinct disadvantage was that the extent of reaction was limited due to the relatively short residence time of the VOCs in the reaction tube.

The smog chamber consisted of a large Teflon bag surrounded by UV lamps. Reactive gas species were introduced into the chamber only once at the beginning of an experiment. Photochemical reactions were initiated through the activation of the UV lamps. A strong advantage of this apparatus was the wide ranges of the extent of photochemical reaction that could be achieved due to the much longer residence times. Details concerning the characterization of this smog chamber have been presented by Bienenstock, Y. (2001) and Barbu, A. (2003). The following sections describe the POM generation experiments using the aforementioned techniques in detail.

3.1.1. Flow Reactor Experiment

The set-up of the flow reactor experiments is shown in Figure 1. The conditions of the POM generation experiment using this apparatus were already established by Collin, F. (personal communication). Isopropyl nitrite (IPN) was synthesized from a mixture of isopropanol/sodium nitrite/sulfuric acid according to the procedure by Noyes (1943). In this experiment, gas-phase IPN, a compound that produces OH radicals, and gas-phase toluene, a precursor of secondary POM, were produced by evaporation from cooled (273 K) bulk IPN and toluene under a gentle flow of pure nitrogen. Production of OH radicals by IPN is made via sequence of following reactions:

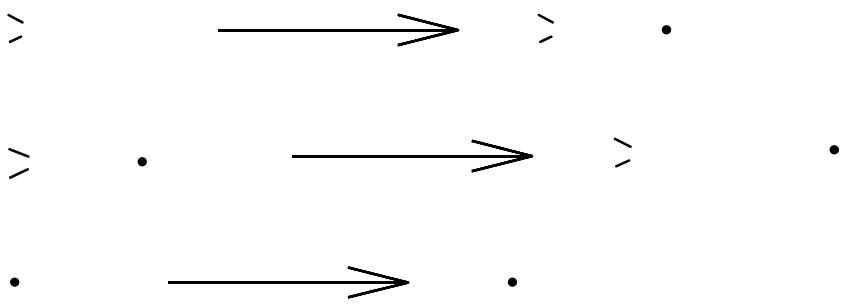

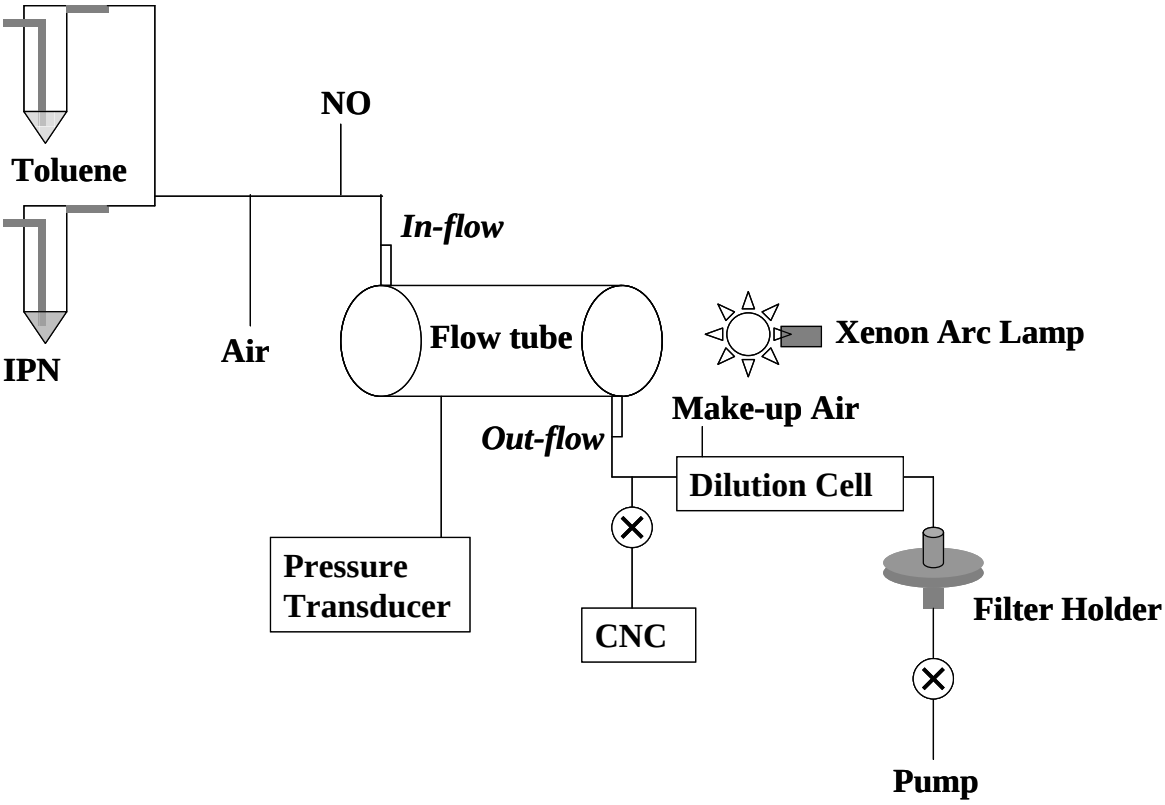

Figure 1. Schematic Diagram of Flow Reactor Apparatus (Courtesy to Hastie, D.).

The evaporated gaseous species were introduced into the flow tube (either 2.5 L or 0.47 L in volume) together with 100 ppm nitrogen oxide (BOC) in nitrogen and synthetic air. The flow rates for IPN, toluene, nitrogen oxide and air were 1.2 mL min^{-1}, 1.9 mL min^{-1}, 33.7 mL min^{-1}, and 740 mL min^{-1}, respectively. The residence time was either 3.2 min or 0.60 min for the larger and smaller flow tubes, respectively. The system was conditioned for several hours before starting any photochemical reactions in order to obtain steady-state concentrations. The initial mixing ratios for IPN, toluene, nitrogen oxide in the reactor were approximately 230 ppm (based on the saturated vapor pressure of ~1.5×10^4 Pa at 273 K, which was calculated with $\Delta_{vapor}H^0$ = 31 kJ mol^{-1} and b.p. = 318 K), 20-40

ppm, and 5 ppm, respectively. The fraction of toluene consumed was determined by measuring the toluene concentration at the exit of the reactor with and without the UV lights on. These measurements were made by sampling gaseous samples at the exit of the flow tube with a 250 μl gas-tight syringe (Hamilton Co.) and then analyzing the gas with HP 6890A GC-FID instrument (Agilent) equipped with a 0.25 mm i.d. × 30 m × 0.25 μm film thickness DB-5MS capillary column (J&W Scientific). The concentration was then determined by comparison with a (100±5) ppm toluene standard in nitrogen (Scott Specialties, Inc.). Split injections of 1:10 with 1 mL min^{-1} column flow were used. The GC oven was isothermal at 100 ˚C for the duration of the analysis. After determining the initial mixing ratio of toluene, the UV light (1000 W Xenon Arc lamp, Model C-50, Oriel Optical Corp.) was turned on. The reactor was then left for at least 15 min before any samples were collected. The fraction of toluene consumed was varied by changing the size of the reactor tube (using either the 2.5 L or 0.47 L reactor tube) or by varying the focus of the lens on the UV source and thus the UV intensity in the reactor. The POM formed was monitored with a condensation nuclei counter or CNC (Model 3020, TSI). Typical number concentration observed was 2×10^5 particles cm^{-3}, approximately. The size distribution of the generated POM was not measured during the flow reactor experiments. All POM generation experiments were carried out at (298±3) K, however, the actual temperature inside the reactor, which was not measured, was expected to be slightly higher. After confirming POM was being generated, the transfer line to the CNC was closed completely during most of the experiments. The flow out of the reactor was then sent to a small glass cell (labeled the dilution cell in Figure 1) where 5.6 L min^{-1} of

make-up air was added into in order to attain a sufficient flow for filter sampling. Filter sampling was made down stream of this dilution cell.

Four sets of flow reactor experiments (series FR A to FR D) were carried out to collect 21 filter samples in total for total POM carbon analysis. The fraction of toluene consumed was different between the sets of experiments, but was kept constant within the each set. Four to six filter samples with different sampling durations were collected during each set of experiments. In order to test for the extent of evaporation of the secondary POM carbon, six filter samples (EVAP A to EVAP F) were again collected under the condition that the fraction of toluene consumed was kept the same. For compound specific analyses, five filter samples (FR 1 to FR 5) were collected under the different fractions of toluene consumed.

3.1.2. Smog Chamber Experiment

The set-up of the smog chamber experiment is shown in Figure 2. Three experiments were carried out using the 8 m^3 YorkU smog chamber. Air generated by a clean air generator (Aadco 737 pure air generator, Aadco) was continuously introduced into the chamber at 3.3 L min^{-1} during the POM generation experiments in order to compensate for the air flowing out of the chamber. Exiting air was sent to several monitoring instruments, such as a CNC (TSI-3760, TSI), a differential mobility analyzer or DMA (TSI-3071, TSI) coupled with a separate CNC (TSI-3760, TSI), a GC (HP 5890), and a NO_x analyzer (Model 42s, Thermo Environmental Instruments). The theoretical

residence time calculated was approximately 40 hours. Through an injection port on the chamber, 40 mL of pure NO (BOC), 18 μl of liquid toluene (Aldrich), and 250μl of IPN were introduced to the chamber. The injection port was heated so that both toluene and IPN were completely evaporated and introduced into the chamber as gases. The typical mixing ratios of NO, toluene, and IPN (assuming the synthesized IPN was free of impurities and its density was 0.785 g mL^{-1}) in all experiments were approximately 2.5 ppm, 0.5 ppm, and 7 ppm, respectively. Seed particles were also introduced into the chamber. Droplets of ammonium sulfate (0.5 g L^{-1}) were generated by using a collision nebulizer. The droplets were subsequently dried by passing them through a silica-gel dryer tube; the dried seed particles were then introduced into the chamber. Typically, the initial number concentration and the median of the size distribution for the seed particles were ~3×10^3 cm^{-3} and ~100 nm, respectively. These experimental conditions followed a procedure established by J. Auld (personal communication). Prior to turning the UV lamps on, the contents of the chamber was allowed to mix for one hour. During the experiments, the changes in the toluene concentration, the NO_x concentration, and the particle size distribution were measured. The GC-FID was equipped with an automated sampling apparatus, and the toluene abundance was measured every 5 minutes. The CNC and DMS/CNC measurements were simultaneously performed every 5 minutes alongside the GC-FID measurements. The toluene concentration was determined through comparison with calibrations made by a permeation apparatus. Three smog chamber experiments were carried out (SC I – SC III). At the end of each experiment two sets of

filter samples were simultaneously collected for total POM carbon analyses and compound specific analyses.

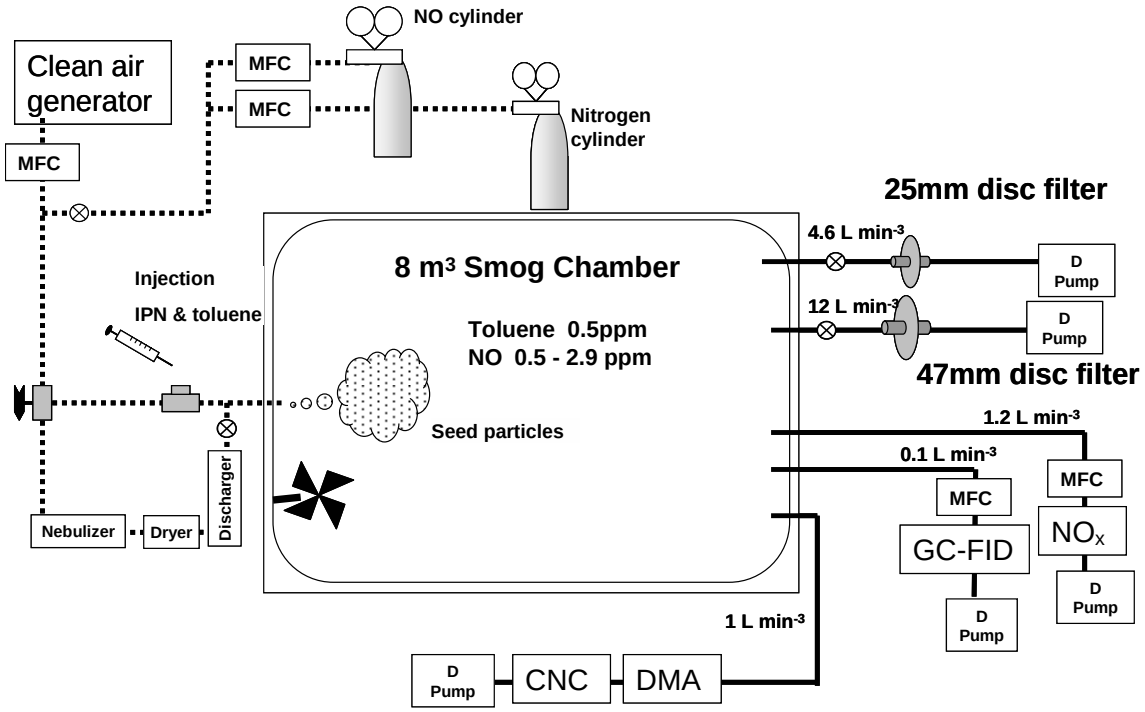

Figure 2. Schematic Diagram of Smog Chamber (Courtesy of Hastie, D.).

3.2. Filter Sampling Secondary POM

A set of two quartz filters (Pallflex Tissuequartz, Pall Corp.) was placed in series for sampling in total POM carbon analyses. For the compound-specific analyses a combination of a Teflon coated filter (Pallflex Fiberfilm, Pall Corp.) on top and a quartz back-up filter for sampling. All quartz filters were pre-cleaned by baking at 1123 K for 12 h prior to use, however, all PTFE coated filters were used without any pre-treatment.

In the flow reactor experiments, the out-flow from the dilution cell of 6.3 L min^{-1} was used. The face velocity for the 25mm disc filters was 1700 cm min^{-1}. The sampling duration made for the flow reactor studies ranged from 30 min and 46 h depending on the production rates of secondary POM.

Two filter samplings were performed parallel for the collection of POM from the smog chamber: one for the analysis of total POM carbon and another is for the analysis of specific product. The filter sizes chosen for the total POM carbon and the compound specific were a 25 mm disc and a 47 mm disc with flow rates of 4.7 L min^{-1} and 12 L min^{-1}, respectively. These flow rates correspond to face velocities of 1300 cm min^{-1} for both filter sizes. The sampling duration for each set of smog chamber experiments was 5 hour, immediately beginning after turning off the UV lights.

3.3. Bulk Sample Analysis

3.3.1. Conversion of Bulk Organic Carbon to CO_2

Bulk organic carbon (i.e. collected filter samples or chemical reference materials) was converted to CO_2 for total carbon yield measurements and for $\delta^{13}C$ measurements via dual-inlet IRMS analyses. The filter sample was sliced into stripes of about ~1 mm and all segments were placed in a 10 inch long × quarter inch o.d. quartz tube, inside of which approximately 1 g of copper oxide (Aldrich) was placed beforehand. For most measurements, copper oxide was used as provided by the supplier. However, pre-baked copper oxide (at 1173 K) was used for analyses of smog chamber samples since it was

found that this pre-cleaning step significantly lowered the background carbon signal. The quartz tube containing the sample and the copper oxide was pre-cooled at 190K for 10 min in a bath of ethanol and dry ice. The tube was then attached to a vacuum line and the air inside was slowly evacuated. The sample was then thermally sealed and the sealed tubes were baked at 1173 K for 12 hours in a muffle furnace.

For the preparation of CO_2 from bulk material, one or two grains of the substance were placed in the quartz tube with copper oxide. Otherwise the procedure was identical to that described above.

3.3.2. Extraction and Quantitative Analysis of CO_2

The extraction of CO_2 from the sample tubes and its quantitative measurement was performed using the vacuum extraction line shown in Figure 3. In the extraction line, impurity of water and nitrogen dioxide (NO_2) was removed using a mixture of ethanol and dryice. After a several steps of the purification of CO_2 inside, the CO_2 extracted was then enclosed in a 1/8″ i.d.×10 in length Pyrex tube for stable carbon isotope measurements.

If necessary, a quantitative measurement of the extracted CO_2 was made before the CO_2 was enclosed in the Pyrex tube. The measurement involved transferring the purified CO_2 in the coil trap 2 to a recovery apparatus similar to the design by Bouton (1991), which was attached to a pressure transducer (Intelligent Transmitter, Series 6000, Paroscientific Inc.). The volume of this measurement apparatus, including the inner volume of the transducer, was calibrated by measuring the pressure and temperature of

standard reference CO_2 ampoules that were prepared from known amounts of a laboratory carbonate standard material (L. Huang, personal communication). The quantity of the sample CO_2 inside the apparatus was determined by measuring the pressure and the temperature according to the ideal-gas law.

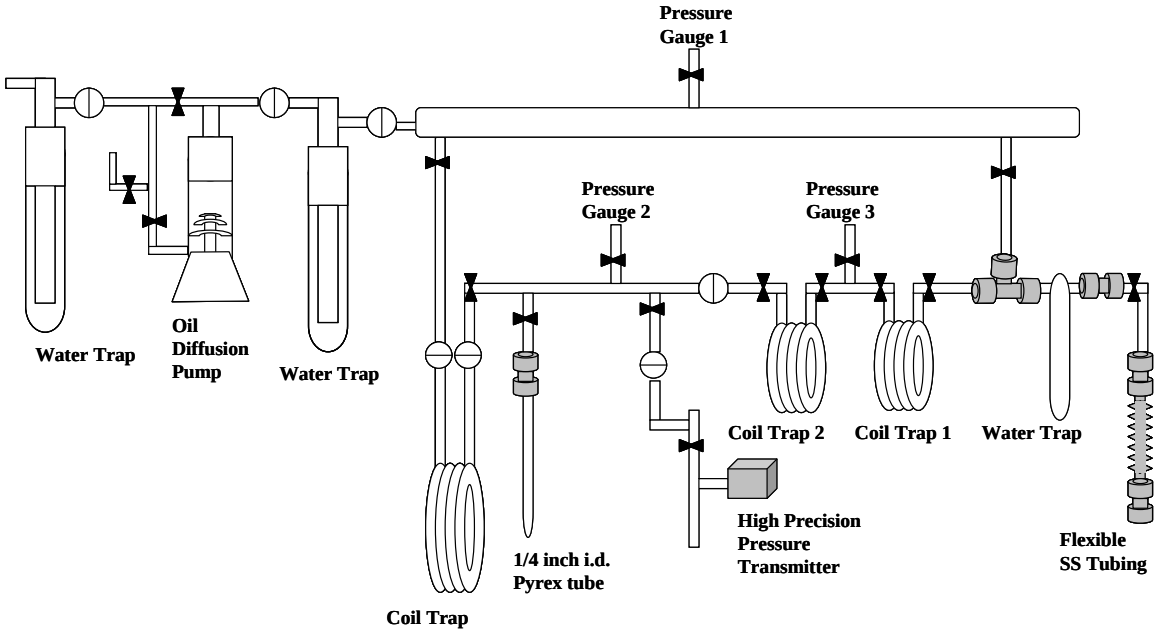

Figure 3. Schematic Diagram of CO_2 Extraction Line (Courtesy of Huang, L.).

3.3.3. Stable Carbon Isotope Measurement By Dual-Inlet IRMS

The extracted sample CO_2 was analyzed for $\delta^{13}C$ by a dual-inlet IRMS (Figure 4). The sample gas in the Pyrex ampoule was introduced into the sample bellow via the flexible stainless steel (SS) tubing, and the sample CO_2 and the reference CO_2 in the bellows were analyzed interchangeably every 8 second in a sequence of $\delta^{13}C$ measurements. The programmed sequence of a single-sample analysis consisted of six measurements for each of the reference and the sample gases at different times. Each CO_2 injection lasted for 20 seconds. The average of the six measurements was used for determination of the $\delta^{13}C$ value.

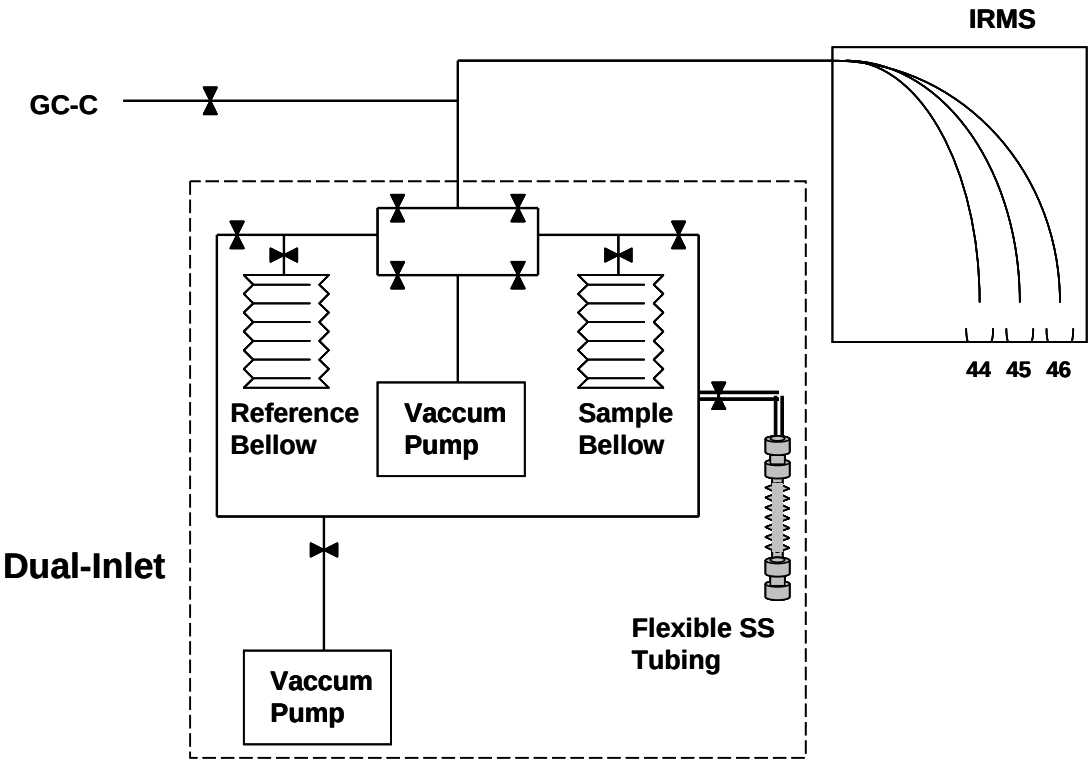

Figure 4. Schematic Diagram of Dual-Inlet IRMS (Courtesy of Huang, L.).

3.3.4. Measurement Test with Reference Materials

The analytical procedure for bulk samples described above was tested with three different reference materials: a laboratory sucrose standard, IAEA-CH-6 (sucrose) and USGS 24 (graphite). The reference values of $\delta^{13}C$ for IAEA-CH-6 and USGS 24 are provided by the International Atomic Energy Agency (IAEA), while that of the laboratory sucrose standard was measured by the stable isotope laboratory of Environment Canada, Downsview. A 2 mg C mL^{-1} solution of the laboratory sucrose or IAEA-CH-6 was prepared in Milli-Q water. Between 10 μl and 50 μl of the standard solution was spiked onto the pre-baked quartz fiber filter. The USGS 24 reference material was spread over quartz fiber filters using a spatula, and the mass of the material was measured with an electronic micro balance. These test samples were then treated in the exact same manner as other secondary POM samples.

3.4. Isotope Fractionation Associated with Evaporation

3.4.1. Isotope Composition of Evaporated Toluene

Evaporated toluene was collected for determination of its isotope ratio using the experimental setup shown in Figure 5 in order to evaluate evaporative isotope fractionation during the flow reactor experiments. Using a similar procedure as for the flow reactor experiments, the bulk toluene was evaporated in a flow of pure nitrogen gas. The evaporated toluene was then transferred into a pre-cooled (190 K) quarter inch o.d. quartz tube containing 1 g of non-baked copper oxide (Aldrich), and the evaporated

toluene was trapped. The preparation and analytical procedures for CO_2 from the trapped toluene were the same procedures as for the other bulk organic samples.

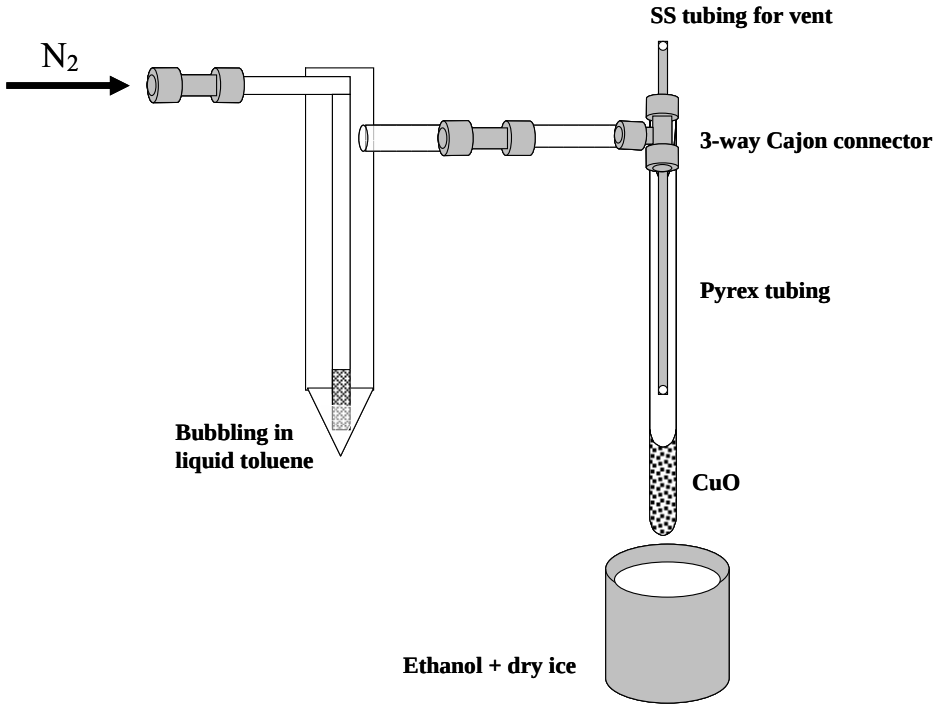

Figure 5. Schematic Diagram for Trapping Experiment of Evaporated Toluene.

3.4.2. Evaporation Test of Secondary POM

Out of 6 filter samples collected under the same fraction of toluene consumed, clean dry air at 6.3 L min^{-1} was pumped down through the three filter samples over 24 hours in order to evaluate the change in the POM carbon and the $\delta^{13}C$ values due to its evaporation. This test was made with non-baked copper oxide.

3.5. Compound Specific Analysis

3.5.1. Analysis of Nitrohydroxy Compounds by GC-C-IRMS

The compound specific analysis targeted the analysis of six nitrophenols, one nitrotoluene, and three methylcatechols (1,2-dihydroxymethylbenzene isomers) shown in Figure 6. Four internal standards were used to quantity these target compounds: Catechol, 2-nitrophenol, 4-ethylresorcinol, and 2,6-dimethyl-4-nitrophenol. The analysis was made by gas chromatography-combustion-isotope ratio mass spectrometry (GC-C-IRMS) shown in Figure 7. After the separation, the effluents were carried by helium carrier gas and introduced into the combustion furnace, at which organic carbons of effluents were converted to CO_2. A make up flow of helium into the combustion tube was mixed with a small flow of pure oxygen (7 mBar above the atmospheric pressure with a capillary tubing) at the head of combustion furnace so that concentration level of oxygen inside the furnace was maintained. The converted CO_2 was introduced to the IRMS inlet with the carrier gas mixture. CO_2 reference gas injections were made from the reference bellow of the dual inlet during a period of a run where no peaks appear. As an option, CO_2 reference gas can be injected from a cylinder via a CO_2 injector (Figure 7), however, this injection method was used only for checking instrument linearity.

Nitrophenol

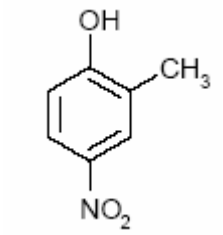

2-methyl-4-nitrophenol

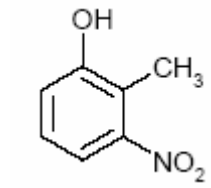

2-methyl-3-nitrophenol

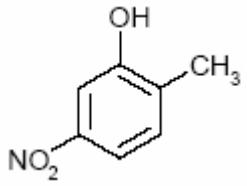

2-methyl-5-nitrophenol

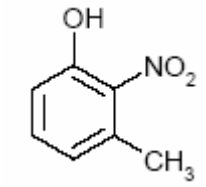

3-methyl-2-nitrophenol

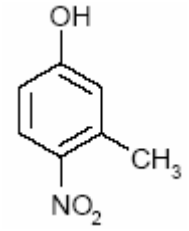

3-methyl-4-nitrophenol

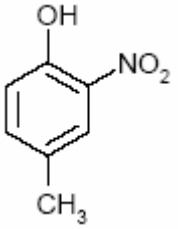

4-methyl-2-nitrophenol

Nitrotoluene ***Methylbenzenediol***

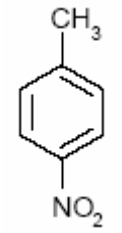

4-nitrotoluene

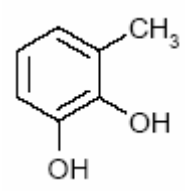

3-methylcatechol

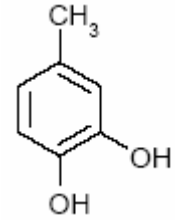

4-methylcatechol

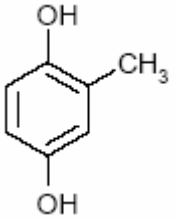

Methylhydroquinone

Internal standard (IS)

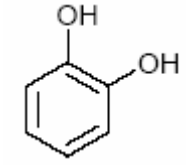

Catechol

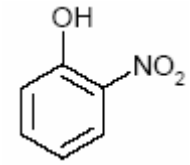

2-nitrophenol

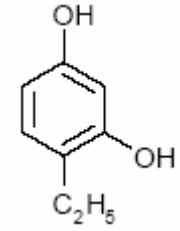

4-ethylresorcinol

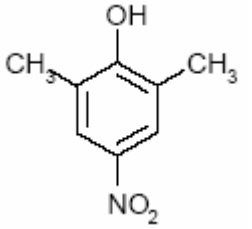

2,6-dimethyl-4-phenol

Figure 6. Standard Substances Tested for Compound Specific Analysis.

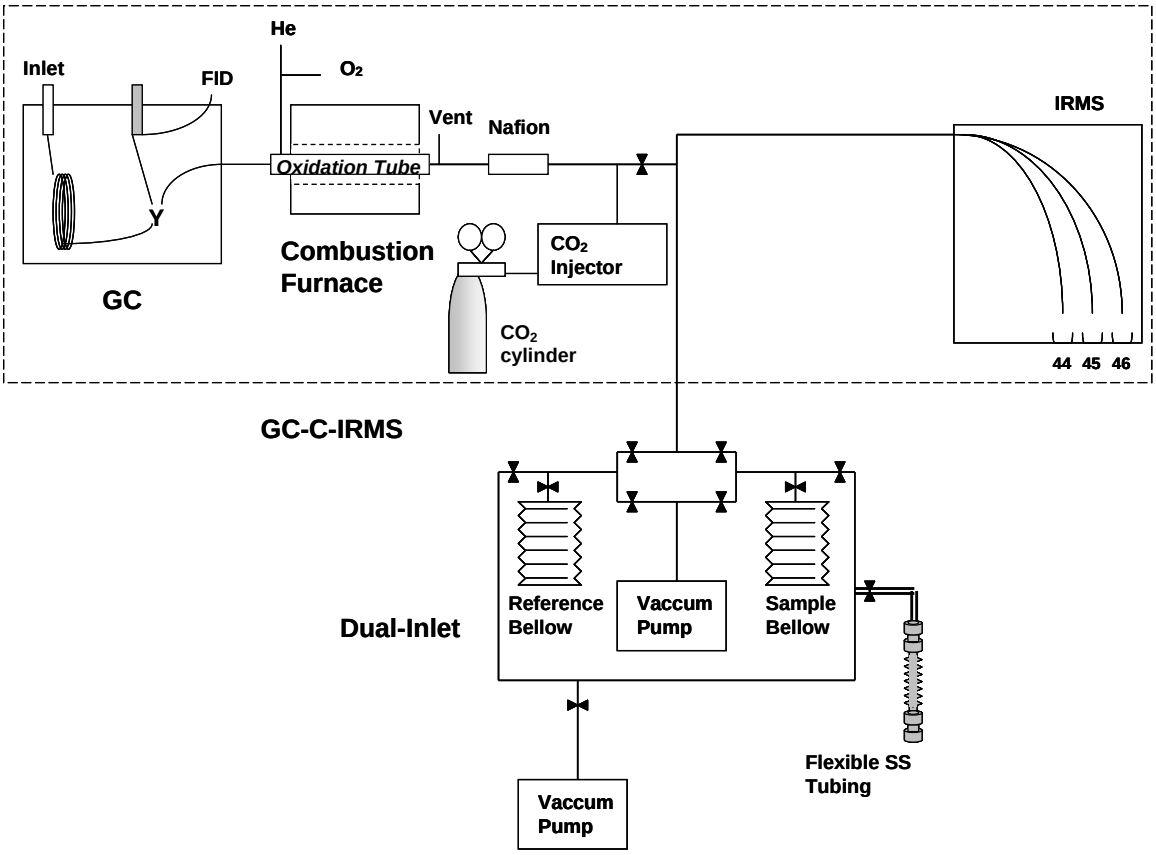

Figure 7. Schematic Diagram of GC-C-IRMS (Courtesy of Huang, L.).

3.5.2. Extraction of Filter Samples

The filter sample was placed in a 60 mL amber glass jar (wide-opened mouth, Chromatographic Specialties Inc.). In advance of the extraction procedure, the jar was etched with a hydrofluoric acid/hydrochloric acid mixture, then silanized with dimethyl-dichloro silane (Aldrich) in order to deactivate the glass surface. The filter samples were extracted with 3 mL of HPLC grade acetonitrile (Aldrich) by agitation in an ultrasonic

bath (FS 60, Fisher Scientific) for 3-5 min. Prior to the extraction, 5 μg C or 24 μg C catechol, 9 μg C or 26 μg C 2-nitrophenol, 6 μg C or 23 μg C 4-ethyl-resorcinol, and 52 μg C or 16 μg C 2,6-dimethyl-4-nitrophenol were all spiked onto the sample filter as the internal standards. The extract was filtered using a micro syringe PTFE filter (0.45 μm pore size, Chromatographic Specialties Inc.) and concentrated in a 5 mL vial (Reacti-Vial Pierce Chemical Co.) under a gentle flow of analytical grade nitrogen gas (Praxair). The residue of the sample filter extracted was rinsed three times with 2 mL of acetonitrile. All of the rinse solutions were filtered and combined together with the first extract. The extract was concentrated at room temperature with a gentle flow of nitrogen gas until the total volume was reduced to ~0.1 mL. An *n*-alkane mixture (C_{17}-C_{19}) (containing 7 μg C each) was spiked to the final concentrated extract in order to evaluate recovery yields. Most of the extracts were analyzed on day of preparation, otherwise they were stored in GC micro vials with crimp caps and placed in a deep freezer for later analysis.

3.5.3. Instrument Linearity

The instrumental linearity of the IRMS under the flow of helium carrier gas was tested by measuring $\delta^{13}C$ values of pure CO_2 gas injected from the CO_2 injector into the carrier gas flow exiting the oxidation furnace (see Figure 7). In this test, the injection of the reference CO_2 gas with defined intensity at the IRMS detectors (5 nA) was made from the reference bellow of the dual-inlet IRMS, and $\delta^{13}C$ values of the sample CO_2 from the CO_2 injector were measured at various signal intensities.

3.5.4. Optimization of GC-C-IRMS for Analysis of Phenolic Compounds

In order to find the best injection method, four different GC injection modes (1:10 split, 1:20 split, splitless, and cold on-column injections) were tested GC-FID. In these tests, a mixture of 5 nitrophenols (in the range of 37-49 ng C for each substance) and 13 ng C n-tetradecane was used. The GC inlet liner used for the split/splitless injections was a Siltek split/splitless deactivated liner (Restek). The retention gap used for the on-column injection was 2 m × 0.32 mm i.d. Siltek deactivated fused-silica capillary (Restek). The inlet temperature for split/splitless injections was kept constant at 520 K, while the inlet temperature program tracking GC temperature (i.e. keeping 5 K lower than the GC temperature) was used for the cold on-column injections. The column used was a 100m × 0.25mm i.d. × 0.5 μm differential Rtx-5SilMS (Restek). The column flow set was at 1 mL min^{-1}. For the split/splitless injections, the following GC temperature program was used: the initial temperature at 373 K was ramped to 538 K at a rate of 5 K min^{-1} and then kept isothermal hold for 8 min. For the cold on-column injection, the initial temperature of 353 K was increased to 403 K at 3 K min^{-1} with isothermal hold for 5 min, then to 443 K at 6 K min^{-1} with no isothermal hold, then to the final temperature of 543 K at 2 K min^{-1} with isothermal hold for 5 min.

The original configuration of the commercially-available combustion furnace was modified in an attempt to reduce the deterioration of phenol peaks through thermal decomposition. First, the heated original interface between the GC and the oxidation furnace was removed in order to shorten the path length that the GC effluents traveled by ~20 cm. Second, the original combustion tube (a 60 cm length × 6.4 mm o.d. quartz tube

containing copper oxide pellets) was replaced with a custom-made combustion tube of 40 cm length × 0.5 mm i.d. × 6.5 mm o.d. gas-tight ceramic tube (Bolt Technical) containing high purity braded Pt, Ni and Cu wires (Alfa Aesar) shown in Figure 8. Since temperature at the entry point of the effluent was critically important, temperature measurements inside the tube were made using a thermo-couple in order to find a region where the temperature settled lower than 553 K. This temperature was chosen since GC-FID analyses demonstrated that no thermal decomposition occurred under this condition. Third, a small flow of pure oxygen was mixed with a stream of make-up helium at the head of the oxidation tube shown in Figure 7. This allowed for having an oxygen-rich environment within the furnace tube at all times.

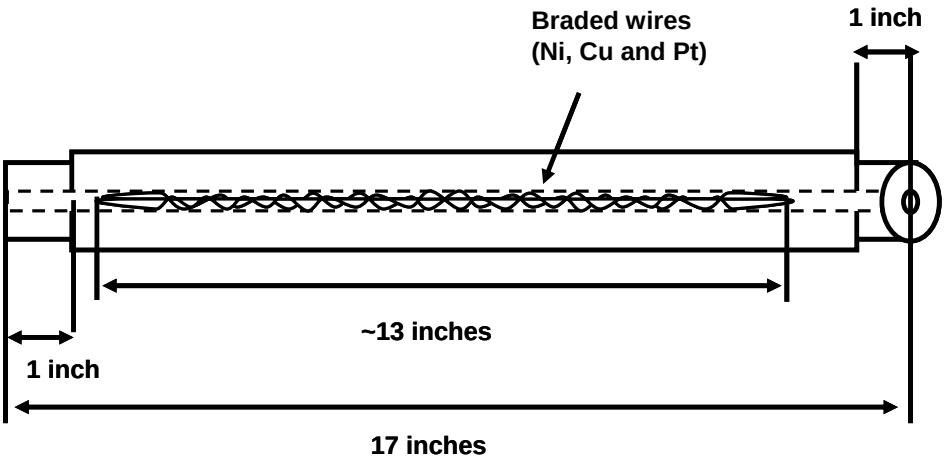

Figure 8. Schematic Diagram of a Gas-tight Ceramic Oxidation Tube.

3.5.5. Derivatization

For the derivatization 10% volume of *N*,*O*-bis-(trimethylsilyl)-trifluoroacetamide (BSTFA, Regis Technology, Inc.) was spiked into the standard solutions and the sample extracts, and then stirred for 5 min at room temperature. BSTFA replaces active hydrogen atoms in –COOH and –OH groups with trimethylsilyl (TMS) groups, as shown in Figure 9, for example.

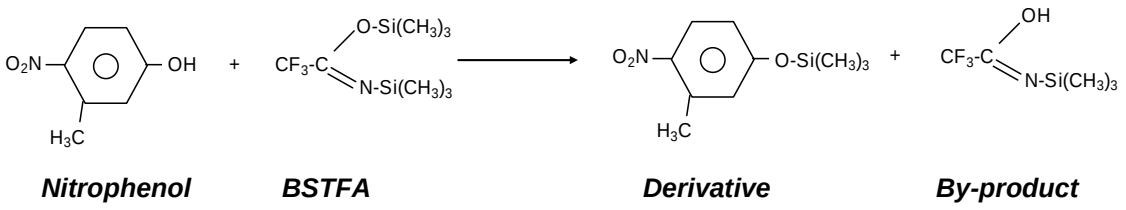

Figure 9. Schematic for Derivatizing Reaction with BSTFA.

The derivatization adds carbon atoms to the original compound. If there is no isotope fractionation occurring during this derivatization, the addition of TMS carbon results in a defined change of the isotope composition of the derivative relative to the starting material. A following mass balance was used in order to obtain the isotope composition of the original compound ($\delta^{13}C_{free}$):

$$\delta^{13}C_{free} = \frac{\#C_{deriv}}{\#C_{free}} \times \delta^{13}C_{deriv} - \frac{\#C_{TMS}}{\#C_{free}} \times \delta^{13}C_{TMS} \qquad (1)$$

where $\#C_{deriv}$, $\#C_{free}$, $\#C_{TMS}$ are the number of carbon atoms of the derivative molecule, the original phenolic compound, and the TMS group(s) added to the original phenol molecule, respectively. $\delta^{13}C_{deriv}$ and $\delta^{13}C_{TMS}$ represent the stable carbon isotope compositions of the derivative and the TMS group, respectively. Values for $\delta^{13}C_{TMS}$ were

determined indirectly by measuring the derivatives of reference substances, whose reference stable carbon isotope compositions were determined by the offline method. The average $\delta^{13}C_{TMS}$ value was then used as the reference $\delta^{13}C_{TMS.}$

3.5.6. Quantitative, Isotope and Qualitative Analysis

Five or six standard mixtures of varying concentration, containing 6 nitrophenols, 3 catechols, and a nitrotoluene were freshly prepared from the stock solutions (92-2800)μg C ml^{-1}. Their TMS derivatives were analyzed by the GC-C-IRMS in order to obtain quantitative and isotopic calibrations.

Qualitative analyses were performed by a GC (CP 3800 GC, Varian) coupled with an ion trap MS (Saturn 2000, Varian). The identification of products was performed through comparisons with retention times of standards and mass spectra from the NIST reference library, or, through data analyses of the fragment ions when no reference retention time and mass spectra were available.

3.5.7. Standard Spike Tests

Standard mixtures containing 10 standard compounds shown in Figure 6 were spiked together with the 4 internal standards onto PTFE coated filters (Pallflex Fiberfilm, 25 mm disc, Pall Corp.). Three *n*-alkanes (C_{17}-C_{19}) of 7 ng C each were spiked onto the final concentrated extract for determination of the extract volume, which allow calculating the recovery yields.

4. Results

4.1. Concentration of Toluene, NO_x and Secondary POM Mass

An example of a calibration plot of toluene measurements during the flow reactor studies is shown in Figure 10. As seen, calibrations made during the flow reactor studies showed excellent linearity ($y = (5.6\pm0.1)\times10^{-4}\ x - (6.7\pm1.0),\ R^2 = 0.999$). The intercept that appeared, corresponding to 10^4 area count, was statistically significant. This high value of the intercept cannot be explained by background signal only, which is $< 10^3$. This intercept is more likely a combination of the background with blank value: possibly cross-contamination in syringe. The smog chamber calibrations performed with a permeation tube containing toluene also showed excellent linearity ($R^2 > 0.98$).

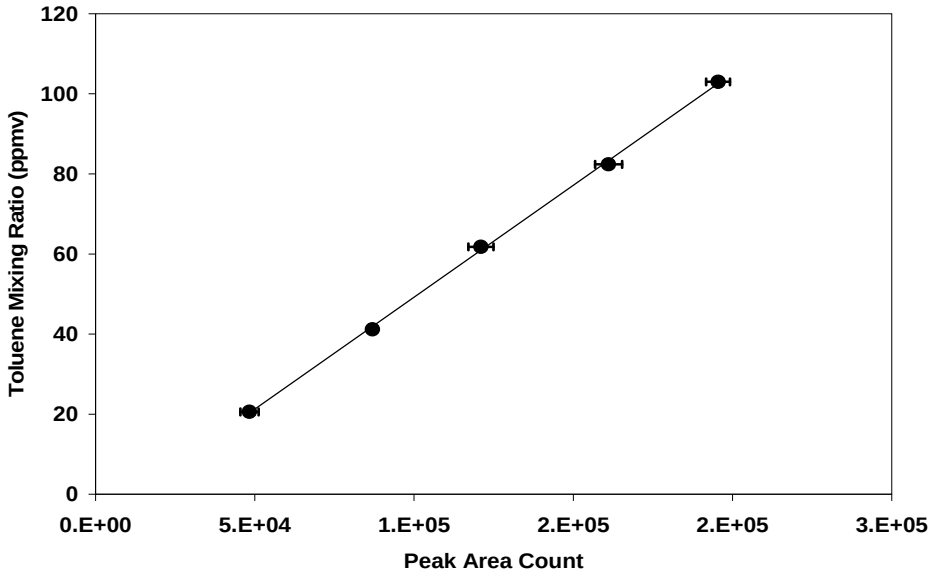

Figure 10. Example Calibration for Toluene during Flow Reactor Experiment.
$y = (5.6\pm0.1)\times10^{-4}\ x - (6.7\pm1.0),\ R^2 = 0.999$. Shown error bars are standard errors.

An example of toluene mixing ratios determined during a flow reactor experiment is shown in Figure 11. For the determination of toluene mixing ratios, at least five measurements were made at steady-state in order to have a defined concentration. The reproducibility of steady-state mixing ratios before and after the start of the toluene+OH reaction was typically 3% or less, which is sufficient to determine the average extent of the toluene reaction. In the example shown, the difference between the average from the 1st-7th injections (before the UV lamp on) and the average from the 8th-16th injections (during the UV lamp on) was (18±2)% (±standard error), relative to the average value from the 1st-7th injections.

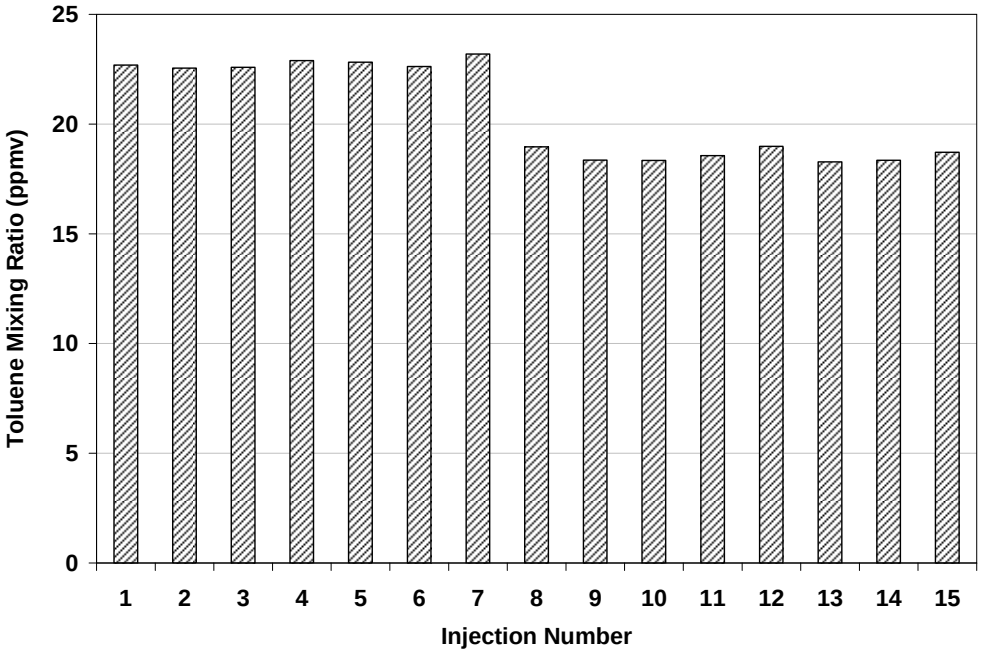

Figure 11. Plot of Toluene Mixing Ratio during Flow Reactor Experiment.
The interval between injections is ~5 min. The UV source was activated immediately following the 7th injection.

An example plot of measured size (diameter) distribution of PM (including seed particles) during the smog chamber experiment is shown in Figure 12. The size distribution data show that the growth of seed particles started immediately following the activation of the UV source. The mono-modal size distribution settled at 340 nm 30 min after activating UV radiation. Based on the results from the size distribution measurements together with typical assumption that all observed particles were spheres, the volume concentration was calculated. The volume concentration of secondary POM was obtained by subtracting the total volume concentration of the seed particles from that of the PM grown. The mass concentration was then calculated by multiplying the volume concentration by 1 g cm^{-3}, assuming that the density of POM formed is 1 g cm^{-3}.

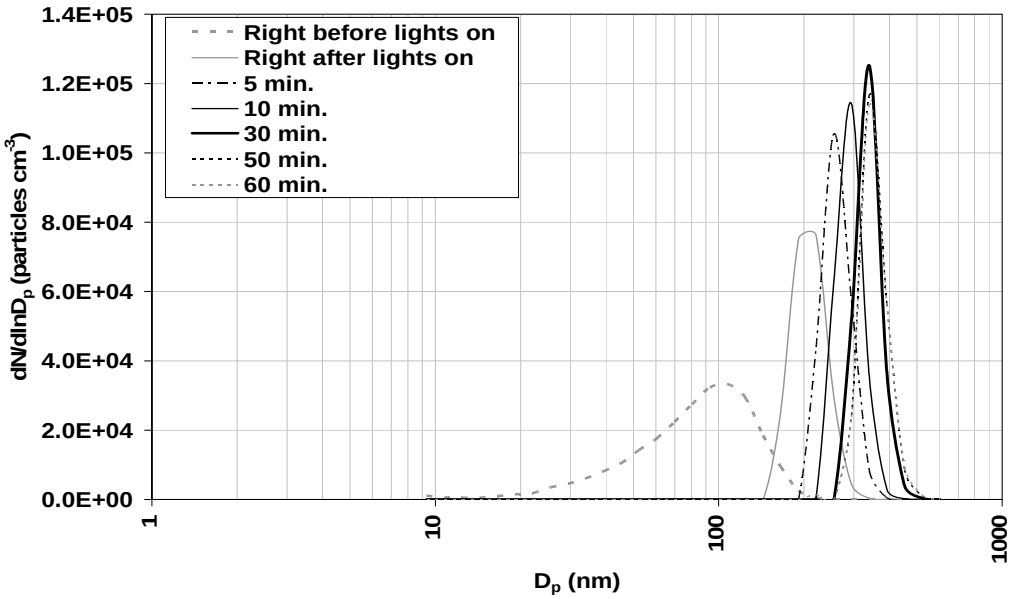

Figure 12. Plot for Size Distribution of Secondary POM Formed during Smog Chamber Experiment (SC I).
The lights were turned off after 55 minutes elapsed time of the lights on.

For more accurate estimation, the rate of wall loss in POM number concentration for a specific particle size bin, [N_{Dp}], was compensated by a first order rate expression (McMurry and Rader, 1985):

$$\frac{d[N_{Dp}]}{dt} = k_{WallLossDp}[N_{Dp}] \quad (2).$$

In this equation the rate constant for a specific particle size bin ($k_{WallLossDp}$) is defined as

$$k_{WallLossDp} = a\exp\left[-0.5\left\{\frac{\ln\left(\frac{D_p}{x_0}\right)}{b}\right\}^2\right] + y_0 \quad (3)$$

where a, b, x_0, and y_0 are the experimentally determined parameters for the YorkU smog chamber by Bienenstock, Y. (2001), and D_p is the median of the size bin (diameter in μm) of particles assumed to be spheres. By using the calculated $k_{WallLossDp}$ for all size bins measured, the overall wall loss rate per unit time was estimated. The estimation demonstrates that the impact of the wall-loss on the POM mass yield (a ratio of the wall-loss corrected mass concentration of POM over the change in mass concentration of toluene, denoted as Y_m thereafter) during the smog chamber experiments is less than 1%. Due to the physical process and its small loss, the impact of wall loss on $\delta^{13}C$ values of the filter samples are thought to be negligible.

An example of time series plot for the mass concentration calculated is shown together with those the toluene and the NO mixing ratios in Figure 13. Time series plot for the other two experiments were similar profiles. The final conditions achieved in the

smog chamber experiments (i.e. just prior to the start of filter sampling as the UV irradiation was turned off) are summarized in Table 1.

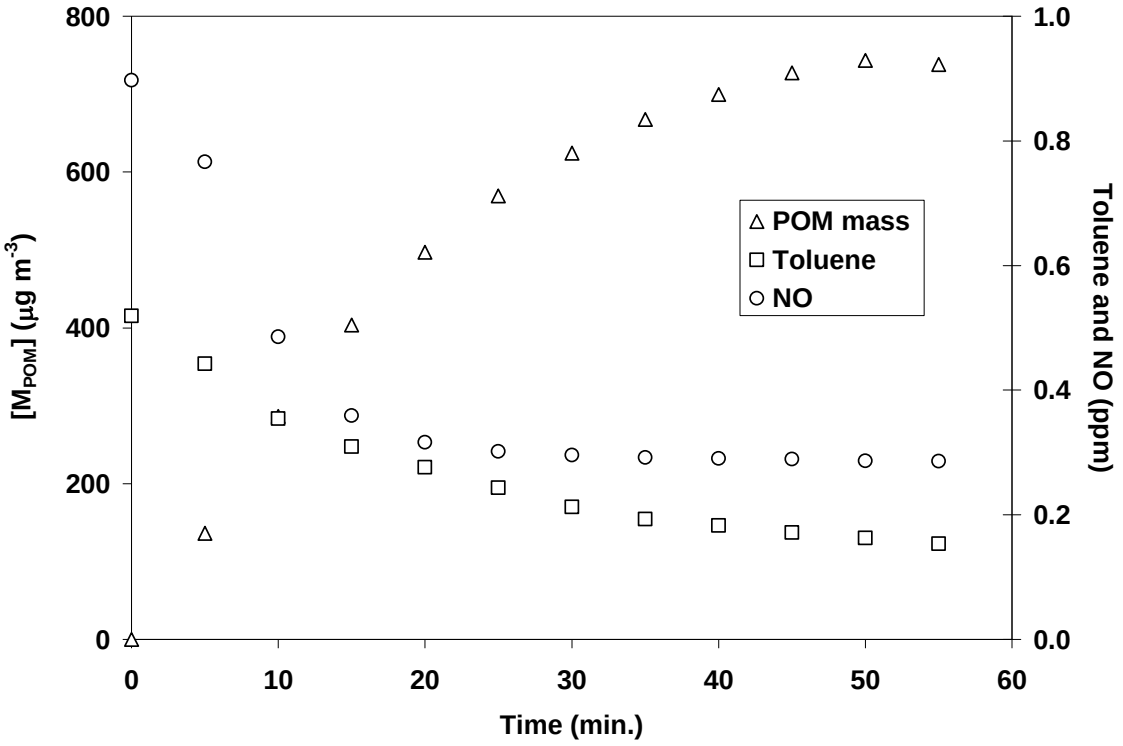

Figure 13. Time Series Plot of POM Mass Concentration, Toluene Mixing Ratio, and NO Mixing Ratio during Smog Chamber Experiment (SC III).
Each point for toluene and NO mixing ratios were one measurement and the average of 30 measurements, respectively. The time of zero indicates the time the UV lights were activated. The lights were deactivated at 50 min.

Table 1 Final Results of Smog Chamber Experiment[a]

Experiment[b]	Toluene consumption[c] (%)	Toluene mass conc. reacted[c] ($\mu g\ m^{-3}$)	POM mass conc.[d] ($\mu g\ m^{-3}$)
SC I	36±4	691±74	260
SC II	69±4	1307±76	747
SC III	71±4	1372±77	755

[a]All the values shown are when the UV lights were turned off (i.e. before the sampling started). [b]Irradiation time was 26 min, 82 min, and 55 min for SC I, SC II, and SC III, respectively. [c]The errors shown are 1σ of the propagated errors according to the 3% error for the measurement of toluene mixing ratios before and after the UV irradiation. [d]The values shown are corrected for wall-loss (see the text for the wall-loss calculation).

4.2. Filter Sampling

The information for sampling POM is summarized in Table 2. The sampling volume taken from the flow reactor was between 0.03 and 2.14 m^3. The mass of POM loaded on the filters from the flow reactor experiments could not be estimated since size distribution nor mass of filter samples were measured. Addition to the sampling information, POM mass loaded on the filter (M_{POM}) is also shown in Table 2 for the smog chamber samples. The estimation was based on the observed POM mass concentrations by the size distribution measurements:

$$M_{POM} = \sum_{n=1} \left\{ [M_{POM}]^n \times V^n \right\} \quad (4)$$

where $[M_{POM}]^n$ and V^n are the average POM mass concentration over a 5 min interval between the *n*th and *n+1*th measurements and the air volume sampled over the same interval between the same number of measurements, respectively. The product of

$[M_{POM}]^n \times V^n$ for each interval was then summed up to obtain the M_{POM}, the total POM mass loaded on the filter. The M_{POM} values calculated are only for the smog chamber samples.

Table 2 Summary of Filter Sampling

Experiment	n	Sampling duration (h)	Sampling flow rate (L min.$^{-1}$)	Sampled volume[a] (m^{-3})	POM mass loaded (M_{POM}) (μg)
Flow Reactor Experiments					
25 mm disc filter[b]					
FR A – FR D	21	0.7-45.3	6.3	0.3-17.1	N/A
25 mm disc filter[b]					
EVAP A – EVAP F	6	1.6-3.3	6.3	0.5-0.8	N/A
47mm disc filter[c]					
FR 1- FR 5	5	2.4-19.0	6.3	0.1-0.9	N/A
Smog Chamber Experiments					
25 mm disc filter[b]					
SC I	1	5.03	4.7	1.42	188
SC II	1	5.10	4.8	1.47	573
SC III	1	5.22	4.7	1.47	608
47mm disc filter[c]					
SC I	1	5.03	12	3.62	480
SC II	1	5.10	12	3.67	1433
SC III	1	5.22	12	3.76	1553

[a]The values shown for the flow reactor samples are determined according to the make-up flow at the dilution cell. [b]Samples are for total POM carbon analyses. [c]Samples are for compound specific analyses.

4.3. Analysis of Bulk Samples

4.3.1. Filter Blank

Results of the blank filter analysis using two different methods (i.e. use of non-baked copper oxide and pre-baked copper oxide) are shown in Table 3. The results demonstrate that the quantity of blank carbon was significantly reduced in the method that used pre-baked copper oxide (ca. 1/10). In contrast, the $\delta^{13}C$ values between the two methods were not significantly different.

Table 3 Results of Blank Filter Analysis

	Carbon mole (μmol C)	$\delta^{13}C$ (‰)
Preparation with non-baked copper oxide (n=14)		
Average	1.1	-22.5
Standard Error	0.1	0.6
Preparation with pre-baked copper oxide (n=14)		
Average	0.2	-22.1
Standard Error	0.1	0.8

4.3.2. Measurement of Reference Materials

The results of quantitative and isotope analyses for the three reference materials as well as their recommended $\delta^{13}C$ values are summarized in Table 4. The $\delta^{13}C$ values shown in the table are the intercepts of linear regression in Keeling plots: A plot of $\delta^{13}C$ as a function of reciprocal of carbon mass (Figure 14).

Table 4 Summary for Measurement of Reference Materials

Reference Material (Oxidation Temperature)	n	Spiked mole (μmol C)	Recovery (%)	$\delta^{13}C^{b}$ (‰)
Preparation method with non-baked copper oxide				
Sucrose (853 K)	3	19 - 47	89 - 98	-11.65±0.01
IAEA-CH-6[a] (853 K)	4	0.92 - 37	66 - 96	-10.4±0.4
USGS 24[a] (853 K)	3	14 - 28	14 - 30	-18±11
Sucrose (1173 K)	3	19 - 47	92 - 99	-12.0±0.2
IAEA-CH-6[a] (1173 K)	4	0.92 - 37	88 - 94	-10.3±0.2
USGS 24[a] (1173 K)	3	14 - 24	72 - 91	-15.9±0.1
Preparation method with pre-baked copper oxide				
IAEA-CH-6[a] (1173 K)	9	1.2 - 34	95 - 100	-10.28±0.08
Reference values				
Sucrose	-	-	-	-11.97±0.09
IAEA-CH-6[a]	-	-	-	-10.449±0.033
USGS 24[a]	-	-	-	-16.0±0.1

[a]IAEA-CH-6 and USGS 24 are the international standards of sucrose and graphite, respectively. [b]The values are shown together with standard errors determined by Keeling plots.

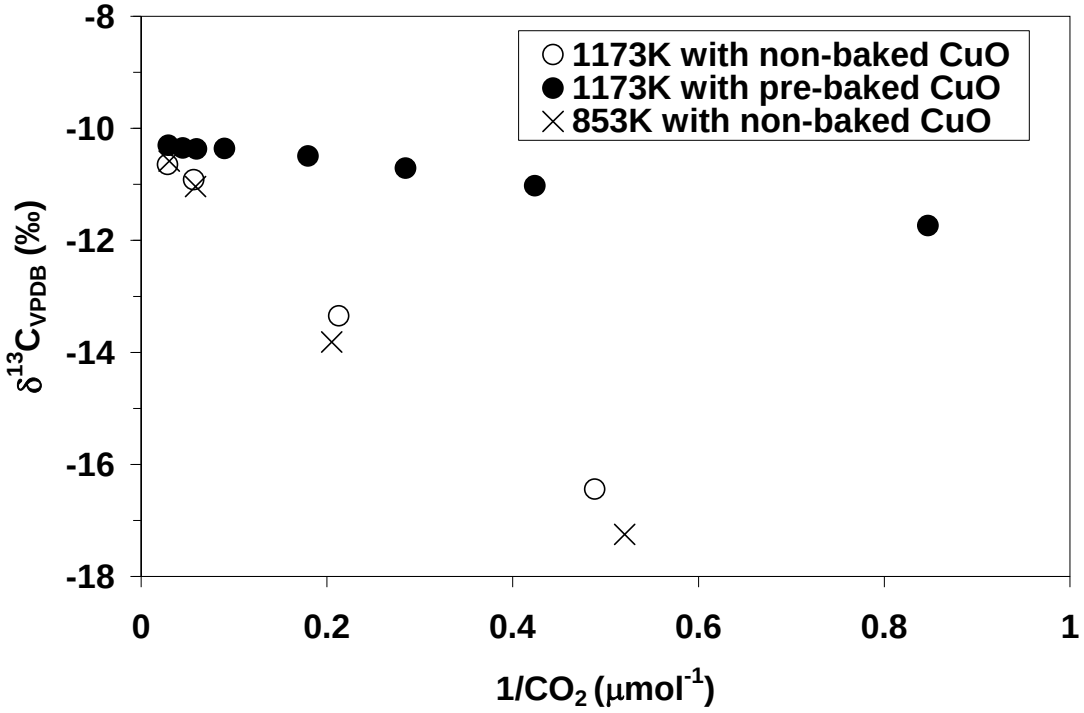

Figure 14. Plot of $\delta^{13}C$ Values Measured for IAEA-CH-6 as Function of Inverse of Carbon Mole Yielded (Keeling Plot).
Open circle, 1173 K oxidation with non-baked copper oxide; cross, 853 K oxidation with non-baked copper oxide; solid circle, 1173 K oxidation with pre-baked copper oxide. The reference $\delta^{13}C$ value for IAEA-CH-6 is (-10.4±0.2)‰. The intercepts (±standard error) from each set of the oxidation methods are (-10.3±0.2)‰, (-10.4±0.4)‰ , and (-10.28±0.08)‰, respectively.

4.3.3. $\delta^{13}C$ Values of Bulk Toluene and Evaporated Toluene

Results of $\delta^{13}C$ analyses for bulk toluene and evaporated toluene are shown in Table 5. Evaporated toluene had on average (0.33±0.02)‰ heavier isotope composition than bulk toluene.

Table 5 $\delta^{13}C$ for Bulk and Evaporated Toluene

Specie	n	Carbon amount (μmol C)	$\delta^{13}C^{a}$ (‰)
Bulk Toluene	3	96 – 102	-27.05±0.02
Evaporated Toluene	6	86 – 252	-26.72±0.01

[a] *The values shown are average ±standard error.*

4.3.4. Results of Filter Sample Analysis

The results of quantitative and $\delta^{13}C$ analyses of secondary POM carbon collected on quartz filters from the flow reactor experiments are summarized in Table 6. The average values of $\delta^{13}C$ and their standard errors shown in the table were determined using Keeling plots.

Similar to the results of the filter sample analysis shown above, the results of the back-up filter analysis for the flow reactor samples are summarized in Table 7. Again, the average $\delta^{13}C$ values and their standard errors shown in the table are determined by Keeling plots.

The results of quantitative and isotope analyses for the filter samples from the smog chamber experiments are summarized in Table 8. The blank corrections were made for the carbon moles and the $\delta^{13}C$ values using mass balance with the blank value of (0.3±0.1)μmol C and (-22.1±1.0)‰ shown in Table 3.

Table 6 Results of Front Filter Analysis for Flow Reactor Samples[a]

Experiment[b]	Sampling duration (h)	Carbon mole[c] (μmol C)	POM C formation rate[d] (μmol C h^{-1})	$\delta^{13}C$ (‰)
FR A				
A-1	9.3	58.3	6.2	-32.07
A-2	3.1	20.1	6.2	-31.38
A-3	6.3	44.0	6.8	-31.89
A-4	9	53.0	5.8	-32.06
A-5	5.5	40.7	7.2	-31.91
A-6	3.4	22.8	6.4	-31.68
Average			6.4[e]	-32.37[f]
Error			0.2	0.08
FR B				
B-1	7.4	2.5	0.20	-30.63
B-2	14.1	3.4	0.17	-31.14
B-3	24.1	5.1	0.17	-31.81
B-4	45.3	6.2	0.12	-31.95
Average			0.16[e]	-32.90[f]
Error			0.02	0.09
FR C				
C-1	5.1	40.7	7.8	-31.93
C-2	3.0	16.1	5.1	-31.99
C-3	15.6	94.1	6.0	-32.54
C-4	8.1	37.0	4.4	-32.36
C-5	16.8	70.6	4.1	-32.58
C-6	3.4	15.8	4.4	N/A[g]
Average			5.3[e]	-32.57[f]
Error			0.6	0.20

[a]All the filter samples were oxidized at 1175K. [b]The fraction of toluene consumed for the flow reactor (FR) series A-D are (15±3)%, (7±1)%, (20±2)% and (29±2)%, respectively. [c]No blank correction was made. [d]Corrected for filter blank values. [e]The values shown are the average of POM formation rate ±standard error. [f]The value shown is the intercept $\delta^{13}C$ value ±standard error determined from Keeling plot (see the discussion concerning correction for blank carbons). [g]Value is not available.

Table 6 Continued.

Experiment[a]	Sampling duration (h)	Carbon mole[b] (μmol C)	POM C formation rate[c] (μmol C h^{-1})	$\delta^{13}C$ (‰)
FR D				
D-1	2.8	20.1	6.8	-31.94
D-2	1.5	9.8	5.9	-31.74
D-3	3.2	20.1	6.0	-31.99
D-4	5.4	32.0	5.7	-32.14
D-5	0.73	4.4	4.6	-31.30
Average			5.8[d]	-32.19[e]
Error			0.4	0.04

Table 7 Results of Back-up Filter Analysis for Flow Reactor Samples[a]

Experiment	Sampling duration (h)	Carbon mole (μmol C)	$\delta^{13}C$ (‰)
FR A			
A-all backup filters	45.5	12.01	-28.20
FR B			
B-1 backup	7.4	0.80	-25.39
B-2 backup	14.1	2.54	-26.45
B-3 backup	24.1	2.55	-26.67
B-4 backup	45.3	2.87	-27.53
average		2.19	-26.51
standard error		0.54	0.51
FR C			
C-1 backup	5.1	3.33	-27.38
C-2 backup	3.0	2.76	-27.29
C-3 backup	15.6	3.63	-28.46
C-4 backup	8.1	2.92	-27.58
C-5 backup	16.8	4.13	-28.40
C-6 backup	3.4	2.53	-26.75
average		3.22	-27.65
standard error		0.34	0.30

[a]All the filter samples were oxidized at 1175K.

Table 7 Continued

Experiment	Sampling duration (h)	Carbon mole (μmol C)	$\delta^{13}C$ (‰)
FR D			
D-1 backup	2.8	1.06	-27.09
D-2 backup	1.5	2.57	-25.70
D-3 backup	3.2	2.87	-27.03
D-4 backup	5.4	3.45	-27.50
D-5 backup	0.73	2.84	-26.43
average		2.56	-26.75
standard error		0.52	0.40
average all		2.7	-27.1
standard error		0.2	0.2

Table 8 Results of Filter Sample Analysis for Smog Chamber Samples[a]

Experiment	Sampling volume[b] (m^{-3})	Carbon mole[c] (μmol C)	$\delta^{13}C$ measured (‰)	$\delta^{13}C$ blank corrected[d] (‰)
SC I	1.42	3.8	-30.760±0.006	-31.5±0.3
SC I back-up	1.42	2.0	-27.743±0.005	-28.9±0.4
SC II	1.47	11.9	-29.639±0.004	-29.83±0.07
SC II back-up	1.47	1.6	-26.912±0.005	-27.5±0.4
SC III	1.47	15.7	-29.716±0.002	-29.86±0.05
SC III back-up	1.47	0.90	-27.955±0.003	-28.5±1.0

[a]All the filter samples were oxidized at 1175K. [b]Collected on 25 mm disc quartz filters at 4.7 L min^{-1} for 5 h. [c]Blank corrections were made. [d]The average blank value(±standard error) of (0.3±0.1)μmol C with (-22.1±1.0)‰ was used in the mass balance for blank correction.

4.3.5. Evaporation Test of Secondary POM

The results of the evaporation tests of secondary POM samples are summarized in Table 9. In overall, (1.3±0.6)% difference for POM carbon yield rate and (0.3±0.2)‰ difference in $\delta^{13}C$ was observed due to evaporation of the organic carbon from the filter samples during pumping the dry air at 6.3 L min^{-1} flow rate for 24 hours.

Table 9 Results of Evaporation Tests of Secondary POM Samples Collected from Flow Reactor[a]

Experiment[b]	Carbon mass[c] (μmol C)	Sampling duration[d] (h)	Carbon yield rate[e] (μmol h^{-1})	$\delta^{13}C$ measured (‰)	$\delta^{13}C$ corrected[c] (‰)
Non-evaporated samples					
EVAP A					
top	18.8	1.6	10.8	-31.205±0.008	-31.75±0.06
back-up	2.1	1.6	0.6	-25.431±0.002	-28.7±0.4
EVAP B					
top	19.9	1.6	11.5	-31.366±0.007	-31.88±0.06
back-up	3.5	1.6	1.5	-25.673±0.004	-27.1±0.2
EVAP C					
top	24.8	2	11.8	-30.979±0.004	-31.37±0.05
back-up	3.4	2	1.1	-25.038±0.003	-26.3±0.2
Average (EVAP A-C) front[f]			11.4±0.5	-31.18±0.14	-31.67±0.19
Average (EVAP A-C) back-up[f]			1.1±0.4	-25.38±0.23	-27.35±0.88
Evaporated samples					
EVAP D					
top	17.8	1.6	10.2	-31.268±0.004	-31.85±0.06
backup	3.0	1.6	1.2	-24.400±0.004	-25.5±0.2
EVAP E					
top	34.5	3.3	10.2	-31.778±0.007	-32.08±0.03
back-up	3.4	3.3	0.7	-24.994±0.009	-26.2±0.2
EVAP F					
top	12.7	1.2	9.7	-31.185±0.011	-32.01±0.09
back-up	2.0	1.2	0.7	-25.386±0.007	-29.1±0.4
Average (EVAP D-F) front[f]			10.1±0.3	-31.41±0.23	-31.98±0.09
Average (EVAP D-F) back-up[f]			0.9±0.3	-24.93±0.35	-26.93±1.36

[a]The blow-off duration for EVAP D, E, and F was ~23 h under a flow of clean dry air at 6.3 L min^{-1}. [b]The extent of toluene reactions for EVAP A, B, C, D, E, and F were (22±5)%, (19.1±0.9)%, (22±3)%, (24±3)%, (21±4)%, and 18.7%, respectively. [c]Blank corrections were made. [d]The duration of POM sampling from the flow reactor. [e]Carbon mass divided by sampling duration. [f]The value shown is the average value ± standard error.

4.4. Compound Specific Analysis

4.4.1. Optimization of Instrumentation

Relative response data (per carbon mass) for the free nitrophenols relative to that of the C_{14} *n*-alkane for different injection methods are shown. Note that these tests were carried out by GC-FID analyses without derivatization.

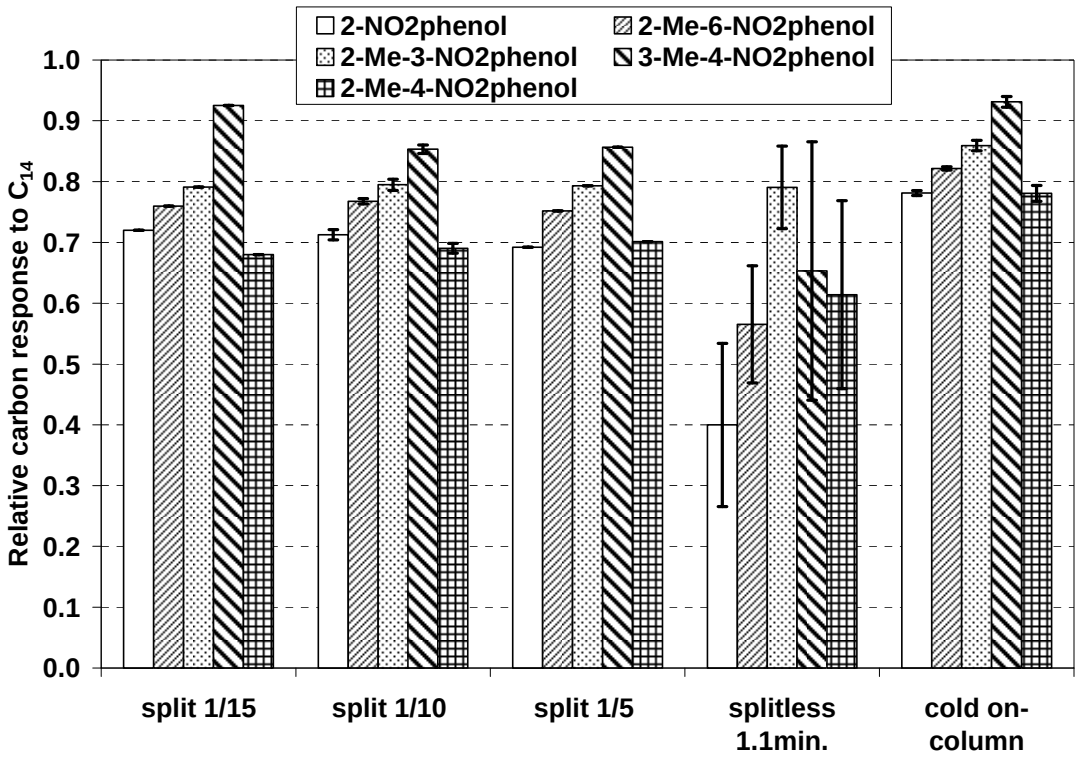

Figure 15. Normalized FID Response (per Carbon Mass) for Nitrophenols for Five Different Injection Methods.
The numbers of replicate measurements are 1, 3, 1, 2, and 3 for split 1/15, split 1/10, split 1/5, splitless, and on-column injections, respectively. The signal response per carbon atom was normalized relative to that of C_{14} n-Alkane. Error bars shown are standard deviation.

4.4.2. Temperature inside the Oxidation Tube

Temperature profiles measured inside the oxidation tube of the combustion furnace are shown in Figure 16.

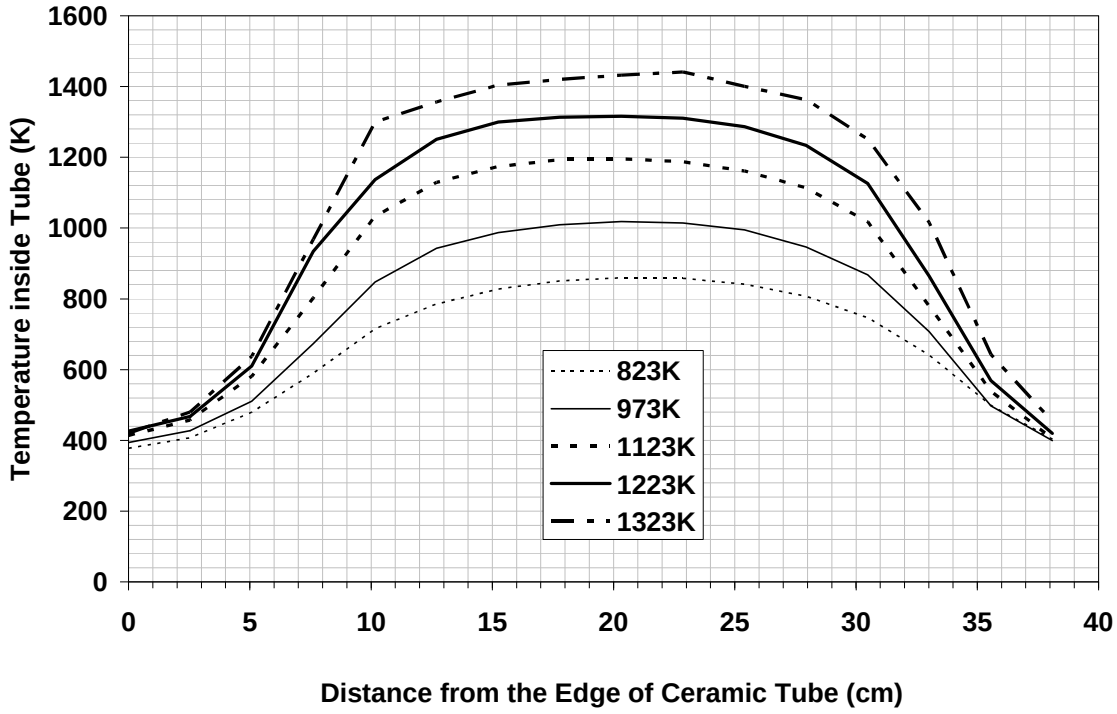

Figure 16. Temperature Profiles inside the Oxidation Tube at Different Set-Point of Furnace Temperature.

4.4.3. Retention Time of Standard Compounds

An example chromatogram for the TMS derivative standard mixture (2–17 ng C of the standards' carbon) is shown in Figure 17. The retention time index for the standard substances obtained by the GC-C-IRMS is shown in Table 10. In total, three replicate

measurements for each of five different concentration levels of standard mixtures were analyzed in order to construct the quantitative and isotope calibrations.

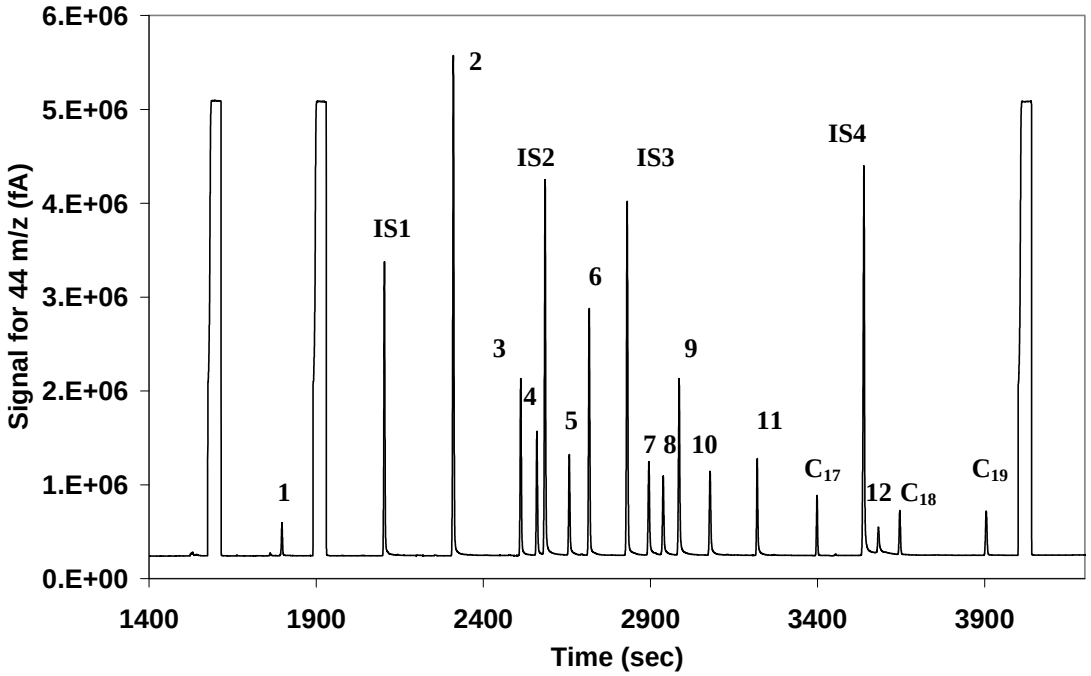

Figure 17. Chromatogram Obtained by GC-C-IRMS Measurement for Oxygenated Aromatic Standard Compounds Derivatized with BSTFA (corresponding to the injection of 2-17 ng C TMS-free standards).
Peaks from 1 to 12 correspond to o-cresol, 4-nitrotoluene, 4-methylcatechol, 3-methylcatechol, 3-methyl-2-nitrophenol, methylhydroquinone, 4-methyl-2-nitrophenol, 2-methly-3-nitrophenol, 2-methyl-5-nitrophenol, 3-methyl-4-nitrophenol, 2-methyl-4-nitrophenol, and 2-hydroxy-5-nitrobenzaldehyde, respectively. Peaks from IS1 to IS4 are the internal standards corresponding to catechol, 2-nitrophenol, 4-ethylresorcinol, and 2,6-dimethyl-4-nitrophenol, respectively. Peaks labeled C_{17}, C_{18}, and C_{19} are n-heptadecane, n-octadecane, and n-nonadecane, respectively. Rectangular peaks are reference CO_2 peaks.

Table 10 Retention Time of Reference Compounds

Peak #[a]	Species	Retention time (min)
IS1	catechol	35.1
2	4-nitrotoluene	38.5
3	4-methylcatechol	41.9
4	3-methylcatechol	42.7
IS2	2-nitrophenol	43.1
5	3-methyl-2-nitrophenol	44.3
6	Methylhydroquinone	45.3
IS3	4-ethylresorcinol	47.2
7	4-methyl-2-nitrophenol	48.3
8	2-methyl-3-nitrophenol	49.0
9	2-methyl-5-nitrophenol	49.8
10	3-methyl-4-nitrophenol	51.3
11	2-methyl-4-nitrophenol	53.7
C17	Haptadecane	56.7
IS4	2,6-dimethyl-4-nitrophenol	59.0
C18	Octadecane	60.8
C19	Nonadecane	65.1

[a]*Peak # corresponds to the peak numbers shown in the chromatogram of Figure 17.*

4.4.4. Average 46/44 Ratio for NO_2 Corrections

The 46 m/z ratios to the 44 m/z for the standard compounds (15-69 ng C injection) are shown in Figure 18. The significant difference observed between non-nitrocompounds and nitrocompounds is due to the impact of NO_2 on the 46 m/z traces. This impact affects the Craig's ^{17}O correction (Allison et al., 1993), which is the correction made on the 45/44 ratio for $^{12}C^{16}O^{17}O$ based on the measured 46/44 ratio, the majority of which is from $^{12}C^{16}O^{18}O$. Thus, use of the 46/44 ratios obtained from the nitrogen-containing compounds was avoided. Instead, the average 46/44 ratios from the measurements of nitrogen-free compounds ($3.9967\times10^{-3}\pm1.4898 \times 10^{-6}$ in the VPDB scale) was used to perform the Craig's corrections for the nitrogen-containing compounds.

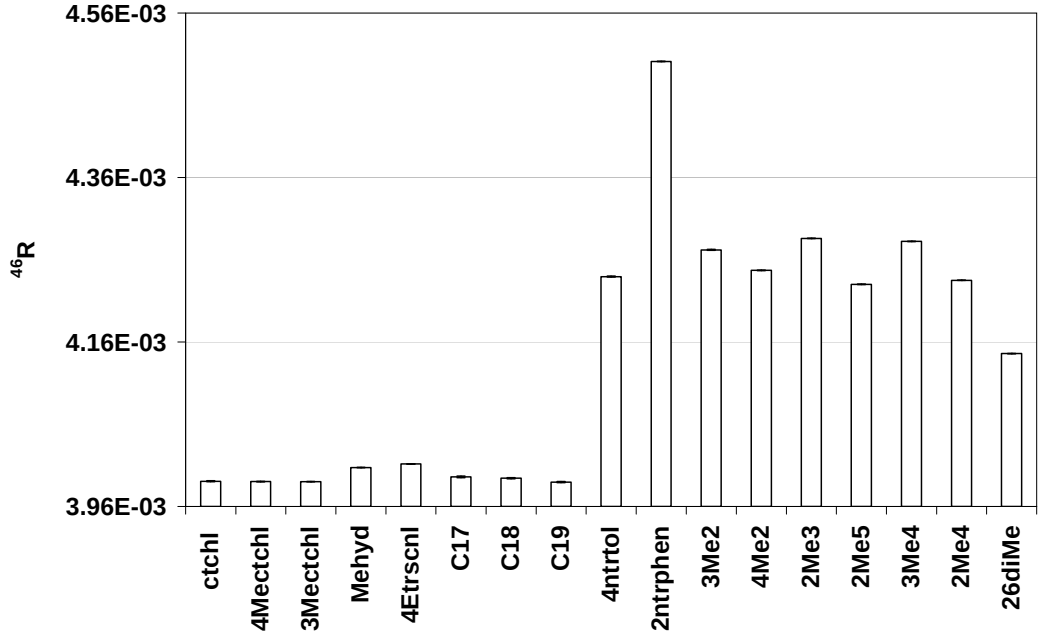

Figure 18. 46 m/z to 44 m/z Ratio of Standard Compounds (15-92 ng C).
The 46/44 ratios are in the VPDB scale. All results were for TMS derivatives, except the C_{17}-C_{19} n-alkanes. See the list of abbreviations for the identification of standard compounds.

4.4.5. $\delta^{13}C$ of the Trimethylsilyl (TMS) Group

The determined reference $\delta^{13}C$ values for the standard compounds were shown in Table 11. Using these reference $\delta^{13}C$ values, the $\delta^{13}C_{TMS}$ was determined by analyzing the derivatives of the standard mixture with high concentration (20-92 ngC μl^{-1}) by the GC-C-IRMS.

The $\delta^{13}C_{TMS}$ determined from individual standard compound is shown in Figure 19. Overall, the average value (±standard error) of (-50.03±0.24)‰ was obtained for the $\delta^{13}C_{TMS}$. It should be noted that the results from 3-methylcatechol and 2-nitrophenol were excluded from determination of the average $\delta^{13}C_{TMS}$ since the baseline separation was not achieved between these compounds. The average $\delta^{13}C_{TMS}$ was taken as the fixed reference $\delta^{13}C_{TMS}$, which was used in Equation 13 with measured $\delta^{13}C$ value for individual TMS derivative in order to obtain TMS-free $\delta^{13}C$ of the original compound.

Table 11 Reference $\delta^{13}C$ Values of Standard Compounds Determined by Offline Method

Specie name	Abbreviation	n	$\delta^{13}C_{VPDB}$ (±SD) (‰)
4-nitrotoluene	4ntrtol	3	-27.26±0.05
catechol (IS1)	ctchl	3	-27.79±0.10
4-methylcatechol	4Mectchl	3	-24.44±0.02
3-methylcatechol	3Mectchl	3	-24.12±0.00
2-nitrophenol (IS2)	2ntrphen	3	-27.73±0.01
3-methyl-2-nitrophenol	3Me2	3	-27.53±0.02
Methylhydroquinone	Mehyd	7	-26.63±0.08
4-ethylresorcinol (IS3)	4Etrscnl	4	-26.77±0.04
4-methyl-2-nitrophenol	4Me2	3	-26.90±0.01
2-methyl-3-nitrophenol	2Me3	3	-26.66±0.01
2-methyl-5-nitrophenol	2Me5	3	-27.20±0.02
3-methyl-4-nitrophenol	3Me4	3	-25.68±0.02
2-methyl-4-nitrophenol	2Me4	3	-27.41±0.04
Haptadecane	C17	3	-29.12±0.03
2,6-dimethyl-4-nitrophenol (IS4)	26diMe	6	-28.99±0.21
Octadecane	C18	3	-28.57±0.04
Nonadecane	C19	3	-35.13±0.01

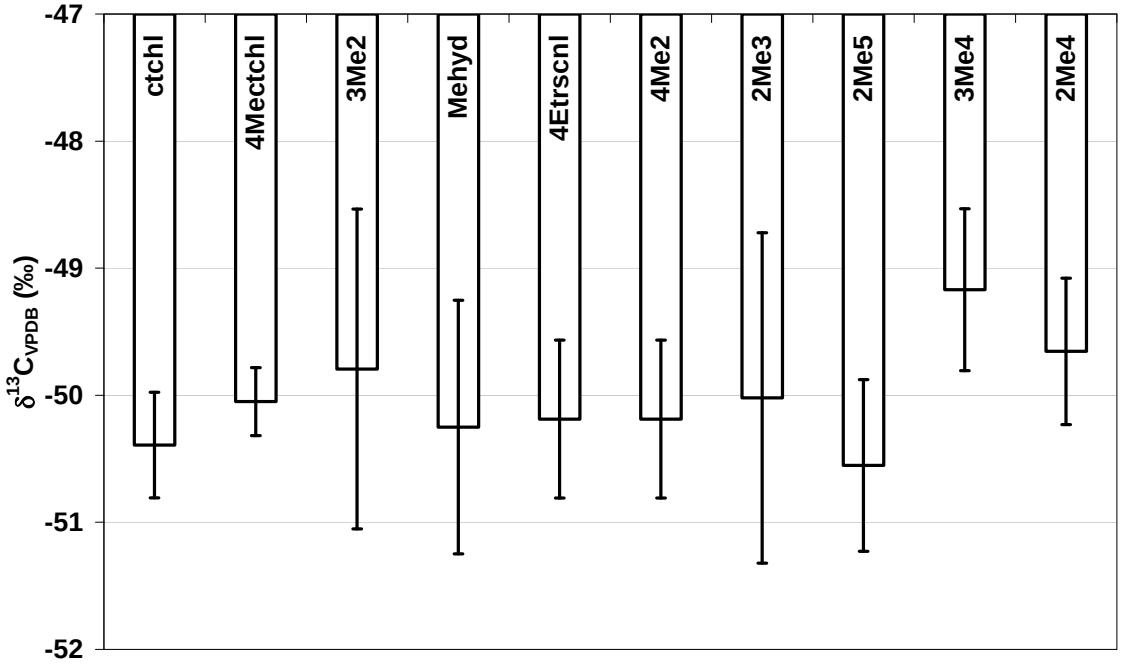

Figure 19. Average $\delta^{13}C$ values of the Trimethylsilyl (TMS) Group of BSTFA Determined from Analysis of Standard Mixture (20-92 ngC μl^{-1}).
Each bar is the average ± standard error value over 9 measurements.

4.4.6. Calibration

An example plot of quantitative calibrations (an internal standard method) made by GC-C-IRMS is shown in Figure 20 (top). The calibrations for all targeted compounds gave r^2>0.98 for the range 2-100 ng C. An example plot of $\delta^{13}C$ values as a function peak area count (i.e. linearity of the isotope measurement) is shown in Figure 20 (bottom). The linearity shown is according to the optimal peak integration found by evaluating peak integration, which is in the similar way to Ricci et al. (1994). According to the linearity plot for 2-methyl-4-nitrophenol, for example, the observed difference between the

measured and the reference $\delta^{13}C$ values was less than ±1‰ for carbon masses as low as 10 ng C.

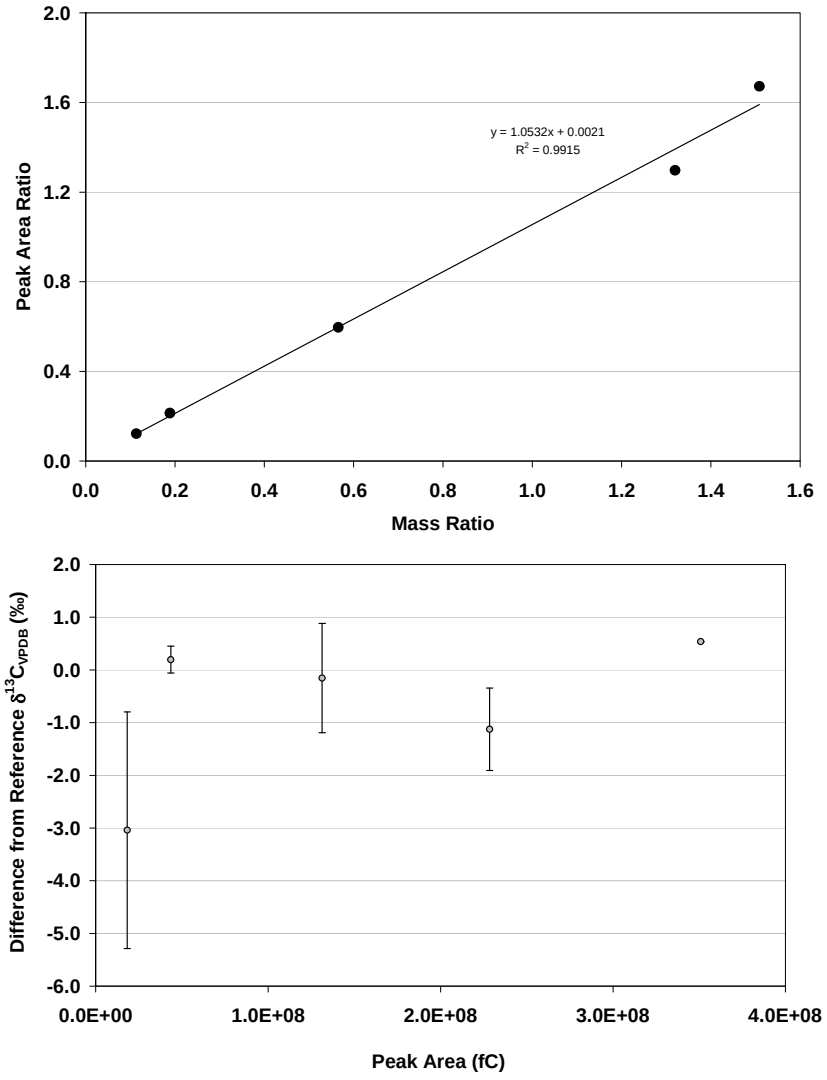

Figure 20. Plot of Quantitative Internal Standard Calibration (top) and of Difference of $\delta^{13}C$ Values Measured from the Reference $\delta^{13}C$ Value (bottom) for 2-methyl-4-nitrophenol.
2,6-dimethyl-4-nitrophenol was used as the internal standard for this calibration.

4.4.7. Measurements of Filter Blank

The analysis of PTFE blank filters demonstrated that there were some contaminants that possibly overlapped with the internal standards (Figure 21): the retention time for contaminant peak 1, at 46.9 min, was close to that of 4-ethylresorcinol (IS3), at 47.2 min; and the retention time of contaminant peak 2, at 58.6 min, was close to that of 2,6-dimethyl-4-nitrophenol, at 59.0 min. Their concentration levels vary sample by sample, depending on how much the extracts were concentrated.

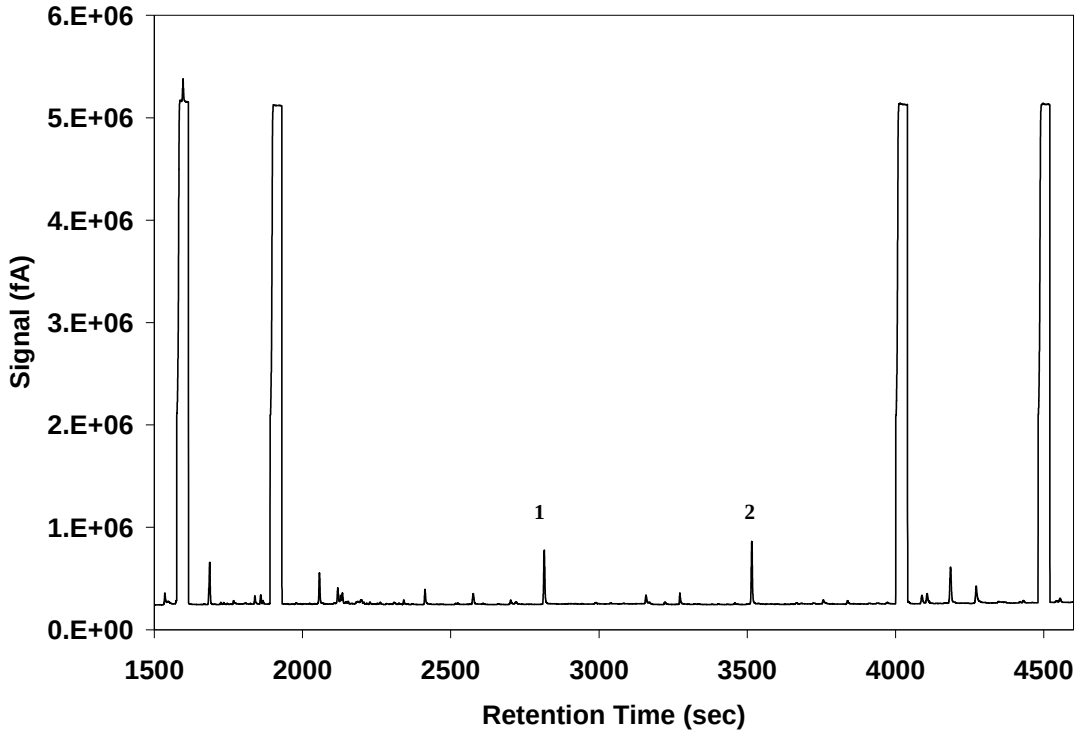

Figure 21. 44 m/z Chromatogram Obtained from Analysis of Blank PTFE Filter Extract.
Contaminant peak 1, 46.9 min, with a signal intensity of 0.75 nA; and contaminant peak 2, 58.6 min, with a signal intensity of 0.84 nA.

4.4.8. Standard Spike Test

The recovery yields and the $\delta^{13}C$ values determined from the analysis of the 14 compounds spiked on filters are shown in Appendix A. On average, the recovery yields were (97±10)%. The average difference (±standard deviation) in $\delta^{13}C$ between the measured and the reference values (i.e., accuracy of the isotope measurements) was (0.76±0.59)‰.

4.4.9. Product Identification

The reference mass spectra (Appendix B) and the retention times (Table 10) obtained from the analyses of the standard compounds derivatized were used for product identification. Figure 22 shows an example of a total ion chromatogram obtained from the analysis of the secondary POM extract by the GC-MS. In total, eight product peaks were detected in the extracts. The mass spectra for unknown products detected in the POM extracts are shown in Appendix C.

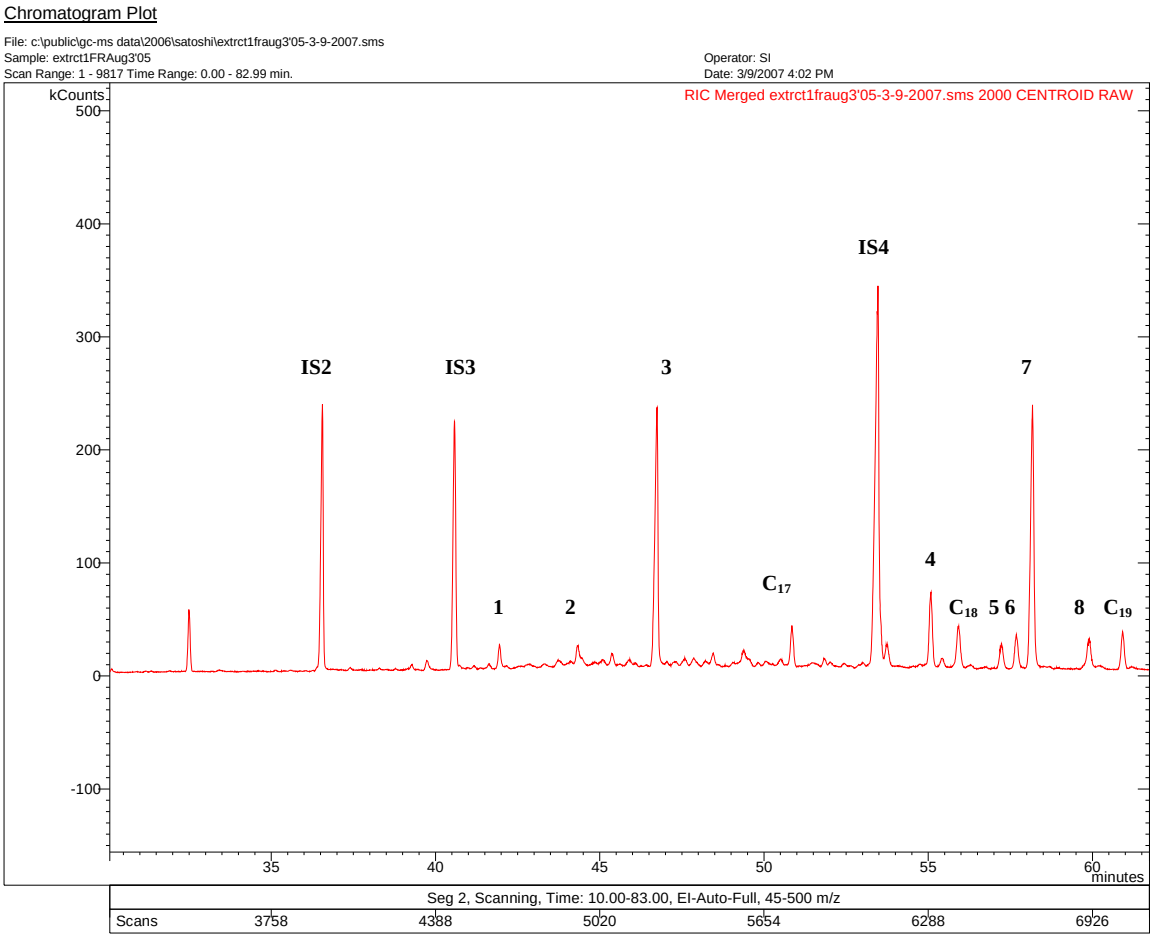

Figure 22. Total Ion Chromatogram Obtained from the Analysis of Secondary POM Extract by GC-MS.

The analysis was made by derivatization with BSTFA. IS2, IS3, and IS4 are the internal standards 2-nitrophenol, 4-ethylresorcinol, and 2,6-dimethyl-4-nitrophenol, respectively. C_{17}, C_{18}, and C_{19} are the internal standards heptadecane, octadecane, and nonadecane, respectively.

4.4.10. Yields and $\delta^{13}C$ Values for Specific Products

$\delta^{13}C$ values for product peaks were determined using Equation (13). For the identified products that the standard mixtures did not contain (the product peak 1, and 4 to 8), the calibrations from the similar standard compounds were used to determine the mass in the extract. The results of quantitative and isotope analyses for secondary POM from the flow reactor experiments (the front filters from the FR 1 – FR 5 experiments) are summarized in Table 12. It should be noted that for the extract of FR 1 there is implication of a problem in spiking the internal standards: the measured concentrations of internal standards in the extract were significantly lower than their concentrations expected, which were approximated based on the amount of internal standards spiked and the volume of extract roughly measured by pipetting. It should also be noted that for the smog chamber samples, most of these peaks were not observed due to their low concentrations (below the detection limit of 3 ng C), except 2-methyl-4-nitrophenol in the extract from the SC II experiment. The yield and the isotope ratio of the 2-methyl-4-nitrophenol determined by a single measurement were 0.042% and -29.26‰, respectively.

Table 12 Summary of Carbon Yields[a] and $\delta^{13}C$ Values for Compound Specific Products

	Product peak 1 (4-nitrophenol)		Product peak 2 (3-methyl-4-nitrophenol)	
	Y_{spec}[b] ±SD (%)	$\delta^{13}C_{spec}$±SD (‰)	Y_{spec}[b] ±SD (%)	$\delta^{13}C_{spec}$±SD (‰)
FR 1	0.148±0.004	-26.68±0.68	0.039±0.001	-36.48±1.83
FR 2	0.170±0.004	-27.79±1.20	0.083±0.002	-33.98±0.21
FR 3	0.133±0.008	-25.09±1.51	0.077±0.006	-31.99±2.72
FR 4	0.019±0.001	-26.43±0.33	N/A[c]	N/A[c]
FR 5	N/A[c]	N/A[c]	N/A[c]	N/A[c]

[a]*The values shown are average values where the uncertainty was determined by the SD from replicate measurements (n=3, 3, 3, 2, and 2 for FR1 to FR5, respectively), and the fraction of toluene consumed was 17%, 27%, 21%, 10%, and 9% for FR1 to FR5, and38%, 70%, and 71% for SCI to SCIII, respectively.* [b]*The values are relative to the reacted toluene carbon.* [c]*No data available due to the saturated peaks in the 45 m/z trace or due to the low concentration in the extract.*

Table 12 Continued.

	Product peak 3 (2-methyl-4-nitrophenol)		Product peak 4 (methylnitrocatechol isomer 1)	
	Y_{spec}[b] ±SD (%)	$\delta^{13}C_{spec}$±SD (‰)	Y_{spec}[b]±SD (%)	$\delta^{13}C_{spec}$±SD (‰)
FR1	3.225±0.015	-32.57±0.25	0.159±0.005	-32.15±0.26
FR2	2.685±0.021	-30.50±0.27	0.110±0.003	-31.61±0.56
FR3	3.198[d]	N/A[c]	0.065±0.002	-30.91±0.55
FR4	0.302±0.011	-33.07±0.70	0.015±0.000	-32.85±0.01
FR5	0.256±0.005	-29.81±0.37	0.015±0.000	-32.43±0.95

Table 12 Continued

	Product peak 6 (methylnitrocatechol isomer 2)		Product peak 7 (methylnitrocatechol isomer 3)	
	Y_{spec}[b]±SD (%)	$\delta^{13}C_{spec}$±SD (‰)	Y_{spec}[b]±SD (%)	$\delta^{13}C_{spec}$±SD (‰)
FR1	0.079±0.002	-33.72±0.64	0.643±0.014	-32.52±0.52
FR2	0.058±0.002	-32.41±0.55	0.477±0.013	-33.98[d]
FR3	0.041±0.001	-35.37±0.86	0.280±0.010	-32.89±0.27
FR4	N/A[c]	N/A[c]	0.061±0.001	-32.73±0.52
FR5	N/A[c]	N/A[c]	0.064±0.000	-33.93±0.26

Table 12 Continued

	Product peak 8 (nitrocatechol isomer)	
	Y_{spec}[b]±SD (%)	$\delta^{13}C_{spec}$±SD (‰)
FR1	0.083±0.003	-30.39±1.02
FR2	0.051±0.001	-30.72±0.60
FR3	0.034±0.001	-32.13±0.63
FR4	0.022±0.001	-33.11±1.16
FR5	0.024±0.000	-32.44±0.60

5. Discussion

5.1. Analysis of Bulk Samples

5.1.1. Validation of Methodology

The analysis of blank filters with non-baked or pre-baked copper oxide shows that the blank values are on average (1.1±0.1) μmol C and (0.2±0.1) μmol C, respectively. The lower blank values with use of the baked copper oxide suggest that impurities in the commercially available copper oxide are likely the major source of carbon. The stated level of purity for copper oxide provided by the supplier was 99.9999%, which corresponds to 100 μg of impurities for every 1 g of the copper oxide. Compared to the average blank value of 1 μmol C with a use of non-baked the copper oxide, the expected carbon content of the impurity is ~10%. The blank $\delta^{13}C$ values from uses of both baked copper oxide and non-baked copper oxide were both -22 ‰ (Table 3). This same $\delta^{13}C$ value implies that the blank carbon left after baking the copper oxide is the residue of the blank carbon in the copper oxide (i.e. no fractionation after the oxidation at the high temperature) or that the carbon from another source having the exact same $\delta^{13}C$, such as carbonate in the quartz tube or the quartz filter.

The measurements of the three reference materials demonstrate that oxidation at both 853 K and 1173 K are adequate for the sucrose standards, while only the higher temperature oxidation at 1173 K is sufficient for the elemental carbon (Table 4). The recovery yields of the laboratory sucrose standard and the IAEA-CH-6 sucrose show that

the oxidation at 853 K resulted in slightly lower yields than the oxidation at 1173 K. Evidence of incomplete oxidation, such as gray spots on filters baked at 853 K, was observed. Nevertheless, the results of the $\delta^{13}C$ measurements show no significant difference between the oxidation at 853 K and 1173 K. For the USGS 24 (soot) standard the recovery yields at 853 K was very poor (<24%), while that at 1173 K was higher than 70%.

The measured $\delta^{13}C$ values for these reference materials vary over a wide range, and these values do not always agree with the $\delta^{13}C$ values recommended for these reference materials by IAEA. The values, however, systematically depend on the inverse carbon mass, as demonstrated by a Keeling plot (Figure 14). The very good linear dependency, with different slopes for the different preparation methods, suggests that the variation of $\delta^{13}C$ values was not due to the incomplete oxidation. Rather, the variation was because CO_2 from the reference materials was mixed with a constant quantity and $\delta^{13}C$ of another carbon source: the blank carbon. The method with 1 g of the pre-baked copper oxide proves that indeed the slope becomes closer to zero compared to the method with 1 g of non-baked copper oxide. This improvement is critical as only one or two samples with small amount of carbon are available, such as the samples from the smog chamber experiments. A mass balance is the only way to correct for the blank value for such a set of samples. Regardless of the blank impact, the results demonstrate intercepts of linear regression lines from the three preparation methods statistically point to the same intercept, reflecting the $\delta^{13}C$ values of blank-free sample carbon; (-10.3±0.2)‰, (-10.4±0.4)‰, and (-10.25±0.08)‰ for the 1173 K oxidation with non-baked copper oxide,

the 853 K oxidation with non-baked copper oxide, and the 1173 K oxidation with pre-baked copper oxide, respectively. These values are in good agreement with the reference value of (-10.449±0.033)‰, thus for the samples analyzed here a Keeling plot is a valid methods to determine a blank impact-free $\delta^{13}C$ value when multiple samples for the same conditions with different masses of carbon are available.

5.1.2. Isotope Fractionation Associated with Evaporation and Adsorption

The results of $\delta^{13}C$ measurements for evaporated toluene show the lighter isotope composition of bulk toluene than that of evaporated toluene by (0.33±0.02)‰ (Table 5). This small inverse evaporative carbon isotope fractionation for toluene agrees with observations by Harrington et al. (1999). To date, normal fractionation at evaporation (faster evaporation of light isotopomers than heavy isotopomers) has been found for oxygen isotopes in water (Hoefs, 1980) and in carbon dioxide (Grootes et al., 1969) as well as for hydrogen isotopes in methanol and ethanol (Wang and Huang, 2003). Inverse fractionation at evaporation (i.e. slower evaporation of light isotopomers than heavy isotopomers) has also been reported for hydrogen and/or carbon isotopes in aromatic compounds (Harrington et al., 1999; Wang and Huang, 2003), in n-alkanes and methyl-tert-butyl (Wang and Huang, 2003), in chlorinated hydrocarbons (Huang et al. 1999) and in carbon dioxide (Grootes et al., 1969). Although it has been suggested that the different type of isotope fractionation were due to different types of intermolecular forces (the normal fractionation is thought to be due to van der Waals force, while the inverse is thought to occur when hydrogen bonding dominates), the theory still cannot explain all

the evaporative isotope fractionations observed. The process of evaporative isotope fractionation seems complex and current theoretical understanding of isotope fractionation and the results here are insufficient to explain these phenomena.

The analysis of the backup filters show evidence that some organic carbon is collected on the backup filters (Table 7). The combustion of seven back-up filters from series A of the flow reactor experiments (FR A) combined into one sample gave 12.0 μmol CO_2 in total with the $\delta^{13}C$ value of -28.2‰. The measurement results for individual back-up filters from the series B to D of the flow reactor experiments (FR B-D) show that, in spite of the considerable variability of the carbon mass and the $\delta^{13}C$ values, the mass was on average (1.7±0.2) μmol C in excess of the blank value from the use of non-baked copper oxide. Obviously, this difference is statistically significant. Similarly, there is highly significant difference in $\delta^{13}C$ between the backup filter and the blank value by (-4.6±0.6)‰, which corresponds to the blank corrected $\delta^{13}C$ value of (-30.3±0.8)‰ for the backup filter on average. The analysis of the back-up filters from the smog chamber experiments also shows the similar results: on average 1.4±0.6 μmol C in excess of the blank carbon and its blank corrected $\delta^{13}C$ value of (-28.9±1.0)‰ (Table 8). In overall, it was consistently observed that there were always some additional carbons on the backup filters, and their $\delta^{13}C$ values were significantly lighter than the $\delta^{13}C$ values of toluene, suggesting that the additional carbon was at least partly due to the oxidation products. The blank corrected $\delta^{13}C$ values for the additional carbons on the backup filters were also consistently larger by (5.2±0.9)‰ on average, suggesting that the additional carbon on the backup filters was not due to penetration of particulate carbons from the front filters

since penetration of particulate carbons through the front filter was expected to result in the same $\delta^{13}C$ values between these filters.

For the back-up filters from the flow reactor experiments, linear regression analysis was performed between carbon mass (or $\delta^{13}C$) of the back-up filter and the total carbon mass of all oxidation products (all products in the gas-phase and the particulate phase) in the air volume sampled, which was determined by the concentration of toluene reacted times the sampling volume (Table 13). The analysis shows some evidence of systematic dependencies: Larger loading, more additional carbon and lighter $\delta^{13}C$ value. Moreover, the intercepts derived from the linear regressions are not identical to the blank values. These are likely indications of loading-dependent process of the oxidation products occurring at the back-up filter. However, the values are very small.

The evaporation tests with the POM samples show some evidence of evaporation loss: the formation rate of POM carbon was lowered by 1.3±0.4 μmol C h^{-1} after pumping the clean air through the filter samples for 24 h at the flow rate of 6.3 L min^{-1}, which is the same rate as that for filter sampling from the flow reactor experiments (Table 9). This difference is small, but statistically significant. The difference of 1.3±0.4 μmol C h^{-1} corresponds to (12±4)% carbon relative to the average of the non-evaporated front filter samples, meaning that (12±4)% was lost by pumping the clean air through the samples. The isotope measurements show the results that on average the $\delta^{13}C$ value of the evaporated front filter is higher than that of the non-evaporated front filter by (0.3±0.2)‰. The difference is almost insignificant. The small evaporation loss from the front filter samples did not cause significant change in $\delta^{13}C$.

Table 13 Dependence between Carbon Mass of Oxidation Products Loaded and Carbon Mass or Stable Carbon Isotope Ratio of Back-up Filter

Experiment[a]	Carbon Mass Slope[b]	Carbon Mass Intercept (μmol C)	$\delta^{13}C$ Slope[c] (‰ μmol C^{-1})	$\delta^{13}C$ Intercept (‰)
FR B	$(1.2\pm0.8)\times10^{-4}$	1.2±0.7	$(-1.5\pm0.4)\times10^{-4}$	-25.4±0.4
FR C	$(9.0\pm2.3)\times10^{-5}$	2.5±0.2	$(-1.1\pm0.2)\times10^{-4}$	-26.7±0.2
FR D	$(1.0\pm2.0)\times10^{-4}$	2.2±0.9	$(-2.3\pm0.9)\times10^{-4}$	-25.9±0.4

All raw values used in this linear regression analysis are non-blank corrected values.
[a]The extents of toluene consumption for FR B – FR D are (7±1)%, (20±2)%, (29±2)%, respectively. ***[b]****Carbon moles of the back-up filter divided by mol C of toluene reacted.*
[c]*The $\delta^{13}C$ value of the back-up filter divided by mol of C for the toluene reacted.*

The results of the back-up filter analysis for the evaporation tests (Table 9) show that the formation rate of the blank-corrected carbon mass and $\delta^{13}C$ value are on average (1.1±0.4) μmol C h^{-1} and (-27.4±0.9)‰ for the non-evaporated backup filters (EVAP A-C) as well as (0.9±0.2) μmol C h^{-1} and (-26.9±1.4)‰ for the evaporated backup filters (EVAP E-F), respectively. Comparison between the evaporated and non-evaporated backup filters indicates that there is no difference in the additional carbon mass on the backup filters. In the previous discussion, it is evident for EVAP D-F that the 12% of carbon was lost from the front filters by evaporation, therefore, the results here indicates that the process occurring at the backup filters is not just accumulation of some products. It is well known that semi-volatile compounds adsorb/desorb on filter media (McDow, 1999), therefore, no further additional carbon observed at the evaporated backup filters is explained by that the adsorption/evaporation processes occurring at the used back-up filter was in the steady-state. There are two possible explanations for the additional

carbons with heavy isotope composition on the backup filters: (1) the compounds that were inverse isotope fractionated when evaporated from the front filters were adsorbed on the backup filters, or (2) the some gas-phase products having heavier isotope composition than that of the POM were selectively collected on the backup filters. Confirmation of the case (2) will possibly be done by compound-specific $\delta^{13}C$ analysis for products found in the back-up filter extracts and in the gas-phase, however, the measurements will be very due to small sample size on the backup filters.

5.1.3. $\delta^{13}C$ and Yield of POM

The analysis of the filter samples show that the $\delta^{13}C$ values of the formed POM was significantly smaller than the initial $\delta^{13}C$ of the toluene precursor (Table 6). The range of the differences was from (-2.78±0.07)‰ to (-6.18±0.09)‰, depending on the fraction of toluene consumed. The $\delta^{13}C$ values for the secondary POM carbon was compared with the predicted $\delta^{13}C$ values for toluene and the sum of all the products calculated using Equations 5 (Figure 23). The initial $\delta^{13}C$ value for toluene of (-26.72±0.01)‰, and ${}^{OH}\varepsilon_{C7H8}$ of (5.95±0.28)‰ (Anderson et al., 2004) were used for the calculation as a function of the fraction of toluene consumed. It was found that, regardless of seeded or non-seeded experiments, the observed $\delta^{13}C$ values of the secondary POM formed from the flow reactor and the smog chamber were almost identical to the $\delta^{13}C$ curve predicted for the sum of all the products. That is, there is seemingly no further carbon KIE after the first reaction step, implying that the initial

reaction step is possibly the rate-determining step in the sequence of reactions leading to the formation of POM carbon. Anderson (2004) points out that the OH-addition to the aromatic ring is responsible for the $^{OH}\varepsilon_{C7H8}$ of (5.95±0.28)‰, therefore, the agreement between here imply that the OH-addition channel is responsible for the production of secondary POM under our experimental condition.

The dominance of the KIE at the initial step in the sequence of reactions leading to the POM formation is somewhat surprising since it is expected that complex and numbers of reactions that possibly have significant KIEs are likely involved in the formation of condensable products. For example, ring-opening products, such as methylglyoxal and maleic anhydride, have been often found in the POM produced by the toluene+OH reaction (Forstner et al., 1997; Jang and Kamens, 2001; Sato et al., 2007) and by xylene+OH reaction during the YorkU flow reactor experiments (Bennet, J., personal communication) as well as in the gas-phase by the toluene+OH reaction during the YorkU smog chamber experiments (Auld, J., personal communication). Therefore, it is not too speculative to expect that ring-opening products exist in the POM analyzed here. There are numerous studies reporting that a large number of complex reaction steps are involved in the formation of ring-opening products, including the cleavage of aromatic ring C-C bonds (Shepson et al., 1984; Tuazon et al., 1984; Bandow et al., 1985; Grey et al., 1985; Bierbach et al., 1994). It is expected that the reaction step of bond cleavage of aromatic ring has a significant carbon KIE. Nevertheless, the observation that only the KIE at the initial reaction step is predominant in the overall KIEs seemingly indicates that the first step is the rate-determining step. There are three possibilities that

can explain the unexpected results under our experimental condition: (1) only the first reaction step has substantial KIE and subsequent reactions of the intermediate(s) of condensable products does not have significant KIEs; (2) if there were significant KIEs on subsequent reactions of the intermediate(s), these reactions are already completed under our experimental condition and the secondary POM is a part of the end products (Rudolph, 2007), (3) isotopic compositions of specific products in the POM, which are produced via different reaction mechanisms, cancel out each other. These possibilities can be confirmed by compound specific analysis. In any case, the findings here demonstrate that the KIE at the initial reaction determines the $\delta^{13}C$ of POM carbon, regardless of the level of the initial toluene concentration (from 0.5 ppm to 40 ppm), the toluene/NO_x ratio (from 0.25 to 8), or the type of formation (i.e. with or without seed particles).

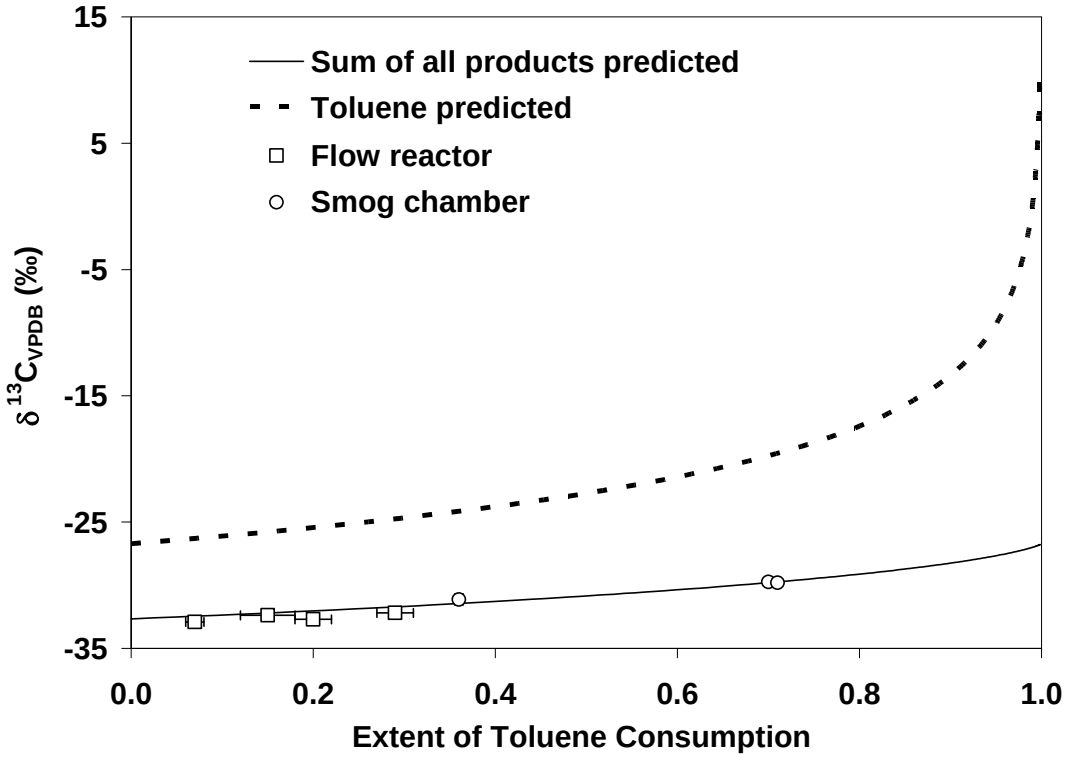

Figure 23. Plot of $\delta^{13}C$ for Secondary POM Formed by OH Radical Induced Reactions of Toluene as Function of Fraction of Toluene Consumed.
The POM from the flow reactor experiments (square) and from the smog chamber experiments (circle) are shown. As comparison, predicted $\delta^{13}C$ for toluene (dotted curve) and for the sum of all products (solid curve) are shown. The initial $\delta^{13}C$ of (-26.72±0.01)‰ for toluene and the KIE of (5.95±0.28)‰ (Anderson et al., 2004) were used for this calculation.

The good agreement of the $\delta^{13}C$ values between the observed $\delta^{13}C$ for the POM and the predicted $\delta^{13}C$ for the sum of all products over the wide range of fraction of toluene consumed implies that by-products from the photolysis-initiated reactions of IPN, acetone, did not likely contribute significantly to formation of POM carbon since contribution of different reactant that has a different KIE would cause a different $\delta^{13}C$ profile. If so, a combination of the following two possibilities must occur in order to

result in the same fractionation: (1) the laboratory-made IPN with isopropyl alcohol from several different batches had the same $\delta^{13}C$ value by coincidence every time, and (2) the over all KIEs leading to the formation of condensable by-products from IPN must be identical to the KIE for the toluene+OH reaction.

A simple mass balance, shown as Equation 4, allows for the estimation of $\delta^{13}C$ values for the products remaining in the gas-phase when the $\delta^{13}C$ values and concentration for the secondary POM and the sum of all products are known. The results of the calculations are shown in Table 14. The difference between $\delta^{13}C$ for POM and the calculated $\delta^{13}C$ for the sum of all gas-phase products is very small.

Table 14 Summary of $\delta^{13}C$ Measurements of Secondary POM and Predicted $\delta^{13}C$ Values for the Sum of All Products and for the Sum of All Gas-phase Products

Experiment	Toluene Reacted (%)	$\delta^{13}C$ POM (‰)	$\delta^{13}C$ All Prod. (‰)	$\delta^{13}C$ Gas Prod. (‰)
FR A	15±3	-32.37±0.08	-32.0±0.3	-32.0±0.3
FR B	7±1	-32.90±0.09	-32.3±0.3	-32.3±0.3
FR C	20±2	-32.57±0.20	-31.9±0.3	-31.8±0.3
FR D	29±2	-32.19±0.04	-31.5±0.2	-31.5±0.2
SC I	36±7	-31.50±0.30	-31.6±0.2	-31.6±0.3
SC II	70±7	-29.83±0.07	-30.0±0.2	-30.1±0.2
SC III	71±7	-29.86±0.05	-30.0±0.1	-30.0±0.2

The initial $\delta^{13}C$ of toluene used in the calculations were (-26.72±0.01)‰ and (-27.05±0.02)‰ for the flow reactor samples (FR) and the smog chamber samples (SC), respectively.

The POM carbon yields (Y_C) from the analysis of the filter samples are summarized in Table 15. For the flow reactor samples, the Y_C values from the flow reactor experiments were calculated by dividing the POM carbon formation rate (Table 6) by the rate of toluene carbon reacted (i.e. the flow rate of the toluene carbon mass before the UV on times the fraction of toluene reacted during the experiment). The Yc values for the smog chamber samples were determined by dividing the measured carbon mass of the filter samples (Table 8), C_{POM}, by the carbon mass of toluene reacted in the air volume sampled ($^{sampled}\Delta C_{C7H8}$). Determination of $^{sampled}\Delta C_{C7H8}$ requires a several step calculation. First of all, based on the mass concentration measurements of toluene by GC, the total mass of residual toluene in the air volume sampled (^{sampled} M_{C7H8}) was estimated by a calculation likewise Equation 14, for POM mass loaded on filter;

$$^{sampled}M_{C7H8} = \sum_{n=1}\left[M_{C7H8}\right]^n \times \Delta V^n \quad \text{or} \quad ^{sampled}M_{C7H8} = n\Delta V\sum_{n=1}\left[M_{C7H8}\right]^n \qquad (5)$$

where n is the number of mass concentration measurements for toluene since the filter sampling started, $[M_{C7H8}]^n$ is the average mass concentration of toluene between *n*th and (*n+1*)th toluene measurements, and ΔV^n is the air volume sampled for the same interval between the *n*th and the (*n+1*)th measurements. Note that $\Sigma\Delta V^n = n\Delta V$ when the flow rate for the sampling is constant. Using the estimated ^{sampled} $M_{C7H8,}$ the carbon mass of residual toluene in the air volume sampled ($^{sampled}C_{C7H8}$) is then calculated as follows:

$$^{sampled}C_{C7H8} = {}^{sampled}M_{C7H8} \times \frac{7\times 12}{MW_{C7H8}} \qquad (6)$$

where 7 is the carbon number of toluene molecule, 12 is the atomic mass of carbon, MW_{C7H8} is the molecular weight of toluene (92 g mol^{-1}), respectively. Therefore, the $^{sampled}\Delta C_{C7H8}$ can be expressed as follows:

$$^{sampled}\Delta C_{C7H8} = {}^{sampled}C_{C7H8} \times \frac{1-f}{f} \quad (7)$$

where f is the fraction of residual toluene at the end of the experiment. Finally, Y_C is determined by dividing C_{POM} by $^{sampled}\Delta C_{C7H8}$.

Table 15 Results of Yield of POM Carbon (Y_C) from Flow Reactor and Smog Chamber Experiment

Experiment	Toluene Processing (%)	POM C yield Y_C (%)
FR A	15±3	8±2
FR B	7±1	0.4±0.1
FR C	20±2	5±1
FR D	29±2	4±1
SC A	36±7	7.3±0.4
SC B	70±7	18±2
SC C	71±7	21±3

Errors shown are standard errors.

The Y_C data from Table 15 give interesting insight into formation mechanisms of the POM: instead of showing a constant value, which is expected from the results of $\delta^{13}C$ measurements presented earlier that the initial reaction step is the rate-determining step for the formation of POM carbon, the Y_C is proportional to the fraction of toluene

consumed (Figure 24). The increase indicates the products are the second or higher generation products. The obtained linear regression for this increase is:

$$Y_C(\%) = \frac{[C_{POM}]}{\Delta[C_{C7H8}]} \times 100 = (30.1 \pm 2.9) \cdot \frac{\Delta[C_{C7H8}]}{[{}^0C_{C7H8}]} - (2.5 \pm 1.3) \quad (8)$$

where $[{}^0C_{C7H8}]$ is the initial carbon concentration of toluene and $\Delta[C_{C7H8}]$ is the carbon concentration of toluene consumed (i.e. $[{}^0C_{C7H8}] - [C_{C7H8}]$). The r^2 of this regression is 0.963, highly correlated. The division of $\Delta[C_{C7H8}]$ by $[{}^0C_{C7H8}]$ is the same as 1-*f* where *f* is the fraction of residual toluene defined in Chapter 2.1. Note that the impact of wall loss on $\delta^{13}C$ values of the filter samples from the smog chamber is negligible according to its small wall-loss of POM mass observed (see the later discussion for the wall-loss for more detail), however, the wall-loss for the flow reactor samples has not been investigated. It should also be noted that for the linear regression shown in Figure 24 the point for the series FR A experiments (the point of 8% Y_C at 15% fraction of toluene consumed) has been excluded since the absolute concentration measurements for toluene have not been made (Irei et al., 2006). Due to the limited number of points available, we cannot exclude that the high correlation observed between the Yc and the fraction of toluene consumed may be by coincidence. As discussed shortly for the mass yield of POM, it is known that Y_m eventually levels off (i.e. becomes constant) after a certain point of toluene consumption due to the different regime of formation mechanisms (Hurley et al., 2001; Sato et al., 2004). Although such a turning point may also exists somewhere in the Y_C plot here, the high correlation based on the available data points indicates that, at least under our experimental condition, the formation mechanism in the flow reactor and the

smog chamber is in the regime of OH reaction suggested by Hurley et al. and Sato et al. In terms of magnitude of POM carbon yield, the results here are similar to the maximum Yc value of 4.9% at ~30% of toluene consumption by Izumi and Fukuyama (1990) as well as the Y_C of 5%-19% from o-cresol+OH studies by Grosjean (1984). The observed negative intercept of the linear regression indicates that formation of POM carbon requires some induction time for products to saturate in the gas-phase. Using Equation (19), the carbon concentration of POM ($[C_{POM}]$) can be expressed as follows:

$$[C_{POM}] = (30.1 \pm 2.9) \cdot \frac{\Delta[C_{C7H8}]^2}{[{}^0C_{C7H8}]} - (2.5 \pm 1.3) \cdot \Delta[C_{C7H8}] \qquad (9).$$

Equation (20) suggests that the concentration of POM carbon has a polynomial dependence on the $\Delta[C_{C7H8}]$ and the inverse of the $[{}^0C_{C7H8}]$. This seems somewhat strange since this contradicts to the partitioning theory: higher initial concentration of toluene results in higher product concentration in the gas-phase and the condensed phase. However, Hurley et al. (2001) and Sato et al. (2004) also found similar dependency based on mass concentration that the lower initial toluene concentration resulted in higher yield of POM formed.

An application of Equation (20) should be noted: under the assumption that the product yields obtained under the conditions of the laboratory experiments can be extrapolated to atmospheric studies, Equation (20) allows estimating $[C_{POM}]$ theoretically by making atmospheric measurements for toluene only. This application requires some other conditions that (a) no additional toluene is input into the air mass during the reaction, (b) toluene and the secondary POM formed are homogeneously mixed in the air

mass, and (c) wet/dry deposition of the secondary POM is negligible. These conditions are possibly met at some locations in remote area where toluene and its photochemical products are carried to by middle or long range transport. For example, Thompson et al. (2003) has demonstrated in a case study at Alert, Canada, that with use of Rayleigh type fractionation (i.e. Equation (3)) isotope measurements of VOCs provide the valuable information of reaction processing, such as $\Delta[C_{C7H8}]/[^{0}C_{C7H8}]$. Since conventional concentration measurements give $[C_{C7H8}]$, combination of concentration measurements with $\delta^{13}C$ measurements will provide theoretical $^{0}[C_{C7H8}]$ (the initial concentration of toluene with respect to the air volume where $[C_{C7H8}]$ is in at a receptor site). This makes an estimation of $\Delta[C_{C7H8}]$ possible, consequently allowing estimation for the $[C_{POM}]$ and the Y_C formed by toluene+OH reaction in the atmosphere by using Equation (19) and (20).

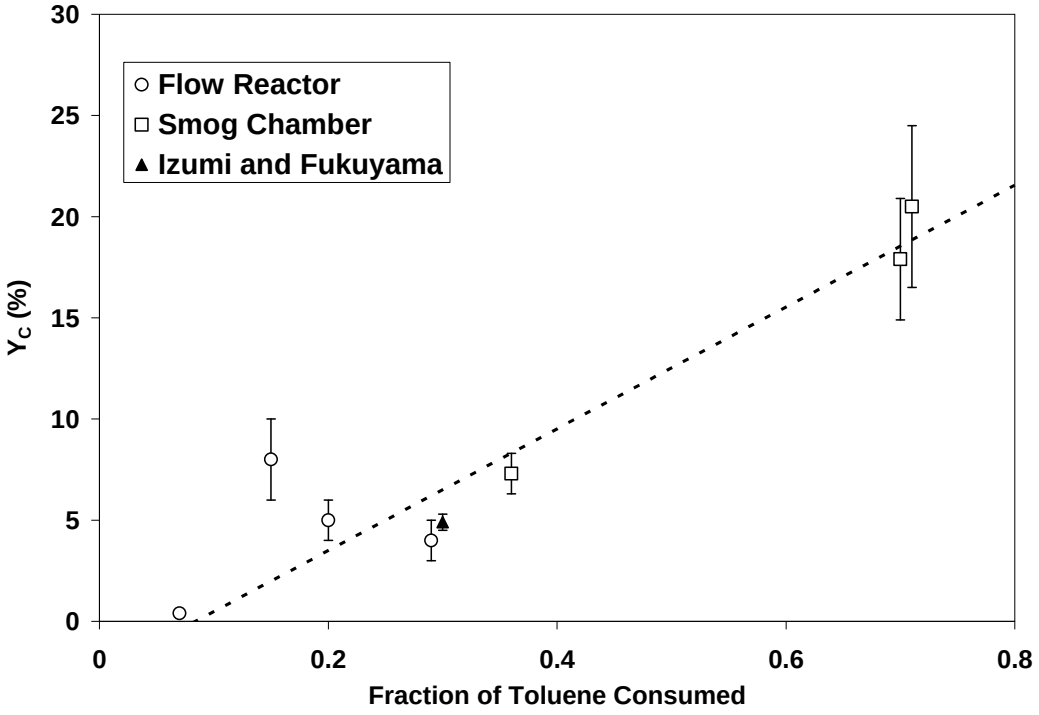

Figure 24. Yield of Observed Total POM Carbon (Y_C) as Function of Fraction of Toluene Consumed.
Square plot is for the flow reactor and circle plot for the smog chamber experiments The linear regression shown as a dotted line is the approximation for the observed Y_C: Y_C in % = (30.1±2.9) ·Δ[C_{C7H8}]/[$^0C_{C7H8}$] - (2.5±1.3), and r^2 = 0.963. See the text for the wall loss compensation and exclusion of the outlier for the linear approximation.

Plots of wall-loss corrected POM mass concentration (M_{POM}) and Y_m are shown in Figure 25. Compared to the other laboratory studies, the Y_m observed are unique: there is no time delay between the UV lights on and the detection of POM formation, and the toluene consumption is very fast (Figure 13). Furthermore, the 37%, 57%, and 55% of Y_m observed for SC I, SC II, and SC III are substantially higher than the Y_m values from other studies, which are typically ~10% or less (Gery et al., 1985; Izumi and Fukuyama, 1990; Odum et al., 1997; Johnson et al., 2004), even compared with the highest reported

value of ~20% in Takekawa et al. (2003) as well as with the previous results using the same YorkU smog chamber, yielding ~14% in Stroud et al. (2004). The major difference of the experimental condition between the YorkU chamber studies and the other studies is use of different chemical for the source of OH radicals: IPN for the YorkU experiments, and methylnitrite, propene, HONO, or hydrogen peroxide in the other studies. Therefore, it is possible that IPN may have caused such different results in the Y_m. Significantly different yields from the previous YorkU smog chamber studies by Stroud et al. may be explained by different quality of the lab-made IPN used. Johnson et al. (2004) point out that acetone, the by-product of IPN photolysis, may be responsible for the high yield of POM. As discussed earlier for the isotope ratio of the total POM, however, acetone likely did not contribute to the formation of particulate carbon. This implies that, for some reason, use of IPN may help components having small amount of carbon to contribute to the formation of PM. On the other hand of these unique results, the profiles in the plots of POM mass concentration formed ($[M_{POM}]$) as a function of toluene mass concentration reacted, $\Delta[M_{C7H8}]$ (Figure 25) are similar to those in the early stage of the POM formation observed by others (Izumi and Fukuyama, 1990; Odum et al., 1997; Hurley et al., 2001; Sato et al., 2004;), which have polynomial increases, again indicating the second generation product. Both the results from Hurley et al. (2001) and Sato et al. (2004) indicates that such a polynomial profile in the plot of $[M_{POM}]$ as a function of $\Delta[M_{C7H8}]$ changes to a linear profile when the reaction with ozone takes over the production, such a linear profile was not observed here. This is probably explained by quenching ozone with high concentration of NO.

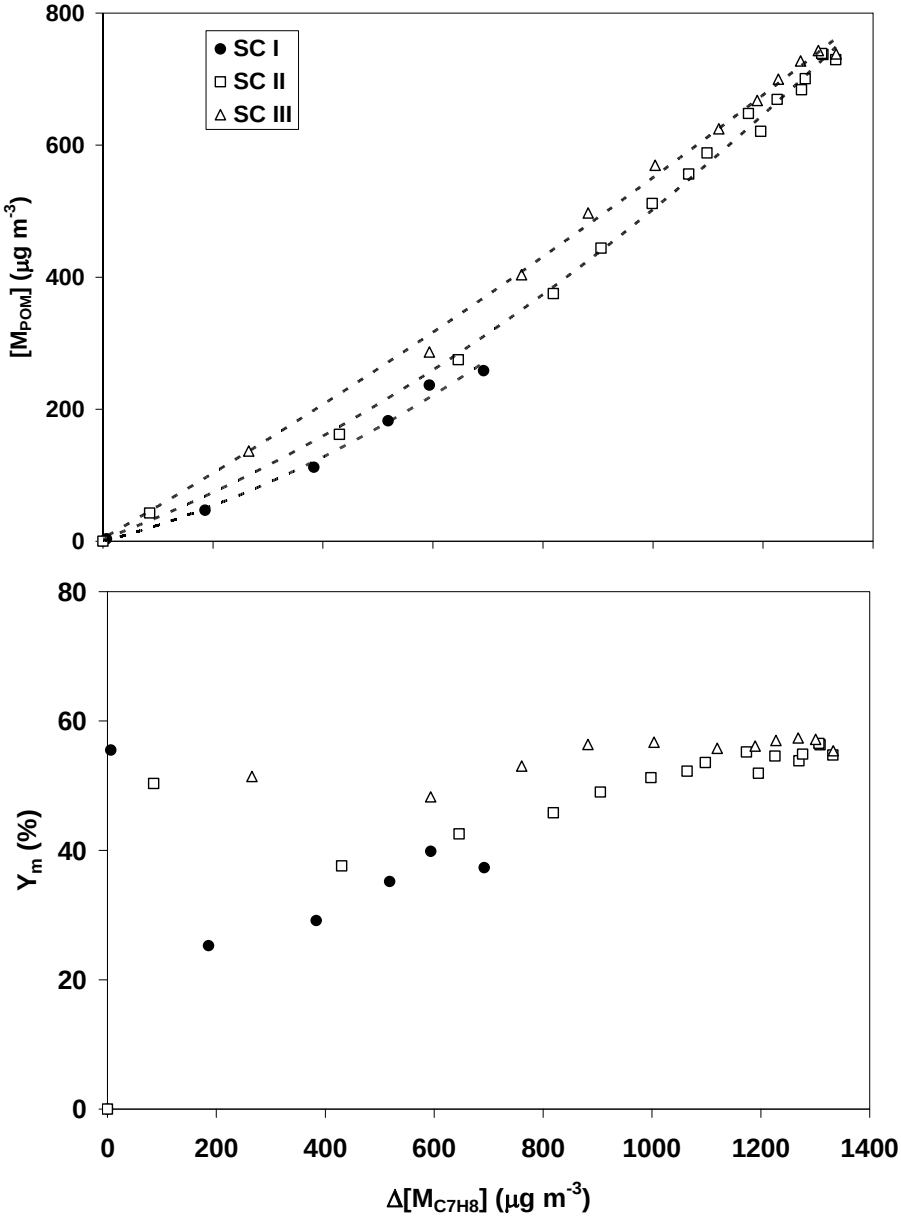

Figure 25. Plot of POM Mass Concentration Formed (top) and POM Mass Yield (bottom) as Function of Mass Concentration of Toluene Reacted during Smog Chamber Experiment.
Polynomial curve fits are shown in the plot of POM mass concentration.

A comparison between the POM mass loaded on the filter and POM carbon measured from the smog chamber experiments reveals the carbon content of the POM: (24.3±2.6)%, (24.9±0.8)%, and (31.0±0.6)% at 36%, 70%, and 71% fraction of toluene consumed, respectively. It should be noted that the calculated uncertainties for the carbon contents do not include the uncertainty for the size distribution measurements and hidden bias due to evaporation loss of semi-volatile compounds from the particulate phase. However, they include ±0.1 μmol measurement uncertainty of carbon measurement, which is smaller than 1% of the carbon yielded from these POM samples. According to the methodology tests conducted with IAEA-CH-6, the recovery yields obtained by the method with use of pre-baked copper oxide were better than 95% when the sample size was more than ~1 μmol C. Since the minimum amount of the POM carbon yielded from the smog chamber experiments is 3.8 μmol C, the impact of carbon loss during the CO_2 extraction should be small. Also note that available data for the carbon contents are only three, therefore, more data are needed to draw more reliable finding.

The carbon contents found are substantially lower than expected. Izumi and Fukuyama (1990) report carbon content values of (49±2)% for the secondary POM formed from 18 different cyclic/aromatic hydrocarbons, which is approximately a factor of two higher than the carbon contents found in this study. Table 16 provides a list of carbon content for compounds that were often observed in the secondary POM formed from the photo-oxidation of toluene. It is clearly seen that methylnitrophenol, methylglyoxal and citraconic anhydride have significantly higher carbon contents than the actual carbon content observed. The carbon contents for formic acid, PAN, and a

product found from the acid-catalyzed heterogeneous reactions of glyoxal determined by Liggio et al. (2005) show the similar values. It has been recently suggested that the density of secondary POM formed in lab studies is substantially higher than 1.0 g cm^{-3}: e.g. experimentally determined value of 1.4 g cm^{-3} by Alfarra et al. (2006). With use of the high densities, the carbon content calculated becomes further lower, approximately by 16-20%. Such values are too low to be solely due to organic carbon. This discrepancy is explained by that inorganic components, such as nitric acid and nitrous acid, and/or organic compounds containing substantial amount of heteroatom may have been contributing to the mass of the secondary PM, or by that significant amount of semi-volatile organic carbon on the POM was evaporated during the sampling. Sato (2008) reports very recently that significant amount of nitrate was found in the extract of PM formed by photo-oxidation of isoprene in the smog chamber. This indicates that those nitrates possibly originate from organic nitrate (i.e. R-NO_3). The isotope data discussed earlier suggest that the POM carbon is not contributed by the IPN carbon, carbons of the impurities in the IPN (i.e. isopropanol) and/or carbons of by-products from the IPN (i.e. acetone), thus, a possible explanation for the high Y_m is that the by-product or the impurity of IPN somewhat made inorganic components contribute to the mass of secondary PM formed in our experiments.

Table 16 List of Carbon Compositions for Typical Products Observed in Secondary POM

Specie	C#	MCW g C mol^{-1}	MW g mol^{-1}	Carbon content (%)	C#/MW
Methylbenzoquinone	7	84	122.12	69	0.0573
Acetone	3	36	58.08	62	0.0517
Methylnitrophenol	7	84	153.14	55	0.0457
Citraconic anhydride	5	60	112.08	54	0.0446
Glyoxal	2	24	58.04	41	0.0345
Acetic acid	2	24	60.05	40	0.0333
1,4-butenediol	4	48	88.11	54	0.0454
Formic acid	1	12	46.03	26	0.0217
PAN	2	24	121.05	20	0.0165
Product C in Liggio	4	48	170.00	28	0.0235

5.2. Compound Specific Stable Carbon Isotope Analysis

5.2.1. Optimization of Instrumentation

The injection tests using the GC-FID showed that on-column injection was the best method in order to attain reproducible and maximal injections of substances onto the GC column (Figure 15). Thus, this method was used for the compound-specific analyses here. However, it should be noted that relative carbon responses of free nitrophenols

(signal intensity per mole of carbon) sometime decreased by up to 30% relative to the response of tetradecane (C_{14} n-alkane). This was due to the loss of the free nitrophenol inside the retention gap and/or the GC column since restoration of the retention gap and solvent rinsing of the GC column improved the relative responses.

In order to find the optimal spot in the oxidation tube, the target temperature between 523 K and 553 K at the introduction point was sought since the analysis by GC-FID, which operated under the FID temperatures of 523-553 K, did not show significant thermal decomposition of the nitrophenols. Based on the temperature measurement made inside the combustion furnace (Figure 16), the optimal location under the 1223 K furnace operation was 3.7 cm from the edge of the oxidation tube, at which the temperature difference from the furnace fell from 1223 K to approximately 523 K.

5.2.2. Validation of Compound Specific $\delta^{13}C$ Analysis

The results of standard spike tests (Appendix A) with three different concentration mixtures showed that the recovery yields of the 10 target compounds and the four internal standards were on average (97±10)% (±standard deviation). The average of the differences between the measured $\delta^{13}C$ values and the reference $\delta^{13}C$ values for the 14 compounds and the three *n*-alkanes were (-0.17±0.88)‰ (±standard deviation). This validates the overall methodology for both the quantitative and the $\delta^{13}C$ measurements. Even though the recovery yields were good, the measured $\delta^{13}C$ values of catechol and 2,6-dimethyl-4-nitrophenol were less accurate than the other nitrophenols. For catechol, the peaks deteriorated after many injections, even with injections of only standard

solutions. Through replacement of the retention gap and solvent-rinsing the GC column the peak shapes were often improved. Therefore, it is concluded that the loss was due to unknown chemical reactions with thermally decomposed products in the capillary system. In the case of 2,6-dimethyl-4-nitrophenol, it was earlier stated that a contaminant peak from blank filter potentially overlapped with 2,6-dimethyl-4-nitrophenol. This is the most likely reason why $\delta^{13}C$ values for 2,6-dimethyl-4-nitrophenol tend to shift to lighter $\delta^{13}C$ values.

The true extraction efficiency of the nitrohydroxy aromatic compounds from POM samples could not be evaluated since no reference PM material containing these target compounds was available. However, the efficiency should be good since the secondary POM generated here consists of polar substances only, which are highly soluble in acetonitrile. Complete dissolution of colored substances on the filter samples was clearly observed immediately after adding acetonitrile. This observation supports the expectation of a high efficiency for the extraction of the photooxidation products from the particulate phase.

5.2.3. Product Identification

A list of identified products is summarized in Table 17. In total, seven species out of the eight products observed in the particulate phase were identified using retention times (comparison with the reference retention times in Table 11), mass spectra from GC-MS analyses (Appendix C), and 46 m/z traces from GC-C-IRMS analyses to identify the presence of the NO_2 group. Only the product peak 5 (Figure 22) was not identified

successfully. Comparison with NIST reference mass spectra did not allow for peak identification, nor did the analysis of the fragment ions give a good idea of the structure. Moreover, significant deterioration of its peak shape was observed in the GC-C-IRMS chromatogram was observed for the product peak 5. This deterioration made the isotope ratios and the quantitative values unreliable

Based on the retention time as well as the mass spectra, peaks 2 and 3 were identified as 3-methyl-4-nitrophenol and 2-methyl-4-nitrophenol, respectively. These products were observed in the POM formed from the photo-oxidation of toluene by Forstner et al. (1997), Jang and Kamens (2001), and Sato et al. (2007).

Peaks 4, 6, 7, and 8 showed very similar mass spectra to each other, however, all of them had different retention times compared to the reference compounds. Therefore, product identification was attempted by the analysis of the fragment ions in the mass spectra (Appendix B). The product peaks 4, 6, and 7 peaks showed the highest mass of 313 m/z, and the product peak 8 showed that of 298 m/z; these ions are possibly the molecular ion. The predominant signal at 73 m/z followed by the 45 m/z signal in the mass spectra of all these product peaks suggest that the products are TMS derivatives similar to catechol/methylcatechol. The enhanced 46 m/z signal observed by GC-C-IRMS measurements also suggests that these compounds contained a nitro group. Thus, it is likely that the product peaks 4, 6, and 7 are methylnitrocatechols (MW = 313), and the product peak 8 is a nitrocatechol (MW = 298).

Unique mass spectra were observed for product peak 1 (Appendix C). Even though its retention time was close to that of 2-methyl-5-nitrophenol, there was no

indication in its fragment-ion masses that the product should be a methylnitrophenol. The appearance of 73 m/z and 45 m/z signal in mass spectra suggests a TMS derivative, signifying the product contains OH or COOH group(s) in its structure. The derivative has the highest mass of 211, possibly the molecular ion. The high 46 m/z signal from the IRMS measurement was evidence for content of nitro group. The possible structure based on these clues is a nitrophenol (2-, 3-, or 4-nitrophenol). As shown in Appendix C, all fragment ions that appeared can be explained by possible fragment ions from a nitrophenol. Although it is not included in the standard mixture here, analysis made for 3-nitrophenol had a retention time of ~ 45 min, which is substantially shorter retention time than that of the product peak 1. The only possible structure left is, therefore, 4-nitrophenol. Comparison with the retention time index for the nitrophenol isomers determined with a different separation column (Mitchell and Veron, 1972) also support this identification.

Table 17 Summary of Peak Identification of Compounds Found in the Extract of the Flow Reactor Sample

Peak number[a]	Retention time (min.)	Identified substance Substance	Type of identification[b]
1	48.9	4-nitrophenol (4ntrphen)	MS & 46
2	51.3	3-methyl-4-nitrophenol (3Me4)	RT, MS,& 46
3	54.0	2-methyl-4-nitrophenol (2Me4)	RT, MS,& 46
4	60.7	Methylnitrocatechol isomer 1 (Mentrctchl 1)	MS & 46
5	62.5	Unknown	
6	63.3	Methylnitrocatechol isomer 2 (Mentrctchl 2)	MS & 46
7	63.4	Methylnitrocatechol isomer 3 (Mentrctchl 3)	MS & 46
8	64.8	Nitrocatechol isomer (ntrctchl)	S & 46

[a]*The peak number corresponds to the peak number in Figure 22.* [b]*RT, MS, and 46 indicate the method of identification by reference retention time, mass spectra, and 46 m/z (identification of nitrocompound), respectively.*

5.2.4. $\delta^{13}C$ and Yield of Specific Products

The $\delta^{13}C$ plot for the specific products as a function of fraction of toluene consumed is shown in Figure 26 and Figure 27. It should be noted that in Figure 26 the point of -29.2 ‰ at 0.7 fraction of toluene consumed, which is from the SC II experiment, may have a significant bias: This $\delta^{13}C$ value was determined from a small signal intensity, which is between the lowest two points in the linearity plot (Figure 20 (b)) where the accuracy of $\delta^{13}C$ measurements significantly drops. Assuming that the offset of the $\delta^{13}C$ measurements (the difference between the value measured and the value supposed to be) between these two lowest points in Figure 20 (b) becomes smaller proportionally to the signal intensity (i.e. applying the first approximation), the approximated measurement bias for the uncorrected value of -29.2 ‰ is ~ +0.7 ‰. Its bias-corrected $\delta^{13}C$ value, therefore, is -28.5 ‰. In Figure 26 and Figure 27, the $\delta^{13}C$ values for many of the products, except 4-nitrophenol, seem to be distributed near the predicted $\delta^{13}C$ for the sum of all products (equal to the $\delta^{13}C$ value for the total POM carbon). For each sample, differences in $\delta^{13}C$ between each specific product and the sum of all products predicted are listed in Table 18. The average differences (±standard deviation) over the five samples are (5.40±1.21)‰ for 4-nitrophenol, (-2.42±2.08)‰ for 3-methyl-4-nitrophenol, (0.65±1.38)‰ for 2-methyl-4-nitrophenol (including the value from the SC II experiment, which is not shown in Table 18), (-0.03±0.59)‰ for methylnitrocatechol isomer 1, (-2.03±1.39)‰ for methylnitrocatechol isomer 2, (-1.25±0.78)‰ for methylnitrocatechol isomer 3, and (-0.20±1.01)‰ for nitrocatechol isomer. It should be pointed out that the

difference smaller than ~2‰ becomes insignificant due to the relatively large standard deviations derived from the small size of the data set. Therefore, the $\delta^{13}C$ differences for the methylnitrophenols and the methylnitrocatechols are insignificant, but it is significant only for 4-nitrophenol.

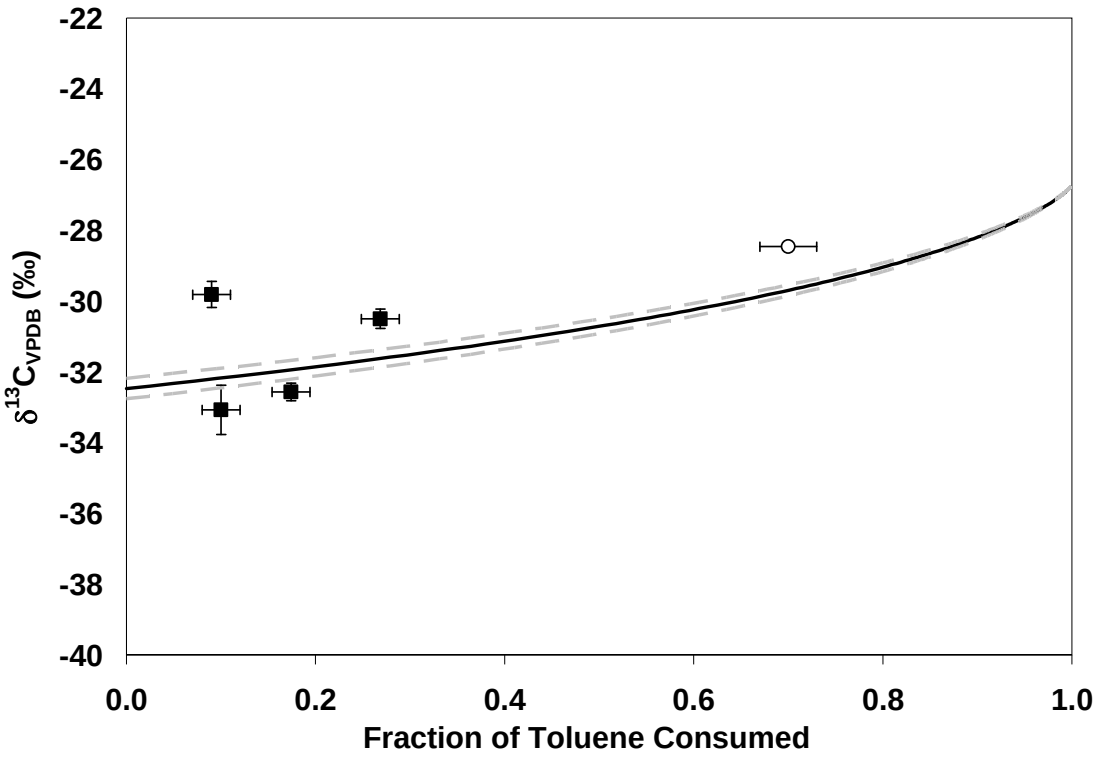

Figure 26. Plot of $\delta^{13}C$ for 2-methyl-4-nitrophenol in POM as Function of Fraction of Toluene Consumed.
Plots shown are from the flow reactor experiments (solid squares) and the smog chamber experiment (open circle). As a comparison, the predicted $\delta^{13}C$ for the sum of all products (solid line) and its 1σ standard error (dotted lines) are shown.

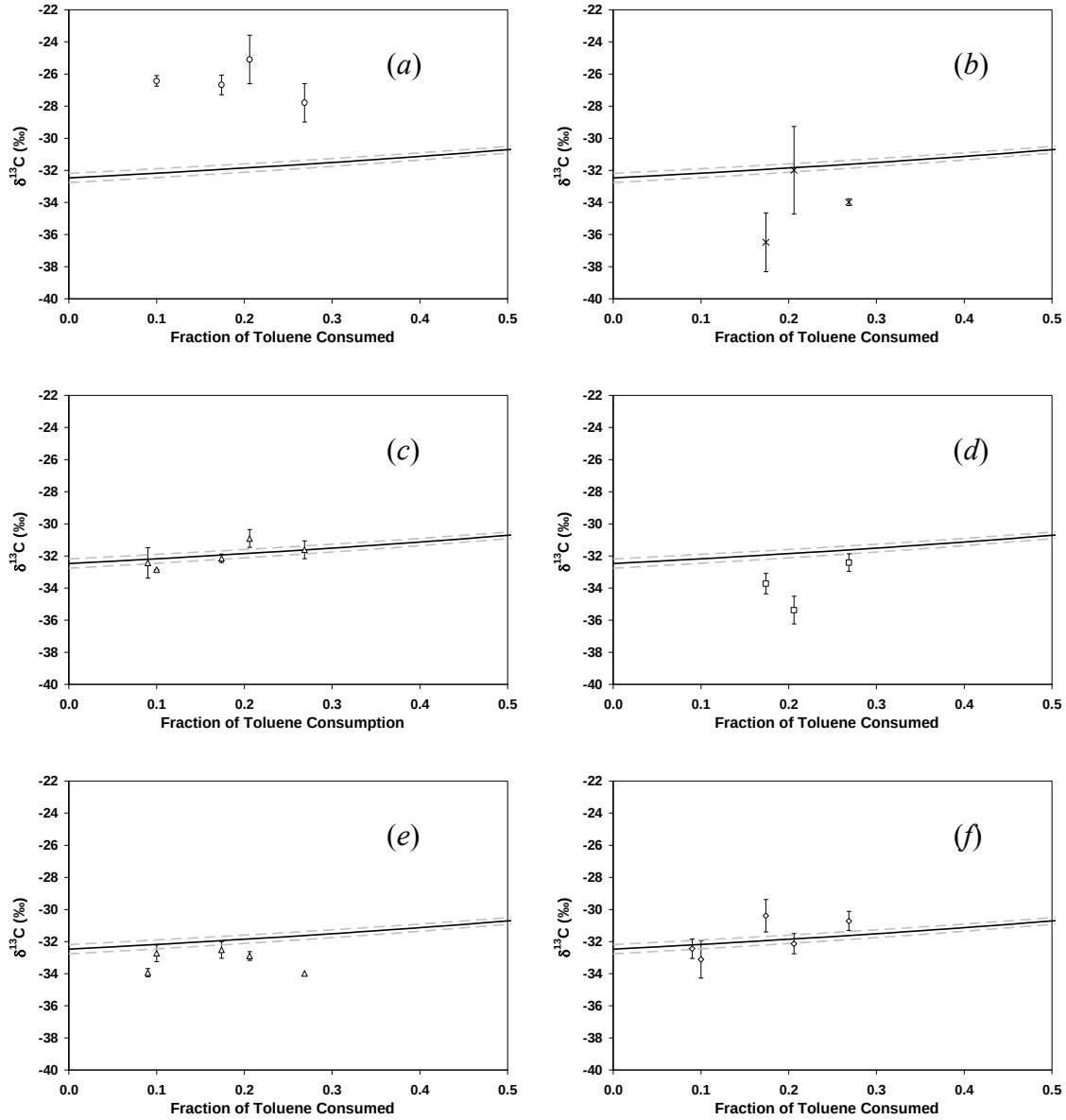

Figure 27. Plot of $\delta^{13}C$ for Compound Specific Product in Secondary POM as Function of Fraction of Toluene Consumed: (a) 4-nitrophenol, (b) 3-methyl-4-nitrophenol, (c) Methynitrocatechol isomer 1, (d) Methynitrocatechol isomer 2, (e) Methylnitrocatechol isomer 3, and (f) Nitrocatechol isomer.

All plots are from the flow reactor experiments. As a comparison, the predicted $\delta^{13}C$ for the sum of all products (solid line) and its 1σ standard error (dotted lines) are shown.

Table 18 Differences between Predicted $\delta^{13}C$ Values for Sum of All Products and Measured $\delta^{13}C$ Values for Specific Product[a,b] for Flow Reactor Experiment

Sample ID	FR1	FR2	FR3	FR4	FR5
$\Delta c_{C7H8}/^{0}c_{C7H8}$[c]	0.17	0.27	0.21 (‰)	0.10	0.09
4ntrphen	5.27±0.50	3.84±0.88	6.75±1.10	5.75±0.35	N/A[c]
3Me4	-4.53±1.32	-2.36±0.29	-0.36±1.94	N/A	N/A
2Me4	-0.62±0.31	1.33±0.32	N/A	-0.89±0.55	2.40±0.37
Mentrctchl1	-0.20±0.32	0.02±0.47	0.93±0.46	-0.67±0.25	-0.22±0.72
Mentrctchl2	-1.77±0.52	-0.78±0.46	-3.53±0.66	N/A	N/A
Mentrctchl3	-0.57±0.44	-2.35±N/A	-1.05±0.32	-0.55±0.45	-1.72±0.31
ntrctchl	1.56±0.76	0.91±0.49	-0.29±0.51	-0.93±0.86	-0.23±0.49

[a]The values shown are obtained by the measured value minus the predicted value. [b]Errors shown are standard deviations of three replicate measurements. [c]Fraction of toluene consumed. [c]Data are not available due to either very small signal or saturation in 45 m/z signal.

Postulated reaction mechanisms by others provide valuable information to evaluate isotope fractionations observed (Figure 28). It is well known that the toluene+OH reaction ($k = 5.96\times10^{-12}$ cm^3 $molecule^{-1}$ s^{-1}) has two channels at the initial step: the OH-addition to the aromatic ring (1a channel shown in the figure) and H-abstraction from the methyl group (1b channel). The branching ratio of 1a: 1b is typically ~90%: ~10% (Calvert et al., 2002). It should be noted that the KIE of (5.95±0.28)‰ for the toluene+OH reaction previously used for the calculation for the $\delta^{13}C$ of sum of all products is the average carbon KIE over these two channels, however, this average KIE is

dominated by KIE at the 1a channel (Anderson et al., 2005). The addition of an OH radical to an aromatic ring forms a methylhydroxycyclohexadienyl radical, then the methylhydroxycyclohexadienyl radical undergoes a several forward reactions at least (the 2a, 2b, and 2c channels). The 2a channel yields cresols (the first generation product) of 12% - 40% reacted toluene (Grey et al., 1985; Leone et al., 1985; Atkinson and Aschmann, 1994; Smith et al., 1998; Klotz et al., 1998), which are suggested intermediates for methylnitrophenols and methylcatechols (second generation products) by Forstner et al. (1997) via the 3a and 3b channels, respectively. The 2b channel is believed to yield quinones and ring opening products (Calvert et al., 2002). It is known that the rate constant for the sum of 2a and 2b channels (the methylhydroxycyclohexadienyl radical+O_2 reaction) is approximately 5×10^{-16} cm^3 $molecule^{-1}$ s^{-1} (Atkinson, 1994). The methylhydroxycyclohexadienyl radical significantly reacts with NO_2 directly when NO_2 concentration is high (in ppm level). This reaction is depicted as the 2c channel postulated by Zellner et al. (1985). The second order rate constant for the 2c channel is $\sim4\times10^{-11}$ cm^3 $molecule^{-1}$ s^{-1} (Knispel et al.1990). This channel then possibly produces cresol and HONO (Atkinson et al. 1992). Based on rate law calculation with the presence of ppm level NO_2 and 20% of O_2, the rate of 2c channel is competitive with or greater than the rate of sum of 2a and 2b channels. H-abstraction from the OH group of cresol (3a channel) is expected to be the minor path due to relatively small probability of OH attack on the OH substituent of cresol. Even though this channel is more favored than the H-abstraction from the CH_3 substituent, the branching ratio for the H-abstraction channels of the *o*-cresol+OH reaction do not

increase substantially in overall, when compared with the branching ratio for the H-abstraction of the toluene+OH reaction. This was experimentally confirmed by Olariu et al. (2002) that the product from the OH-adduct to cresol was dominant (64% - 73%), while the product from the H-abstraction from cresol was minor (7% - 9%). Known products from the 3a and 3b channels are, at least, methylnitrophenols and methylcatechols, respectively. These products further react with OH radicals, and the rate constant for the methylnitrophenol+OH reaction is in the range from 3×10^{-12} cm^3 $molecule^{-1}$ s^{-1} to 7×10^{-12} cm^3 $molecule^{-1}$ s^{-1} (Bejan et al., 2007), and that for the methylcatechol+OH reaction is in the range from 1×10^{-10} cm^3 $molecule^{-1}$ s^{-1} to 2×10^{-10} cm^3 $molecule^{-1}$ s^{-1} (Olariu et al., 2000). Both of these channels possibly produce methylnitrophenols, which are the products observed in our experiments.

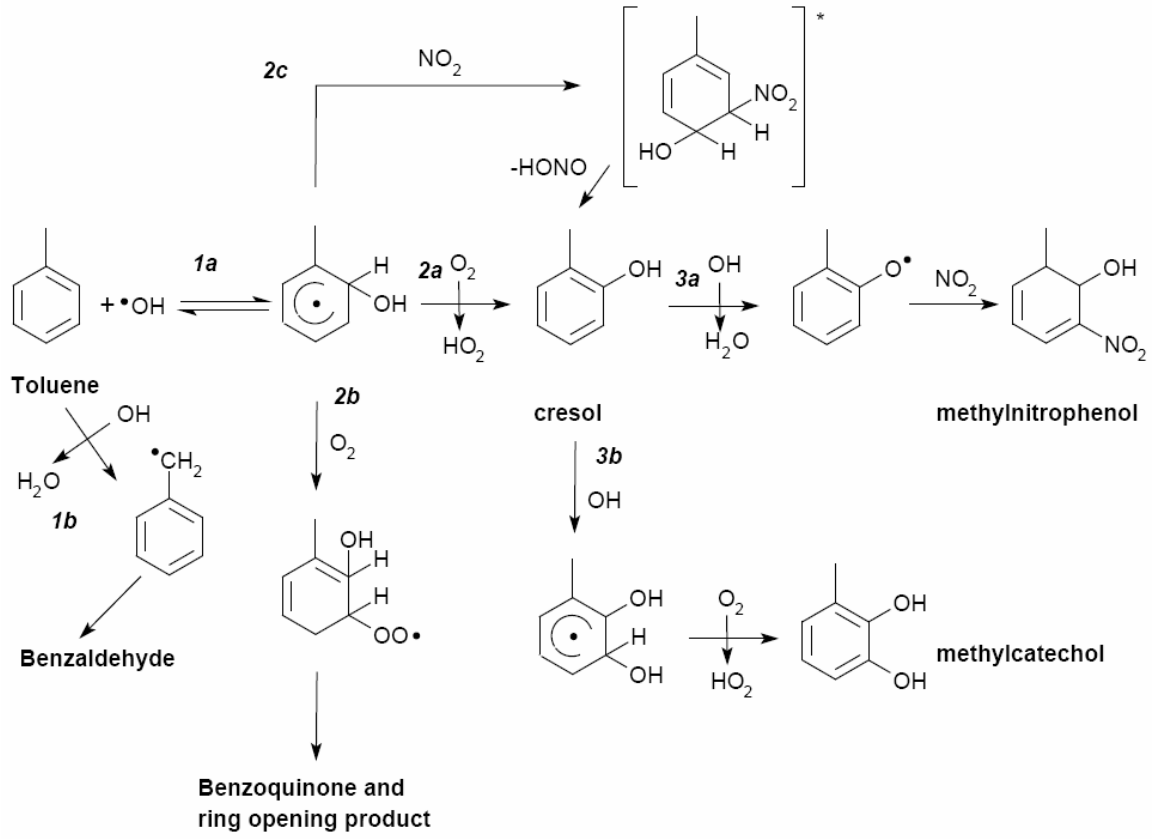

Figure 28. Postulated Toluene+OH Reaction Mechanism for Formation of Some of Oxidation Products.

With expected KIEs occurring at subsequent reactions, the postulated production mechanisms reasonably explain our observations in the isotope ratios for the methylnitrophenols and 4-nitrophenol, but indicate some discrepancies for the methylnitrocatechols. According to the carbon KIE studies for the reactions of NMHCs with OH radical in the gas-phase (Iannone et al., 2003; Anderson et al., 2005), addition reaction of OH radical to unsaturated bond has substantial KIEs, while H-abstraction channel from alkyl-substituent has very small KIEs. Based on their findings, the KIE at the 3a channel (the OH-attack on the substituent) is expected to be negligible (i.e. the ε

value is ~0 ‰) since the H-abstraction reaction occurs at the OH-substituent of cresol, meaning secondary carbon KIE. On the other hand, the 3b channel is expected to have significant KIE since the overall KIE for reaction of aromatic hydrocarbons with OH radical is typically dominated by KIE that occurs at the channel of OH-addition to aromatic ring (Anderson, 2005). Furthermore, it is expected that carbon KIEs of aromatic hydrocarbons have dependency of one over carbon number (Anderson et al., 2004), therefore, the overall carbon KIEs for the toluene+OH, cresol+OH, methylnitrophenol+OH, and methylcatechol+OH reactions are expected to be the similar, ~6 ‰. Together with the rate constants of $(5.9\pm1.5)\times10^{-12}$ cc s^{-1} $molecule^{-1}$ (Atkinson, 1994), $(4.2\pm1.3)\times10^{-11}$ cc s^{-1} $molecule^{-1}$ (Atkinson, 1994), $(\sim5\pm1)\times10^{-12}$ cc s^{-1} $molecule^{-1}$ (Bejan et al., 2007), and $(2.0\pm0.4)\times10^{-10}$ cc s^{-1} $molecule^{-1}$ (Olariu et al., 2000) for the toluene+OH, cresol+OH, methylnitrophenol+OH, and methylcatechol+OH reactions, respectively, the change of isotope ratios for cresol, methylcatechol (the product from the 3b channel), and the product from the methylnitrophenol+OH reaction were estimated (Figure 29). Note that the parameters used are based on the reactions in the gas-phase, therefore, the prediction of isotope ratios made here may not be valid when the reaction speed, mechanism, and KIEs in condensed phase are different from those in the gas-phase. It is clear that the predicted isotope ratio for methylnitrophenol reasonably agrees with the observations, suggesting the postulated mechanism for the production and the loss of methylnitrophenol is consistent with the observation. However, the prediction for methylcatechol seems to have significantly different isotope composition than the

observed methylnitrocatechols. With current available information, it is difficult to conclude whether or not this is implication of unknown mechanisms.

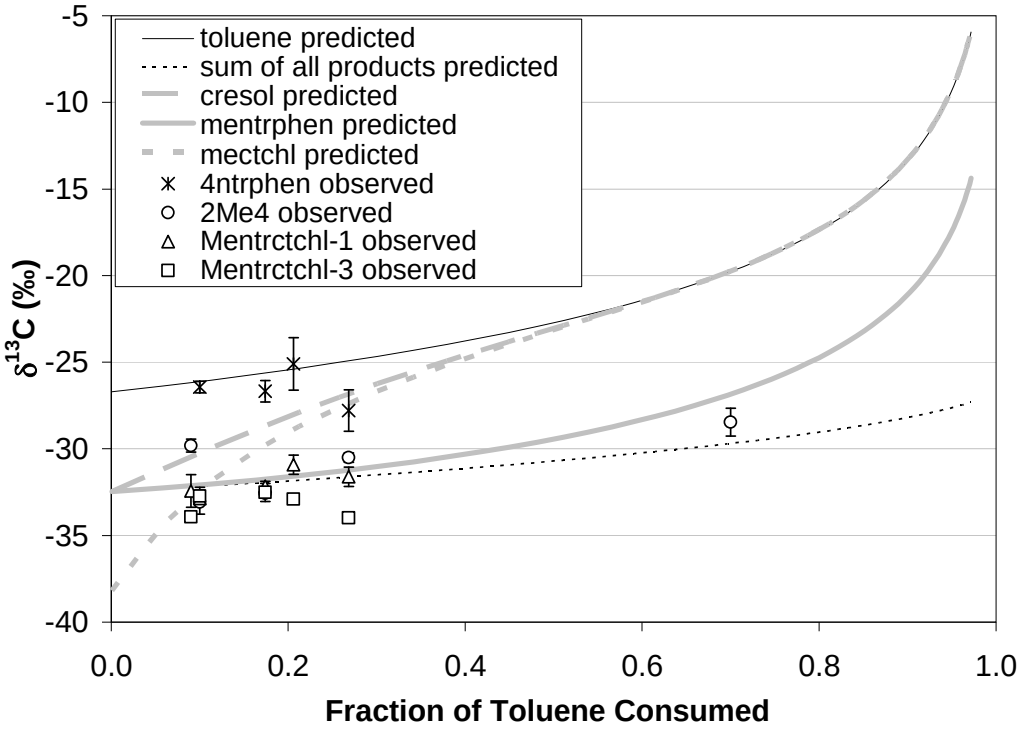

Figure 29. Plot of Predicted Stable Carbon Isotope Ratio for Toluene, Sum of All Products, Cresol, Methylcatechol, and the Third Generation Product, and Observed Stable Carbon Isotope Ratios for Specific Products.

Figure 30 shows the postulated production mechanism for nitrophenol by Jang and Kamens (2001). For the production of 4-nitrophenol, the reaction mechanism must include the reaction with the methyl group on the aromatic ring, indicating that the production is via the 1b channel in Figure 28. There would be substantial fractionations at the initial step (i.e. H-abstraction from the methyl group) and at the reaction step where

benzaldehyde reacts with OH radical (i.e. abstraction of a hydrogen atom from the aldehyde group) since both the reactions are cleavages of C-H bonds, meaning primary carbon KIE. These fractionations are expected to result in light isotope enrichment at the carbonyl group of the reaction product. However, information of carbon isotope fractionation at the aldehyde group will be lost as result of the decarboxylation occurring after the benzaldehyde+OH reaction. As a consequence of the decarboxylation, $\delta^{13}C$ of 4-nitrophenol formed is likely almost identical to that of the aromatic carbon of toluene, which would be represented by the initial toluene isotope composition of ~27‰. The experimental observations are consistent with this expectation.

The carbon yields of specific products relative to toluene carbon consumed (Y_{spec}) show a dependence on the fraction of toluene consumed (Figure 31 and Figure 32) within the flow reactor samples. For example, the yields of 2-methyl-4-nitrophenol (Y_{2Me4}), which is the product with the highest yield found in the POM extracts, increase from 0.3% to 3% as toluene consumption increases (Figure 31). Similarly to 2-methly-4-nitrophenol, the yields for the other products found from the flow reactor samples also depend on the fraction of toluene consumed (Figure 32). When removing outliers at the 0.17 fraction of toluene consumed, which is likely a failure in spiking the internal standards, the dependencies are more evident. In order to approximate the dependency on the toluene consumption, linear regression analysis was performed (Table 19). It should be pointed out that the approximation was made for the flow reactor samples only due to the inconsistent trend between the flow reactor data and the smog chamber data as well as there is only one data point available for the smog chamber experiments.

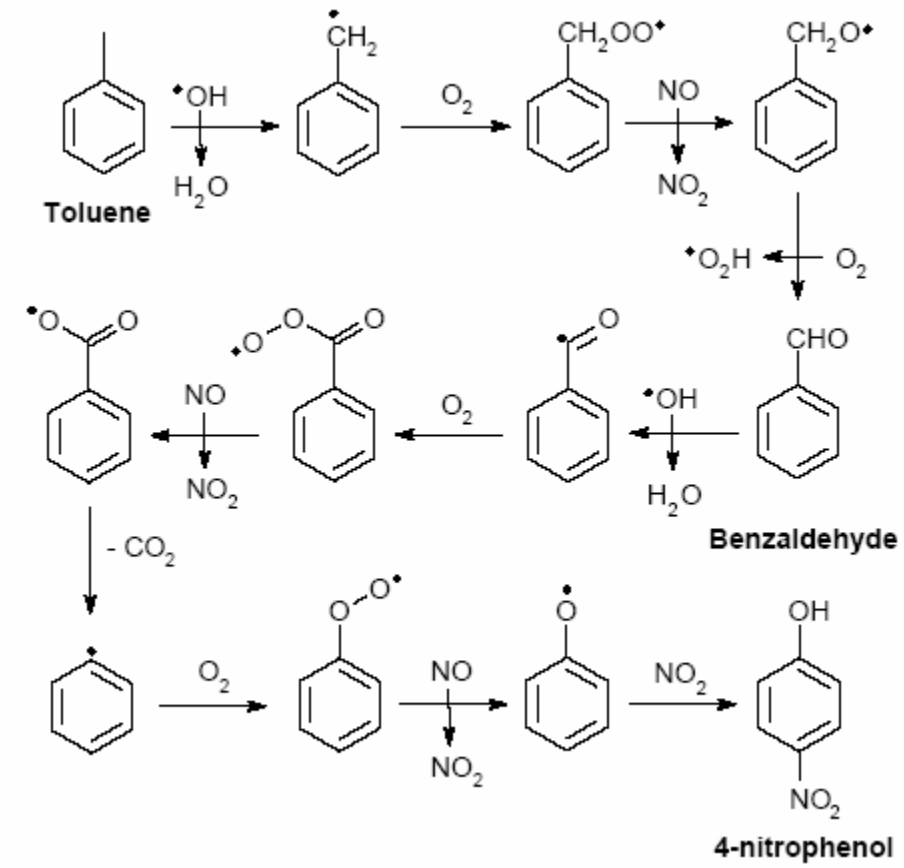

Figure 30. Postulated Production Mechanism for Nitrophenol from Toluene+OH Reaction (Jang and Kamens, 2001).

In contrary to the results of the total POM carbon, the yield dependency on toluene consumption for the specific products observed is inconsistent between the flow reactor samples and the smog chamber samples. For example, the yield for 2-methyl-4-nitrophenol at the 70% of toluene consumption was approximately 0.04% under the condition of the smog chamber experiments, which is three orders of magnitude lower than the yield for the flow reactor experiments estimated from the first approximation found (see the following discussion for the approximation). The inconsistent yields are

found for the other products as well: the amount of these products in the smog chamber samples is too small to be detected. Such low yields are similar to the observations by Forstner et al. (1997) and Sato et al. (2007), who found significant amount of ring-opening products in their POM extracts. A possible explanation for this discrepancy between the flow reactor and the smog chamber samples is (1) different extent of loss process (i.e. reactions) of these products inside the particles, (2) substantially different magnitude of their partitioning to the condensed phase due to their different concentrations in the gas-phase, (3) different weight of branching reactions, possibly due to different initial toluene mixing ratio and/or different toluene/NO_x ratios. In the case of (1), it is expected that such reaction(s) does not change the overall $\delta^{13}C$ of POM, but it most likely would change the $\delta^{13}C$ and yield of each specific product. Unfortunately, this possibility cannot be confirmed with the data available currently due to the large uncertainty on the $\delta^{13}C$ value measured. If (2) is the case, it is expected that the isotope ratios are not affected significantly by partitioning between the gas and the particle phases since the isotope fractionation resulting from phase transitions is only small. The observed difference in the $\delta^{13}C$ values between the two types of experiments is small, which is consistent with a phase transition process that creates a very small isotope fractionation. However, this explanation has some discrepancy with the fact that the observed total POM carbon yields show a consistent trend, regardless of the different magnitude of initial toluene concentration. If the case (2) is true, it must be implying that the consistent yield trend for the total POM carbon is just by coincidence. The case (3) is also possible since the yields of the nitrophenols and nitrocatechols more or less depend

on NO_x concentration since at very high NO_x level the phenoxy radical (the radical formed right after the H-abstraction from OH group of cresol) reacts very fast at competitive rates with NO_2 and O_2 according to the proposed mechanism (Atkinson, 1994). Again, due to the limited number of data, further discussion cannot be made. More yield data under variety of experimental conditions are needed to explore the reaction mechanisms.

Table 20 shows parameters (slopes and intercepts) for linear relationships between the POM carbon yields (Y_C) and the carbon yields of the specific products (Y_{spec}). The parameters were obtained by substituting $\Delta[C_{C7H8}]/[^0C_{C7H8}]$ in the Y_C regression shown in Figure 24 with the re-arranged Y_{spec} regression listed in Table 19 with respect to $\Delta[C_{C7H8}]/[^0C_{C7H8}]$. The comparison physically means carbon content of each specific product in the total POM carbon. It should be pointed out that the quantitative relationship between the total POM carbon and the specific products will require more points under a variety of conditions and a wide range of fraction of toluene consumed before they can be generalized. There are relatively large uncertainties on the intercepts, suggesting that the intercept values are insignificant. This means that the slopes shown in Table 20 are essentially identical to the reciprocal of average relative content of specific product carbon in total POM carbon, therefore, values of one over slopes are also shown together in Table 20. The relative carbon contents in the POM are 3.1% for the 4-nitrophenol, 0.32% for the 3-methyl-4-nitrophenol, 54% for the 2-methyl-4-nitrophenol, 1.8% for the methylnitrocatechol isomer 1, 0.93% for the methylnitrocatechol isomer 2, 7.6% for the methylnitrocatechol isomer 3, and 0.5% for

the nitrocatechol. Note that all of these values were derived from the flow reactor samples. Note that these relative contributions to the total POM carbon are the parameters of F_2 in Equation (11), which is introduced in Chapter 2.2. For the smog chamber samples, the relative content of 2-methyl-4-nitrophenol determined from the single measurement is ~0.02% only, suggesting that the chemical compositions of the smog chamber sample and the flow reactor samples are different.

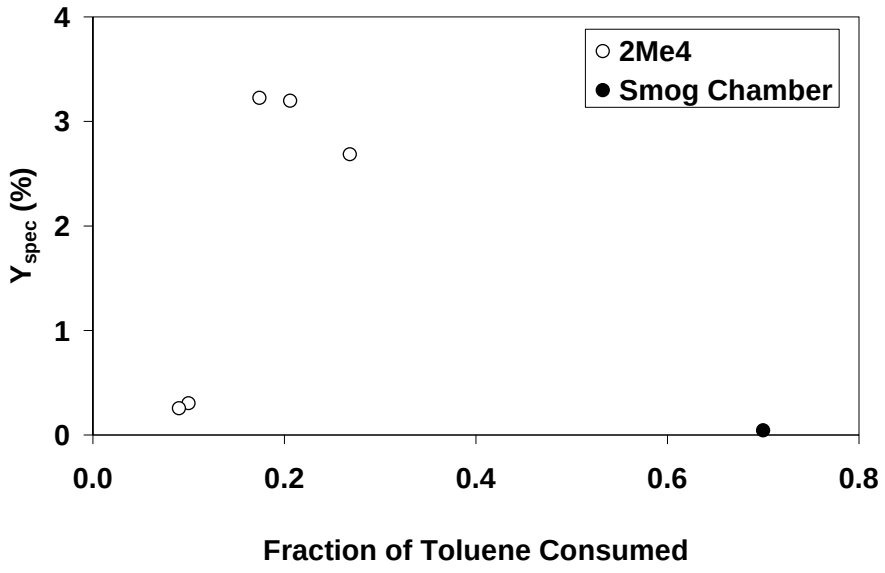

Figure 31. Plot of Carbon Yield for 2-methyl-4-nitrophenol (Y_{2Me4}) as Function of Fraction of Toluene Consumed.

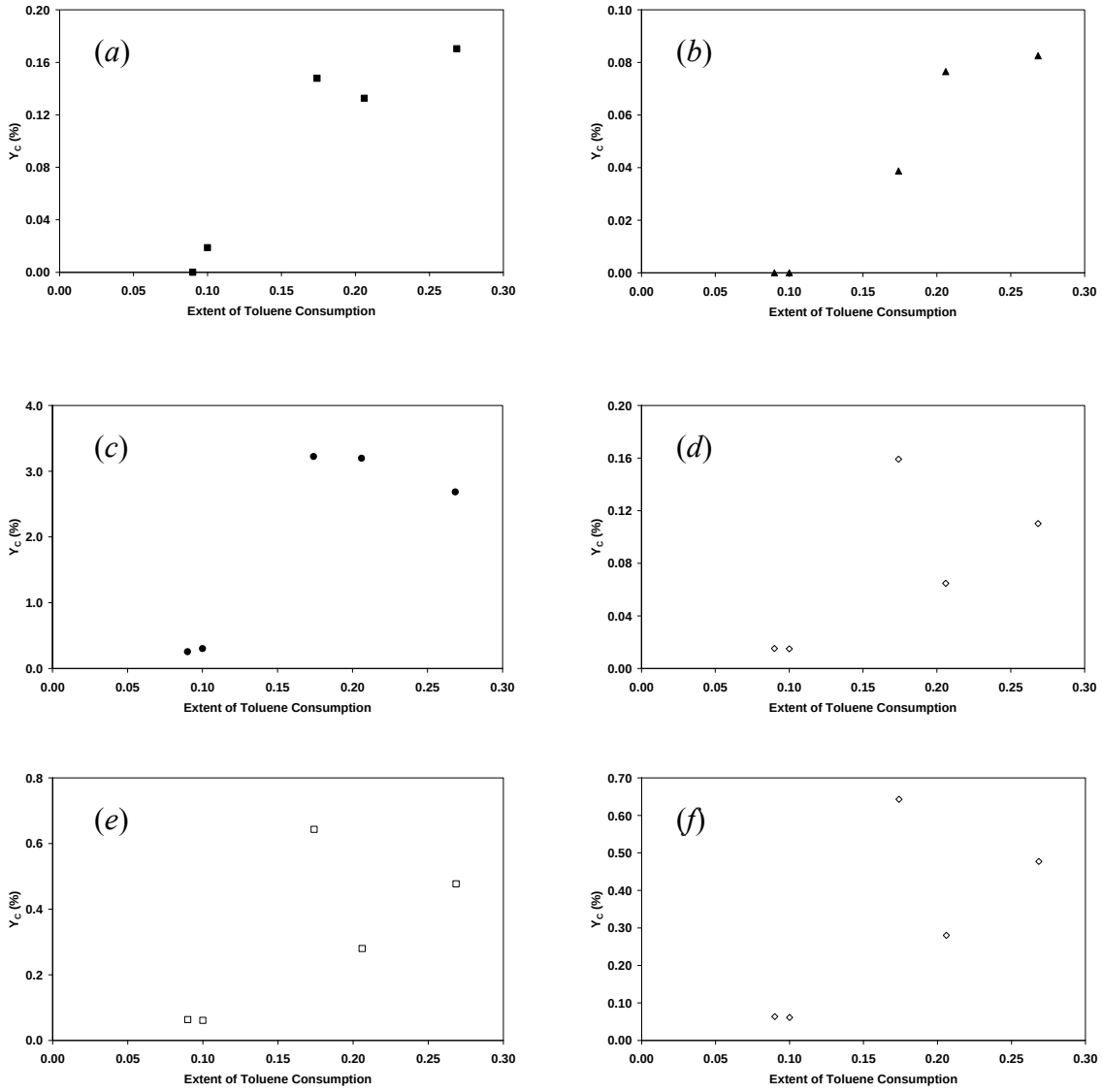

Figure 32. Plot of Carbon Yield for Specific Products as Function of Fraction of Toluene Consumed: (a) for 4-nitrophenol, (b) for 3-methyl-4-nitrophenol, (c) for 2-methyl-4-nitrophenol, (d) for methynitrocatechol isomer 1, (e) for methylnitrocatechol isomer 3, and (f) for nitrocatechol isomer.

Table 19 Results of Linear Regression Analysis for Carbon Yield of Specific Product (Y_{spec}) as Function of Fraction of Toluene Consumed[a]

Product	n	slope±error[b] (Y_{spec} (%) × fraction of toluene consumed^{-1})	intercept±error[b] Y_{spec} (%)	R^2
4ntrtol	3	0.92±0.12	-0.069±0.025	0.9822
3Me4	2	0.096	0.057	1
2Me4	4	16.3±5.4	-1.10±0.98	0.8203
Mentrctchl 1	4	0.527±0.048	-0.0364±0.0087	0.984
Mentrctchl 2	2	0.281	-0.017	1
Mentrctchl 3	4	2.30±0.20	-0.161±0.037	0.9845
ntrctchl	4	0.147±0.029	0.0082±0.0053	0.9264

[a]*The data are from the flow reactor experiments only and the point at a 0.17 fraction of toluene consumed shown in Figure 32 was excluded from the linear regression analysis.*
[b]*The errors shown are standard errors.*

Table 20 Parameters (± propagated standard error[a]) for Linear Regression[b] of Percentage Yield of Total POM Carbon (Y_C) as Function of Percentage Yield of Specific Product Carbon (Y_{spec})

Y_{spec}	Slope	Intercept	1/Slope[c]
$Y_{4ntrphen}$	32.7±5.3	-0.2±1.6	0.031±0.005
Y_{3Me4}	313.5	-20.4	0.0032
Y_{2Me4}	1.85±0.64	-0.5±2.3	0.54±0.19
$Y_{Mentrctchl}$	57.1±7.6	-0.4±1.4	0.018±0.002
$Y_{Mentrctchl2}$	107.10	-0.68	0.0093
$Y_{Mentrctchl3}$	13.1±1.7	-0.4±1.4	0.076±0.010
$Y_{ntrctchl}$	204.8±45.0	-4.2±1.7	0.005±0.001

[a]Propagated standard errors were calculated based on the standard errors for the parameters of the linear regressions presented in Table 19 and the standard errors for the parameters of the linear regression for the total POM carbon (Figure 24). [b]See the text for the calculation. [c]A one over slope for each product indicates the relative carbon concentration of the product to the concentration of total POM carbon (see the text for the detail).

5.3. Novel Method for Studies of Secondary POM Yield

As explained in Chapter 2.2, the yield of total POM carbon (Y_C) can be theoretically determined by a combination of concentrations and $\delta^{13}C$ values for toluene and the sum of all products in a closed system (Equation 10). In this study, the results of $\delta^{13}C$ for the total POM carbon show no apparent evidence for further carbon isotope fractionation after the first step of toluene+OH reaction. This suggests that the term of

$\delta^{13}C_{AllProd}$ in Equation 10 can be simply replaced with the term of $\delta^{13}C_{POM}$ (i.e. $\delta^{13}C_{AllProd} \approx \delta^{13}C_{POM}$):

$$Y_C = \frac{{}^0\delta^{13}C_{C7H8} - \delta^{13}C_{POM}}{\delta^{13}C_{C7H8} - {}^0\delta^{13}C_{C7H8}} \cdot \frac{C_{POM}}{C_{C7H8}} \quad (10).$$

Equation (21) has been presented elsewhere (Irei et al., 2004). Furthermore, F_1 and F_2 (see Chapter 2.2 for definition of F_1 and F_2) derived from the results of the compound-specific studies can be used to replace the $\delta^{13}C_{POM}$ and C_{POM} in the equation above with the isotope ratio and the carbon mass (or carbon concentration) for a specific product in the POM. For example, the compound specific analysis demonstrates that the $\delta^{13}C$ value for 2-methyl-4-nitrophenol ($\delta^{13}C_{2Me4}$) is approximately equivalent to the $\delta^{13}C_{POM}$, which is furthermore equivalent to the $\delta^{13}C_{AllProd}$ (i.e. F_1 in Equation (11) is 1). The analysis also provides that the carbon mass of 2-methyl-4-nitrophenol in the POM (C_{2Me4}) corresponds to 54% of the C_{POM}. Therefore, Equation (21) can be expressed as follows:

$$Y_C = \frac{{}^0\delta^{13}C_{C7H8} - \delta^{13}C_{2Me4}}{\delta^{13}C_{C7H8} - {}^0\delta^{13}C_{C7H8}} \cdot \frac{\frac{1}{0.54} \times C_{2Me4}}{C_{C7H8}} \quad (11).$$

This substitution will reduce measurement interference from other organic carbon existing in ambient samples. Using the parameters based on the results of laboratory studies here, Equation (22) gives opportunities to estimate the yield of secondary POM from the photo-oxidation of toluene by atmospheric measurements since all the variables in the right side of the equations are measurable in atmospheric studies.

6. Conclusion

The study here is the first exploring secondary POM stable isotope ratios in laboratory experiments. The results from the $\delta^{13}C$ measurements for the total POM carbon provide the following novel findings: (1) the $\delta^{13}C$ of the POM was distinctively different from the initial $\delta^{13}C$ of toluene, (2) after the initial reaction step, no further significant carbon isotope fractionation was observed in the sequence of the reactions leading to the formation of the condensable products, (3) according to the mass balance, it is predicted that the sum of the remaining products in the gas-phase must have very similar $\delta^{13}C$ to the secondary POM. Even though no further isotope fractionation seems to indicate that the rate-determining step in the sequence of reactions leading to formation of POM is the first reaction step (i.e. the reaction of OH with toluene), the yields for total POM carbon demonstrate that the POM consists of second or higher generation products, meaning that there are other formation rate limiting step(s) in the sequence of reactions that overall result in only small carbon isotope fractionation.

A method for the compound specific $\delta^{13}C$ analysis for nitro, nitrohydroxy, and hydroxy aromatic compounds was developed. The analysis identified 4-nitrophenol, 3-methyl-4-nitrophenol, 2-methyl-4-nitrophenol, three isomers of methylnitrocatechol, and one isomer of nitrocatechol in the POM extracts. It was found that (1) the $\delta^{13}C$ for the methyl nitrophenols and the methylnitrocatechols were also similar to the predicted $\delta^{13}C$ for the sum of all products, however, the $\delta^{13}C$ for 4-nitrophenol was significantly different from the predicted $\delta^{13}C$ for the sum of all products, (2) the yields of all the

specific products identified in the POM extracts indicate that these products are the second or higher generation products.

Comparison with the prediction based on the postulated reaction mechanism by others indicates that the results were reasonable for 4-nitrophenol and the two methylnitrophenols, however, implication of discrepancy is found for the methylnitrocatechols.

The study here propose a novel concept to study secondary POM using stable carbon isotope ratio: linking results of laboratory studies to atmospheric studies. The experimental results here allow us approximate yield and concentration of secondary POM from the toluene+OH from atmospheric measurements.

In overall, the study here demonstrates the large potential of stable isotope measurements for studies of secondary POM. The study also demonstrates that isotope ratio measurements are useful to explore the reaction mechanisms as well as processing studies in laboratory and ambient studies.

References

Alfarra, M.R., Paulsen, D., Gysel, M., Garforth, A.A., Dommen, J., Prévôt, A.S.H., Worsnop, D.R., Baltensperger, U., Coe, H., 2006. A mass spectrometric study of secondary organic aerosols formed from the photooxidation of anthropogenic and biogenic precursors in a reaction chamber. Atmospheric Chemistry and Physics 6, 5279-5293.

Allison, C.E., Francey, R.J., Meijer, H.A.J., 1993. Recommendations for the Reporting of Stable Isotope Measurements of Carbon and Oxygen in CO2 Gas. IAEA report IAEA-TECDOC-825, 155-162.

Anderson, R.S., Iannone, R., Thompson, A.E., Rudolph, J., Huang, L., 2004. Carbon kinetic isotope effects in the gas-phase reactions of aromatic hydrocarbons with the OH radical at 296 +- 4 K. Geophysical Research Letters 31, L15108/1-L15108/4.

Anderson, R.S., May, 2005. Carbon kinetic isotope effects in the gas-phase reactions of non-methane hydrocarbons with hydroxy radicals and chlorine atoms, Ph.D. Dissertation, York University, Toronto, Canada, 1-252

Anderson, T.L., Charlson, R.J., Schwartz, S.E., Knutti, R., Boucher, O., Rodhe, H., Heintzenberg, J., 2003. Atmospheric science: Climate forcing by aerosols-a hazy picture. Science (Washington, DC, United States) 300, 1103-1104.

Atkinson, R., 1989. Kinetics and mechanisms of the gas-phase reactions of the hydroxy radical with organic compounds. Journal of Physical and Chemical Reference Data. Monograph: No. 1, 1-246.

Atkinson, R., 1994. Gas-phase tropospheric chemistry of organic compounds. Journal of Physical and Chemical Reference Data, Monograph No.2 2, 1-216.

Atkinson, R. and Aschmann, S.M., 1994. Products of the gas-phase reactions of aromatic hydrocarbons: Effect of NO2 concentration. International Journal of Chemical Kinetics 26, 929-944.

Atkinson, R., Aschmann, S.M., Arey, J., 1992. Reactions of hydroxyl and nitrogen trioxide radicals with phenol, cresols, and 2-nitrophenol at 296 +- 2 K. Environmental Science and Technology 26, 1397-1403.

Bandow, H., Washida, N., Akimoto, H., 1985. Ring-cleavage reactions of aromatic hydrocarbons studied by FT-IR spectroscopy. I. photooxidation of toluene and benzene in the NO-air systemx. Bull. Chem. Soc. Jpn. 58, 2531-2540.

Barbu, A.M., February, 2003. Smog Chamber Studies of Aromatic Hydrocarbon Photooxidation by HO Radicals. M.Sc., York University, Toronto, Canada, 1-104.

Bejan, I., Barnes, I., Olariu, R., Zhou, S., Wiesen, P., Benter, T., 2007. Investigations on the gas-phase photolysis and OH radical kinetics of methyl-2-nitrophenols. Physical Chemistry Chemical Physics 9, 5686-5692.

Bienenstock, Y., May, 2001. Chamber Studies of Particulate Production from HO Reactions with Toluene. M.Sc., York University, Toronto, Canada, 1-153. .

Bierbach, A., Barnes, I., Becker, K.H., Wiesen, E., 1994. Atmospheric chemistry of unsaturated carbonyls: Butenedial, 4-oxo-2-pentenal, 3-hexene-2,5-dione, maleic anhydride, 3H-furan-2-one, and 5-methyl-3H-furan-2-one. Environmental Science Technology 28, 715-729.

Crüts, B., van Etten, L., Törnqvist, H., Blomberg, A., Sandström, T., Mills, N.L., Borm, P.J.A., 2008. Exposure to diesel exhaust induces changes in EEG in human volunteers. Particle and Fibre Toxicology 5,

Dockery, D.W., Pope, C.A.,3rd, Xu, X., Spengler, J.D., Ware, J.H., Fay, M.E., Ferris, B.G.,Jr., Speizer, F.E., 1993. An association between air pollution and mortality in six U.S. cities. New England journal of medicine, 329, 1753-9.

Fang, J., Kawamura, K., Ishimura, Y., Matsumoto, K., 2002. Carbon isotopic composition of fatty acids in the marine aerosols from the western north pacific: Implication for the source and atmospheric transport. Environmental Science and Technology 36, 2598-2604.

Forstner, H.J.L., Flagan, R.C., Seinfeld, J.H., 1997. Secondary organic aerosol from the photooxidation of aromatic hydrocarbons: Molecular composition. Environmental Science and Technology 31, 1345-1358.

Gery, M.W., Fox, D.L., Jeffries, H.E., Stockburger, L., Weathers, W.S., 1985. A continuous stirred tank reactor investigation of the gas-phase reaction of hydroxyl radicals and toluene. Int.J.Chem.Kinet. 17, 931-955.

Grootes, P.M., Mook, W.G., Vogel, J.C., 1969. Isotopic fractionation between gaseous and condensed carbon dioxide. Zeitschrift für Physik 221, 257-273.

Grosjean, D., 1984. Atmospheric reactions of ortho cresol: Gas phase and aerosol products. Atmospheric Environment - Part A General Topics 18, 1641-1652.

Harrington, R.R., Poulson, S.R., Drever, J.I., Colberg, P.J.S., Kelly, E.F., 1999. Carbon isotope systematics of monoaromatic hydrocarbons: Vaporization and adsorption experiments. Organic Geochemistry 30, 765-775.

Heberer, T. and Stan, H., 1997. Detection of more than 50 substituted phenols as their t-butyldimethylsilyl derivatives using gas chromatography-mass spectrometry. Analytica Chimica Acta 341, 21-34.

Hoefs, J., 1980. Stable isotope geochemistry. Stable isotope geochemistry.

Huang, L., Sturchio, N.C., Abrajano Jr., T., Heraty, L.J., Holt, B.D., 1999. Carbon and chlorine isotope fractionation of chlorinated aliphatic hydrocarbons by evaporation. Organic Geochemistry 30, 777-785.

Hurley, M.D., Sokolov, O., Wallington, T.J., Takekawa, H., Karasawa, M., Klotz, B., Barnes, I., Becker, K.H., 2001. Organic aerosol formation during the atmospheric degradation of toluene. Environmental Science and Technology 35, 1358-1366.

Iannone, R., 2008. Laboratory and Ambient Studies of Carbon Isotope Fractionation for Atmospheric Reactions of Isoprene and other Volatile Organic Compounds. Ph.D. Dissertation, York University, Toronto, Canada, 1-203.

Iannone, R., Anderson, R.S., Rudolph, J., Huang, L., Ernst, D., 2003. The carbon kinetic isotope effects of ozone-alkene reactions in the gas-phase and the impact of ozone reactions on the stable carbon isotope ratios of alkenes in the atmosphere. Geophysical Research Letters 30, 17/1-17/4.

Intergovernmental Panel on Climate Change, 2001. Climate Change 2001: The Scientific Basis.

Irei, S., Huang, L., Collin, F., Zhang, W., Hastie, D., and Rudolph, J., The 16th International Conference on Nucleation and Atmospheric Aerosols, 2004. Flow Reactor Studies for Stable Carbon Isotopic Composition of Secondary Particulate Organic Matter Generated by Toluene/OH Radical-Initiated Reactions. In: The 16th International Conference on Nucleation and Atmospheric Aerosols

Irei, S., Huang, L., Collin, F., Zhang, W., Hastie, D., Rudolph, J., 2006. Flow reactor studies of the stable carbon isotope composition of secondary particulate organic matter generated by OH-radical-induced reactions of toluene. Atmos.Environ. 40, 5858-5867.

Izumi, K. and Fukuyama, T., 1990. Photochemical aerosol formation from aromatic hydrocarbons in the presence of nitrogen oxides (NOx). Atmospheric Environment, Part A: General Topics 24A, 1433-1441.

Jang, M. and Kamens, R.M., 2001. Characterization of secondary aerosol from the photooxidation of toluene in the presence of NOx and 1-propene. Environmental Science and Technology 35, 3626-3639.

Johnson, D., Jenkin, M.E., Wirtz, K., Martin-Reviejo, M., 2004. Simulating the formation of secondary organic aerosol from the photooxidation of toluene. Environ.Chem. 1, 150-165.

Kawamura, K. and Kaplan, I.R., 1983. Organic compounds in the rainwater of Los Angeles. Environ.Sci.Technol. 17, 497-501.

Klotz, B., Sørensen, S., Barnes, I., Becker, K.H., Etzkorn, T., Volkamer, R., Platt, U., Wirtz, K., Martin-Reviejo, M., 1998. Atmospheric oxidation of toluene in a large-volume outdoor photoreactor: In situ determination of ring-retaining product yields. Journal of Physical Chemistry A 102, 10289-10299.

Lee, P.K.H., Brook, J.R., Dabek-Zlotorzynska, E., Mabury, S.A., 2003. Identification of the major sources contributing to PM2.5 observed in Toronto. Environmental Science and Technology 37, 4831-4840.

Leone, J.A. and Seinfeld, J.H., 1985. Comparative analysis of chemical reaction mechanisms for photochemical smog. Atmospheric Environment - Part A General Topics 19, 437-464.

Leuenberger, C., Czuczwa, J., Tremp, J., Giger, W., 1988. Nitrated phenols in rain: Atmospheric occurrence of phytotoxic pollutants. Chemosphere 17, 511-515.

Liggio, J., Li, S.-., McLaren, R., 2005. Reactive uptake of glyoxal by particulate matter. Journal of Geophysical Research D: Atmospheres 110, 1-13.

McDow, R.S. 1999. Sampling Artifact Errors in Gas/Particle Partitioning Measurements in Gas and Particle Phase Measurements of Atmospheric Organic Compounds. In: Lane, D.A. (Ed.), Adv. Environ., Ind. Process Control Technol., 1999; 2. Gordon and Breach Science Publishers, Netherlands, 105-126.

McMurry, P.H. and Rader, D.J., 1985. Aerosol wall losses in electrically charged chambers. Aerosol Science and Technology 4, 249-268.

Mitchell, P.T. and Vernon, F., 1972. Gas-liquid chromatography of nitrophenols and methyl derivatives. Journal of Chromatography A 65, 487-491.

Na, K., Sawant, A.A., Song, C., Cocker, D.R., 2004. Primary and secondary carbonaceous species in the atmosphere of western riverside county, California. Atmospheric Environment 38, 1345-1355.

Nara, H., Toyoda, S., Yoshida, N., 2007. Measurements of stable carbon isotopic composition of ethane and propane over the western north pacific and eastern indian ocean: A useful indicator of atmospheric transport process. Journal of Atmospheric Chemistry 56, 293-314.

Narukawa, M., Kawamura, K., Takeuchi, N., Nakajima, T., 1999. Distribution of dicarboxylic acids and carbon isotopic compositions in aerosols from 1997 indonesian forest fires. Geophysical Research Letters 26, 3101-3104.

Noyes, W.A., 1943. n-butyl nitrite. Organic Syntheses 2, 108-109.

Odum, J.R., Jungkamp, T.P.W., Griffin, R.J., Forstner, H.J.L., Flagan, R.C., Seinfeld, J.H., 1997. Aromatics, reformulated gasoline, and atmospheric organic aerosol formation. Environmental Science and Technology 31, 1890-1897.

Olariu, R.I., Klotz, B., Barnes, I., Becker, K.H., Mocanu, R., 2002. FT-IR study of the ring-retaining products from the reaction of OH radicals with phenol, o-, m-, and p-cresol. Atmospheric Environment 36, 3685-3697.

Olariu, R.I., Barnes, I., Becker, K.H., Klotz, B., 2000. Rate coefficients for the gas-phase reaction of OH radicals with selected dihydroxybenzenes and benzoquinones. International Journal of Chemical Kinetics 32, 696-702.

Ramanathan, V., Crutzen, P.J., Kiehl, J.T., Rosenfeld, D., 2001. Atmosphere aerosols, climate, and the hydrological cycle. Science (Washington, DC, United States) 294, 2119-2124.

Ricci, M.P., Merritt, D.A., Freeman, K.H., Hayes, J.M., 1994. Acquisition and processing of data for isotope-ratio-monitoring mass spectrometry. Organic Geochemistry 21, 561-571.

Richartz, H., Reischl, A., Trautner, F., Hutzinger, O., 1990. Nitrated phenols in fog. Atmospheric Environment - Part A General Topics 24 A, 3067-3071.

Rudolph, J. 2007. Gas Chromatography-Isotope Ratio Mass Spectrometry. In: Koppmann, R. (Ed.), Volatile Organic Compounds in the Atmosphere, Blackwell Publishing, 388-466.

Rudolph, J. and Czuba, E., 2000. On the use of isotopic composition measurements of volatile organic compounds to determine the \"photochemical age\" of an air mass. Geophysical Research Letters 27, 3865-3868.

Rudolph, J., Czuba, E., Huang, L., 2000. The stable carbon isotope fractionation for reactions of selected hydrocarbons with OH-radicals and its relevance for atmospheric chemistry. Journal of Geophysical Research, [Atmospheres] 105, 29329-29346.

Rudolph, J., Lowe, D.C., Martin, R.J., Clarkson, T.S., 1997. A novel method for compound specific determination of δ13C in volatile organic compounds at ppt levels in ambient air. Geophysical Research Letters 24, 659-662.

Saito, T., Tsunogai, U., Kawamura, K., Nakatsuka, T., Yoshida, N., 2002. Stable carbon isotopic compositions of light hydrocarbons over the western north pacific and implication for their photochemical ages. J.Geophys.Res., [Atmos.] 107, ACH 2/1-ACH 2/9

Sakugawa, H. and Kaplan, I.R., 1995. Stable carbon isotope measurements of atmospheric organic acids in Los Angeles, California. Geophysical Research Letters 22, 1509-1512.

Sato, K., 2008. Detection of nitrooxypolyols in secondary organic aerosol formed from the photooxidation of conjugated dienes under high-NO x conditions. Atmospheric Environment

Sato, K., Hatakeyama, S., Imamura, T., 2007. Secondary organic aerosol formation during the photooxidation of toluene: NOx dependence of chemical composition. Journal of Physical Chemistry A 111, 9796-9808.

Sato, K., Klotz, B., Hatakeyama, S., Imamura, T., Washizu, Y., Matsumi, Y., Washida, N., 2004. Secondary organic aerosol formation during the photo-oxidation of toluene: Dependence on initial hydrocarbon concentration. Bulletin of the Chemical Society of Japan 77, 667-671.

Seinfeld, J.H. and Pandis, S.N., 1998. Atmospheric chemistry and physics: From air pollution to climate change. , 1-1326.

Shinebarger, S.R., Haisch, M., Matthews, D.E., 2002. Retention of carbon and alteration of expected 13C-tracer enrichments by silylated derivatives using continuous-flow combustion-isotope ratio mass spectrometry. Analytical Chemistry 74, 6244-6251.

Smith, D.F., McIver, C.D., Kleindienst, T.E., 1998. Primary product distribution from the reaction of hydroxyl radicals with toluene at ppb NO(X) mixing ratios. Journal of Atmospheric Chemistry 30, 209-228.

Shepson, P.B., Edney, E.O., Corse, E.W., 1984. Ring fragmentation reactions on the photooxidations of toluene and o-xylene. Journal of Physical Chemistry 88, 4122-4126.

Stroud, C.A., Makar, P.A., Michelangeli, D.V., Mozurkewich, M., Hastie, D.R., Barbu, A., Humble, J., 2004. Simulating organic aerosol formation during the photooxidation of Toluene/NOx mixtures: Comparing the equilibrium and kinetic assumption. Environ.Sci.Technol. 38, 1471-1479.

Takekawa, H., Minoura, H., Yamazaki, S., 2003. Temperature dependence of secondary organic aerosol formation by photo-oxidation of hydrocarbons. Atmospheric Environment 37, 3413-3424.

Thompson, A., Rudolph, J., Rohrer, F., Stein, O., 2003. Concentration and stable carbon isotopic composition of ethane and benzene using a global three-dimensional isotope inclusive chemical tracer model. J.Geophys.Res., [Atmos.] 108, ACH 1/1-ACH 1/12.

Thurston, G.D., Ito, K., Hayes, C.G., Bates, D.V., Lippmann, M., 1994. Respiratory hospital admissions and summertime haze air pollution in Toronto, Ontario: Consideration of the role of acid aerosols. Environmental research 65, 271-290.

Tremp, J., Mattrel, P., Fingler, S., Giger, W., 1993. Phenols and nitrophenols as tropospheric pollutants: Emissions from automobile exhausts and phase transfer in the atmosphere. Water, Air, and Soil Pollution 68, 113-123.

Tuazon, E.C., Atkinson, R., Leod, H.M., Biermann, H.W., Winer, A.M., Carter, W.P.L., Pitts Jr., J.N., 1984. Yields of glyoxal and methylglyoxal from the NOx-air photooxidations of toluene and m- and p-xylene. Environmental Science and Technoalogy 18, 981-984.

Wang, Y. and Huang, Y., 2003. Hydrogen isotopic fractionation of petroleum hydrocarbons during vaporization: Implications for assessing artificial and natural remediation of petroleum contamination. Applied Geochemistry 18, 1641-1651.

Zellner, R., Fritz, B., Preidel, M., 1985. A cw UV laser absorption study of the reactions of the hydroxy-cyclohexadienyl radical with NO2 and NO. Chemical Physics Letters 121, 412-416.

APPENDIX

Appendix A Summary of Standard Spike Test

Species	Extraction test I (16– 74 ng C)			Extraction test II (16–74 ng C)		
	Recovery	$\delta^{13}C$	Offset	Recovery	^{13}C	Offset
	%	‰	‰	%	‰	‰
4ntrtol	107 ± 3.2	-27.18 ± 0.08	0.08	99 ± 3.5	-27.19 ± 0.04	0.07
ctchl	104 ± 2.1	-26.39 ± 0.6	1.41	100 ± 0.7	-26.46 ± 0.21	1.33
4Mectchl	100 ± 1.1	-23.46 ± 0.40	0.98	96 ± 0.6	-24.77 ± 0.06	-0.33
3Mectchl	92 ± 1.7	-22.69 ± 0.52	1.43	91 ± 0.6	-23.57 ± 0.23	0.55
2ntrphen	75 ± 21.8	-26.62 ± 0.77	1.11	93 ± 1.7	-27.37 ± 0.58	0.36
3Me2	100 ± 2.9	-27.19 ± 0.22	0.34	96 ± 0.5	-27.65 ± 0.09	-0.12
Mehydqn	103 ± 0.4	-25.82 ± 0.44	0.82	100 ± 0.5	-25.74 ± 0.06	0.90
4Etrscnl	107 ± 0.6	-26.59 ± 0.50	0.18	104 ± 0.6	-26.55 ± 0.17	0.22
4Me2	84 ± 18.3	-28.15 ± 0.49	-1.24	92 ± 0.7	-28.41 ± 0.11	-1.51

Appendix A Continued

	Extraction test I (16 –74 ng C)			Extraction test II (16 –74 ng C)		
Specie	Recovery	$\delta^{13}C$	Offset	Recovery	^{13}C	Offset
	%	‰	‰	%	‰	‰
2Me3	104 ± 3.2	-27.75 ± 0.47	-1.09	97 ± 0.3	-27.62 ± 0.06	-0.96
2Me5	103 ± 3.1	-27.96 ± 0.19	-0.76	94 ± 0.5	-27.58 ± 0.06	-0.38
3Me4	101 ± 2.5	-26.88 ± 0.14	-1.20	93 ± 0.4	-26.28 ± 0.24	-0.61
2Me4	105 ± 2.9	-27.37 ± 0.33	0.04	97 ± 0.6	-28.28 ± 0.18	-0.88
C17	N/A	-29.76 ± 0.13	-0.64	N/A	-29.70 ± 0.09	-0.58
26diMe	103 ± 4.2	-30.28 ± 0.15	-1.29	94 ± 0.3	-30.45 ± 0.25	-1.46
C18	N/A	-29.19 ± 0.04	-0.62	N/A	-29.49 ± 0.08	-0.92
C19	N/A	-35.19 ± 0.22	-0.06	N/A	-35.48 ± 0.17	-0.35

Appendix A Continued

Specie	Extraction test III (23 ngC – 129 ngC)			Extraction test IV (6 ngC – 46 ngC)		
	Recovery	$\delta^{13}C$	Offset	Recovery	^{13}C	Offset
	%	‰	‰	%	‰	‰
4ntrtol	108 ± 0.7	-27.52 ± 0.40	-0.27	112 ± 2.0	-26.97 ± 0.47	0.28
ctchl	101 ± 0.1	-27.63 ± 2.54	0.16	79 ± 2.9	-29.69 ± 1.64	-1.90
4Mectchl	96 ± 0.2	-24.60 ± 0.49	-0.16	82 ± 5.3	-24.50 ± 1.89	-0.06
3Mectchl	89 ± 0.9	-23.14 ± 0.07	0.98	62 ± 7.4	-22.27 ± 0.70	1.84
2ntrphen	85 ± 1.8	-27.24 ± 0.39	0.49	76 ± 12.6	-27.24 ± 1.48	0.48
3Me2	102 ± 0.1	-27.62 ± 0.10	-0.09	99 ± 0.5	-27.23 ± 0.58	0.30
Mehydqn	101 ± 1.3	-25.17 ± 0.13	1.46	89 ± 1.0	-25.06 ± 0.75	1.57
4Etrscnl	108 ± 1.7	-27.21 ± 0.10	-0.44	107 ± 1.4	-26.35 ± 0.14	0.42
4Me2	94 ± 0.5	-28.20 ± 0.56	-1.30	83 ± 8.7	-27.49 ± 0.99	-0.59

Appendix A Continued

	Extraction test III (23 ngC – 129 ngC)			Extraction test IV (6 ngC – 46 ngC)		
Specie	Recovery	$\delta^{13}C$	Offset	Recovery	^{13}C	Offset
	%	‰	‰	%	‰	‰
2Me3	99 ± 0.4	-27.12 ± 0.45	-0.46	104 ± 4.1	-27.17 ± 1.12	-0.51
2Me5	96 ± 0.0	-27.02 ± 0.33	0.18	104 ± 1.0	-27.57 ± 0.80	-0.36
3Me4	93 ± 0.1	-25.72 ± 0.24	-0.04	107 ± 9.0	-26.64 ± 0.54	-0.96
2Me4	97 ± 0.1	-28.45 ± 0.50	-1.05	112 ± 7.6	-27.32 ± 0.58	0.09
C17	N/A	-29.54 ± 0.18	-0.42	N/A	-30.45 ± 0.29	-1.33
26diMe	93 ± 0.1	-31.55 ± 0.07	-2.56	107 ± 7.6	-29.33 ± 0.16	-0.33
C18	N/A	-29.32 ± 0.07	-0.76	N/A	-29.13 ± 0.12	-0.56
C19	N/A	-35.19 ± 0.02	-0.06	N/A	-35.49 ± 0.38	-0.36

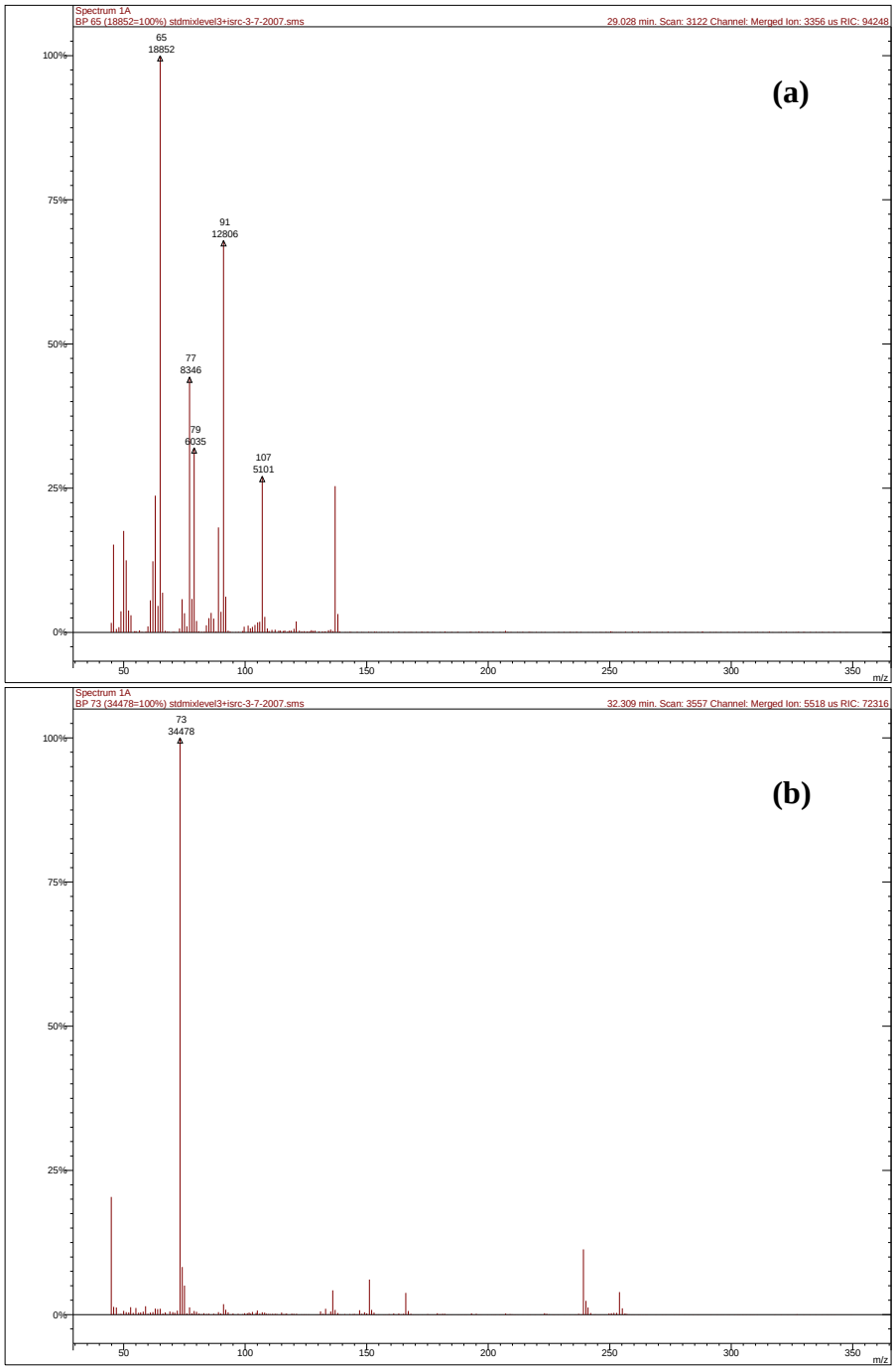

Appendix B. Mass Spectra Obtained from the Analysis of (a) 4-nitrotoluene and (b) Catechol.

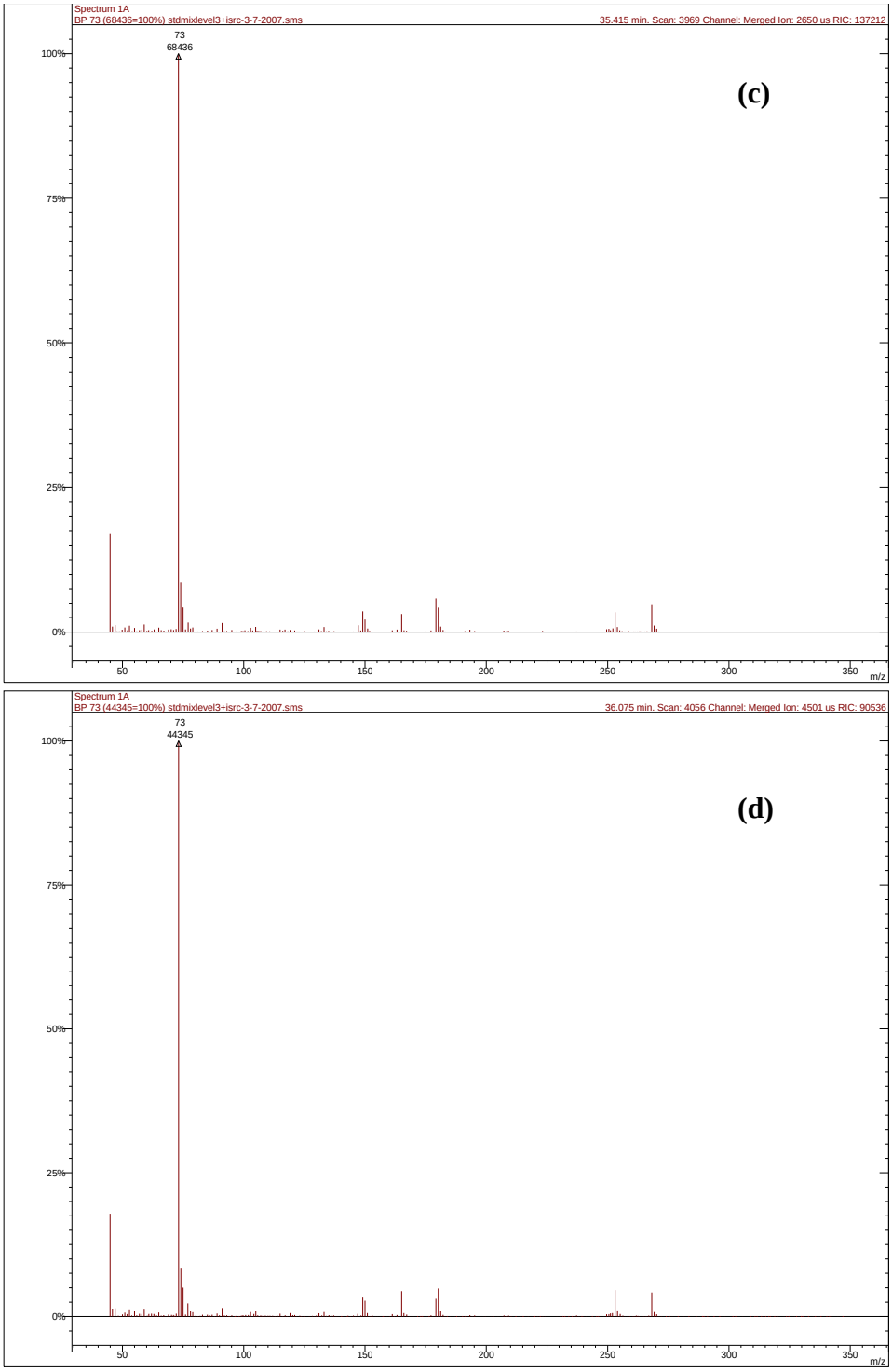

Appendix B. Continued: (c) 4-methylcatechol and (d) 3-methylcatechol.

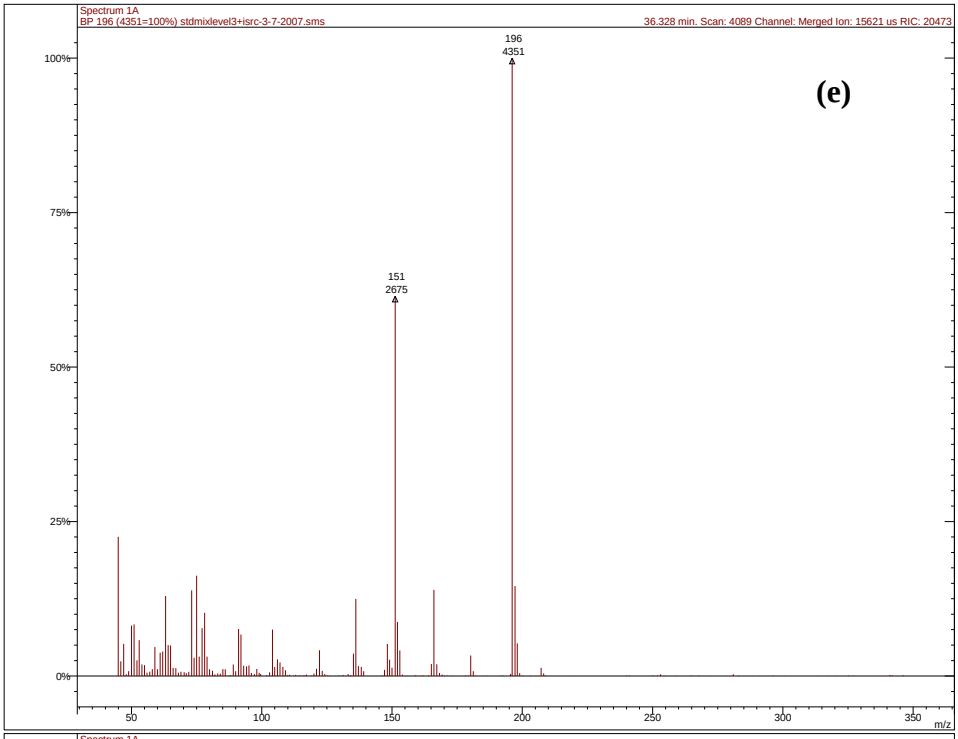
Spectrum 1A
BP 196 (4351=100%) stdmixlevel3+isrc-3-7-2007.sms
36.328 min. Scan: 4089 Channel: Merged Ion: 15621 us RIC: 20473
196
4351
151
2675
(e)
100%
75%
50%
25%
0%
50
100
150
200
250
300
350
m/z

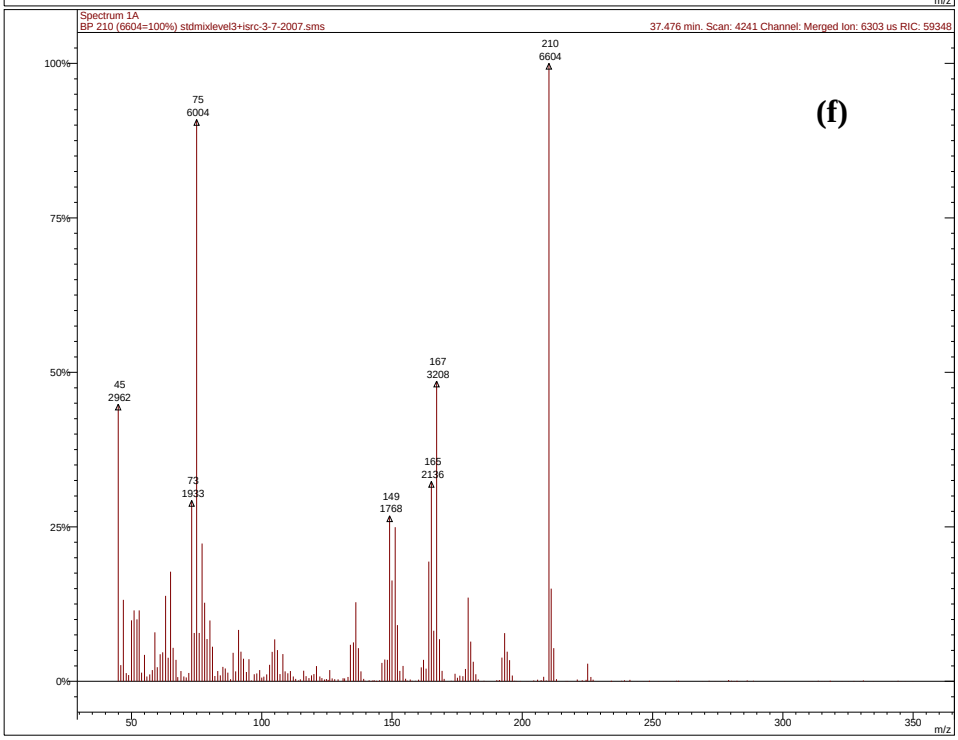
Spectrum 1A
BP 210 (6604=100%) stdmixlevel3+isrc-3-7-2007.sms
37.476 min. Scan: 4241 Channel: Merged Ion: 6303 us RIC: 59348
210
6604
75
6004
(f)
167
3208
45
2962
165
2136
73
1933
149
1768
100%
75%
50%
25%
0%
50
100
150
200
250
300
350
m/z

Appendix B. Continued: (e) 2-nitrophenol and (f) 3-methy-2-nitrophenol.

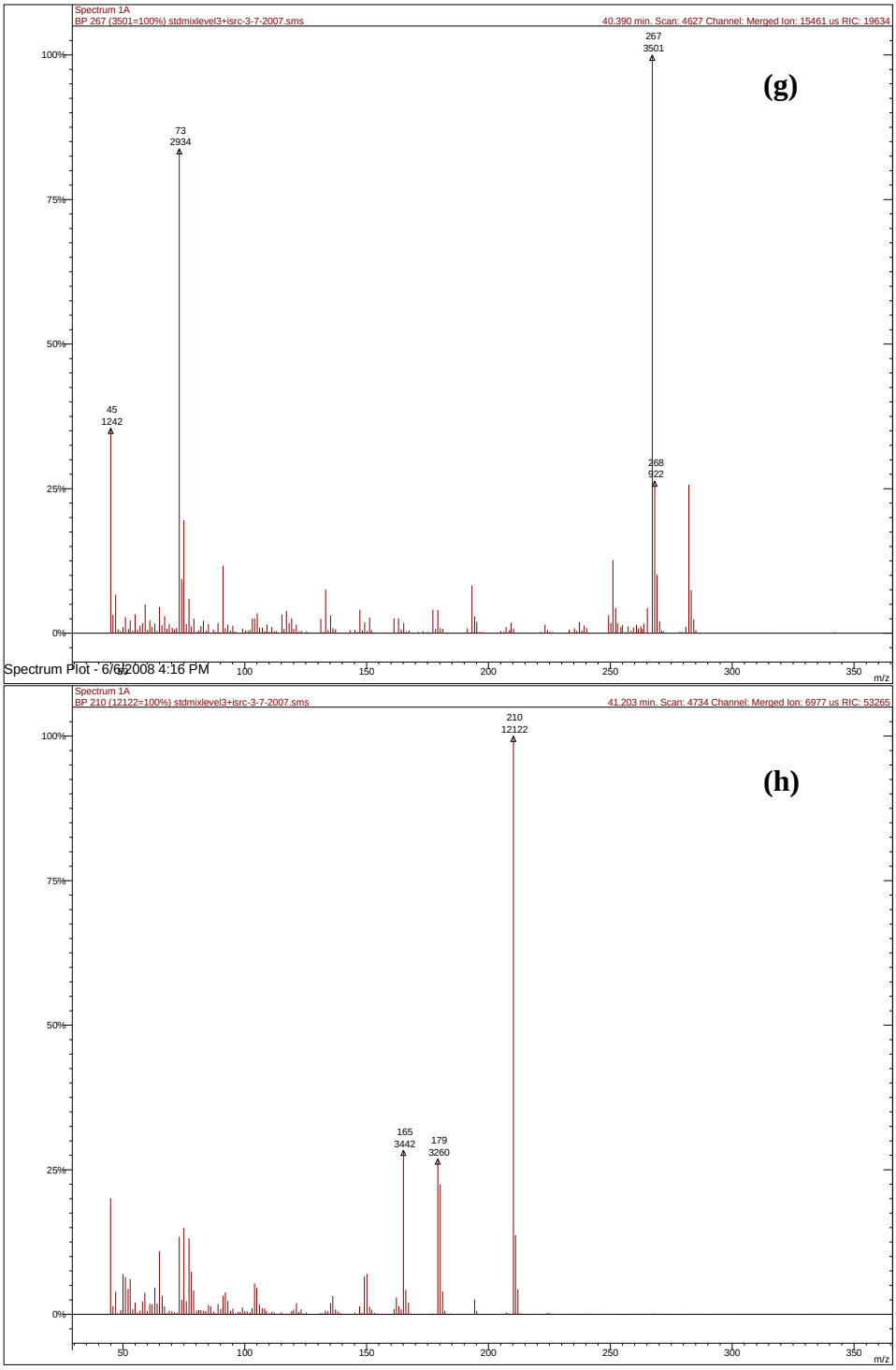

Appendix B. Continued: (g) 4-ethylresorcinol and (h) 4-methyl-2-nitrophenol.

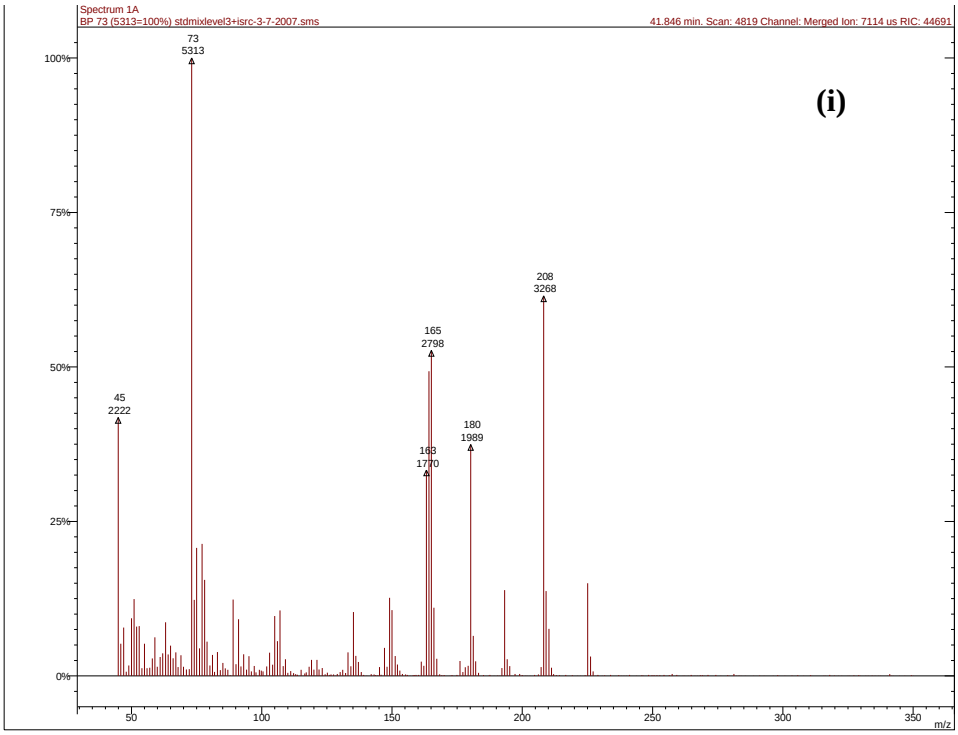
Spectrum 1A
BP 73 (5313=100%) stdmixlevel3+isrc-3-7-2007.sms
41.846 min, Scan: 4819 Channel: Merged Ion: 7114 us RIC: 44691
(i)
73
5313
208
3268
165
2798
45
2222
180
1989
163
1770
100%
75%
50%
25%
0%
50
100
150
200
250
300
350
m/z

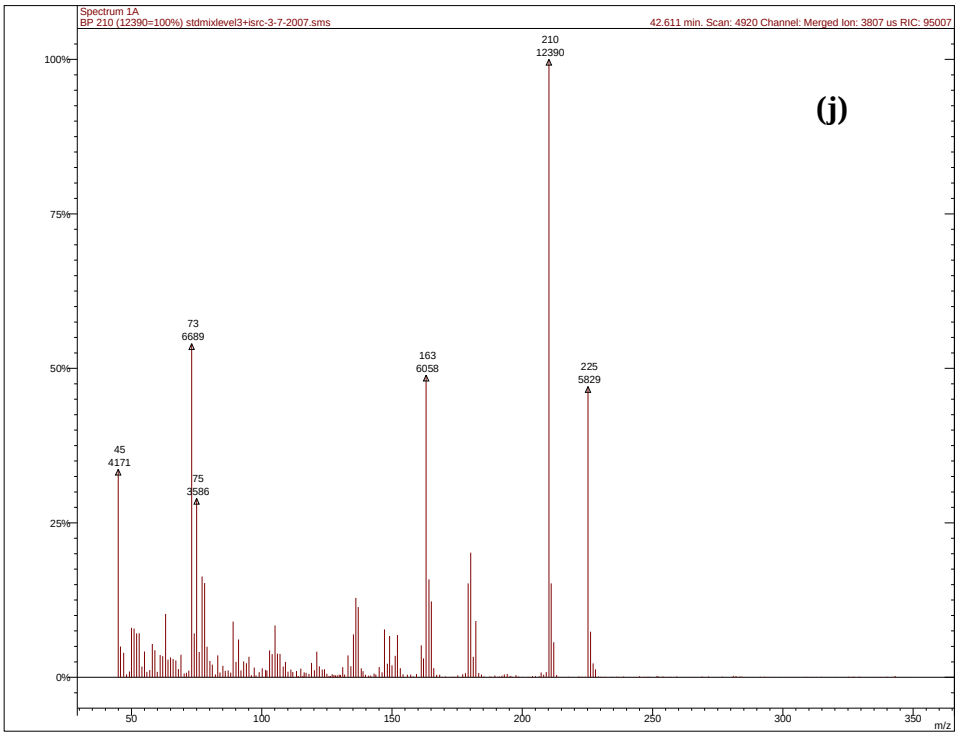
Spectrum 1A
BP 210 (12390=100%) stdmixlevel3+isrc-3-7-2007.sms
42.611 min, Scan: 4920 Channel: Merged Ion: 3807 us RIC: 95007
(j)
210
12390
73
6689
163
6058
225
5829
45
4171
75
3586
100%
75%
50%
25%
0%
50
100
150
200
250
300
350
m/z

Appendix B. Continued: (i) 2-methy-3-nitrophenol and (j) 2-methyl-5-nitrophenol.

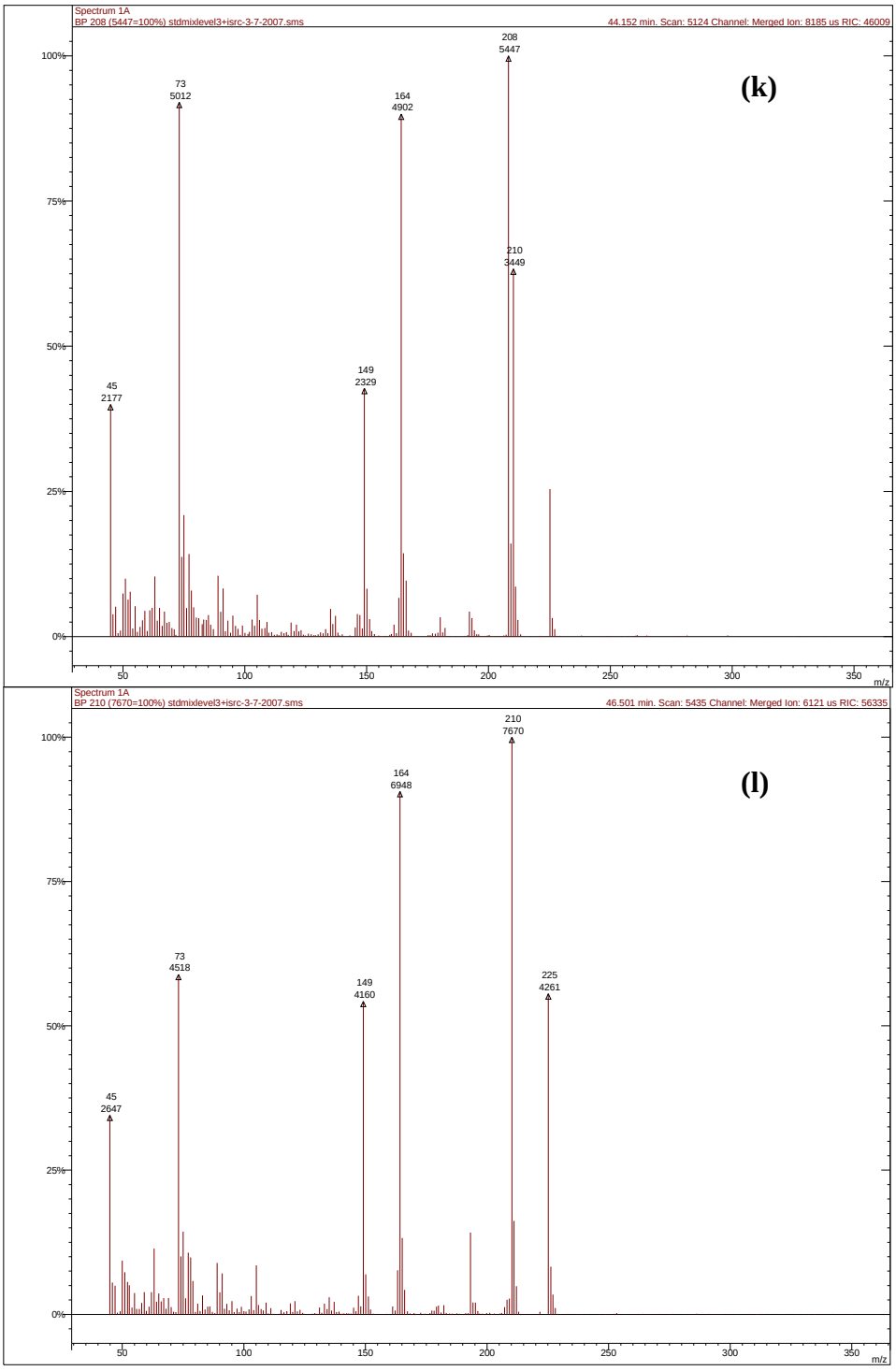

Appendix B. Continued: (k) 3-methyl-4-nitrophenol and (l) 2-methyl-4-nitrophenol.

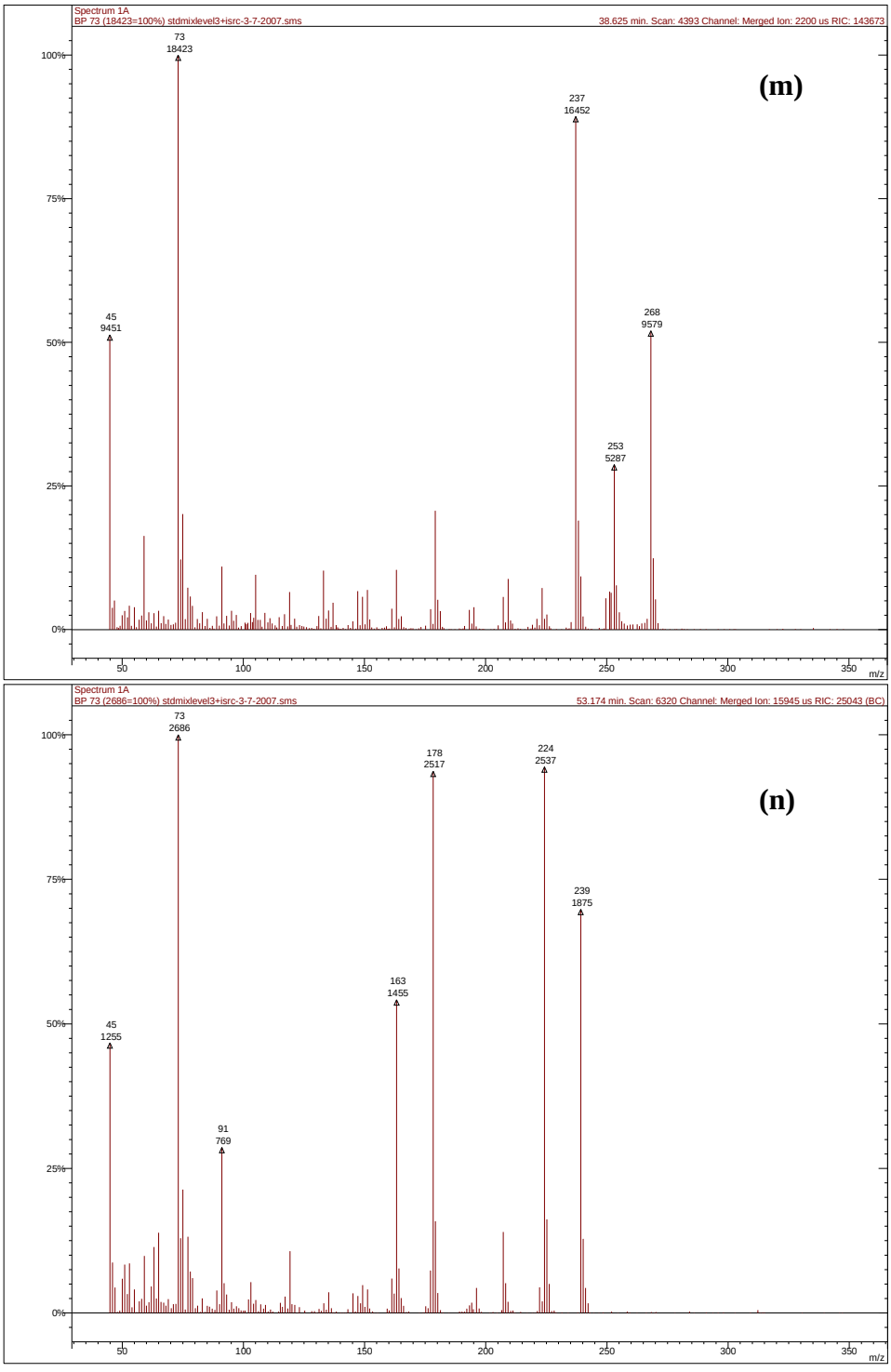

Appendix B. Continued: (m) Methylhydroquinone and (n) 2,6-dimethyl-4-nitrophenol.

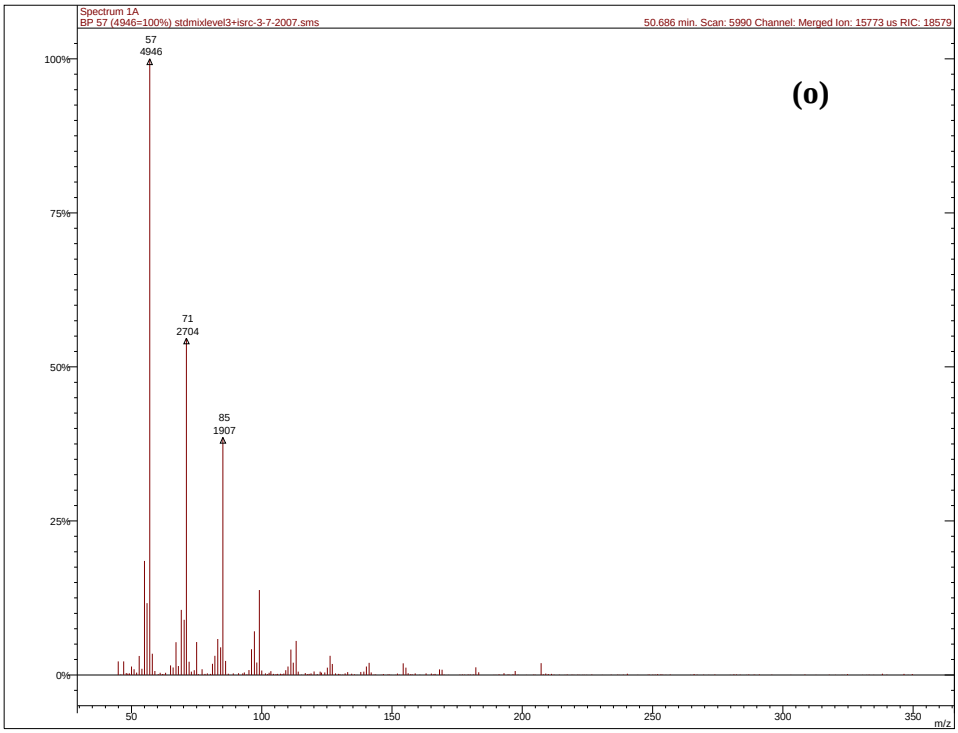

Appendix B. Continued: (o) heptacosane.

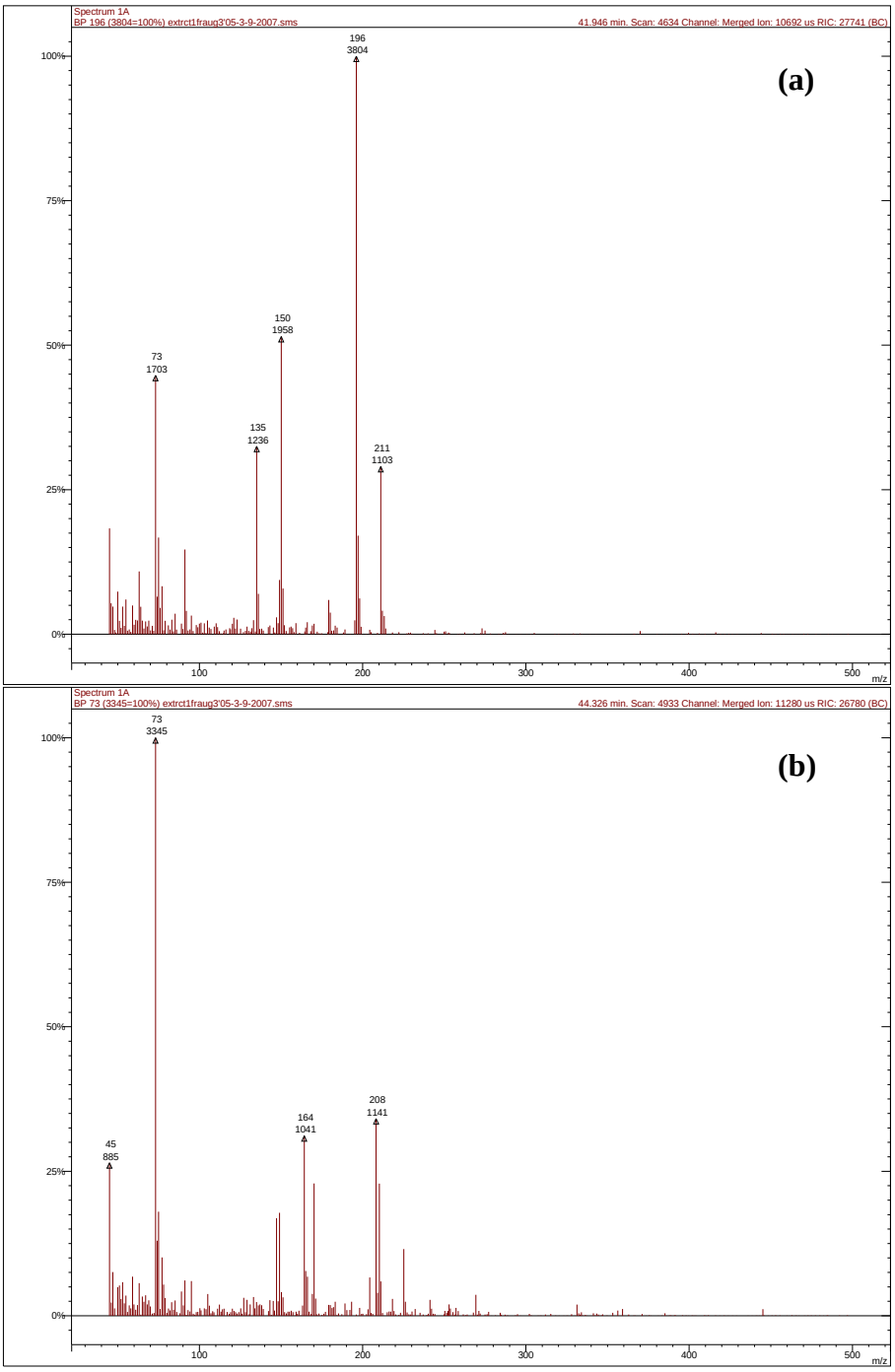

Appendix C. Mass Spectra for: (a) Product Peak 1 and (b) Product Peak 2 found in the Secondary POM Extract.

Peak numbers correspond to those in Figure 22.

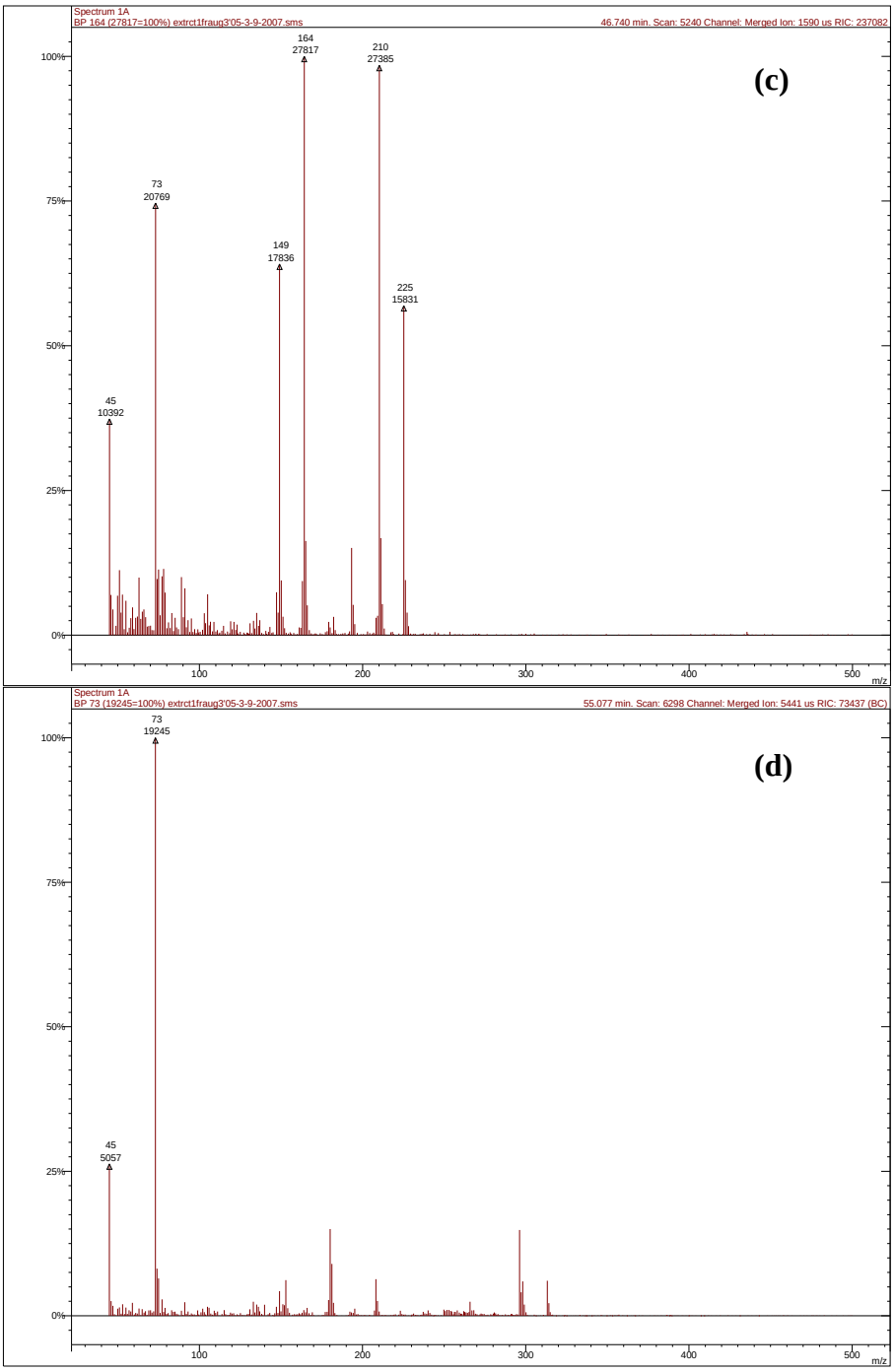

Appendix C. Continued: (c) Product Peak 3 and (d) Product Peak 4.

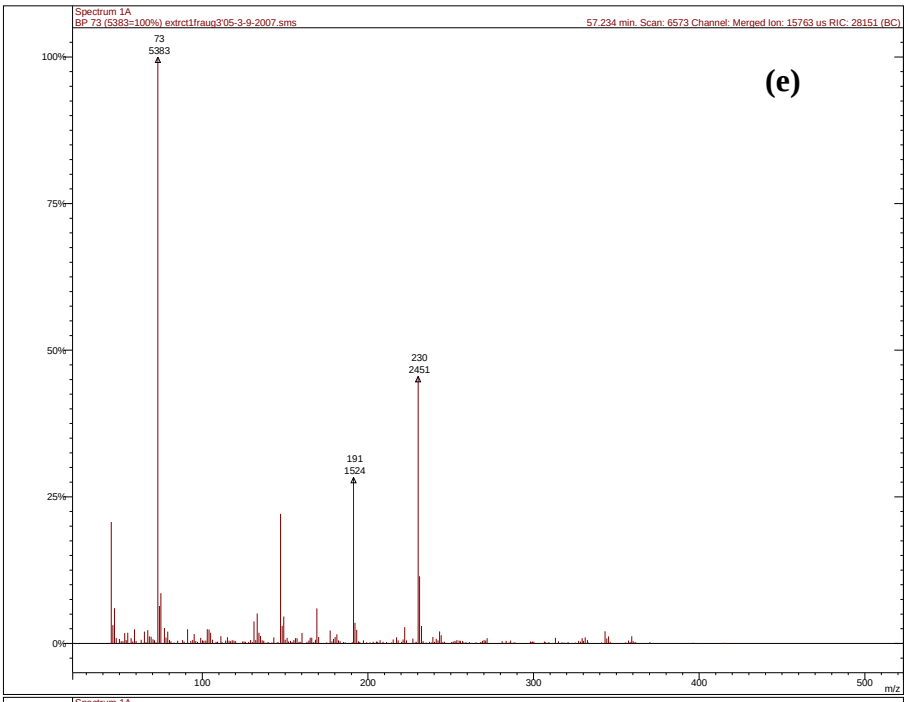

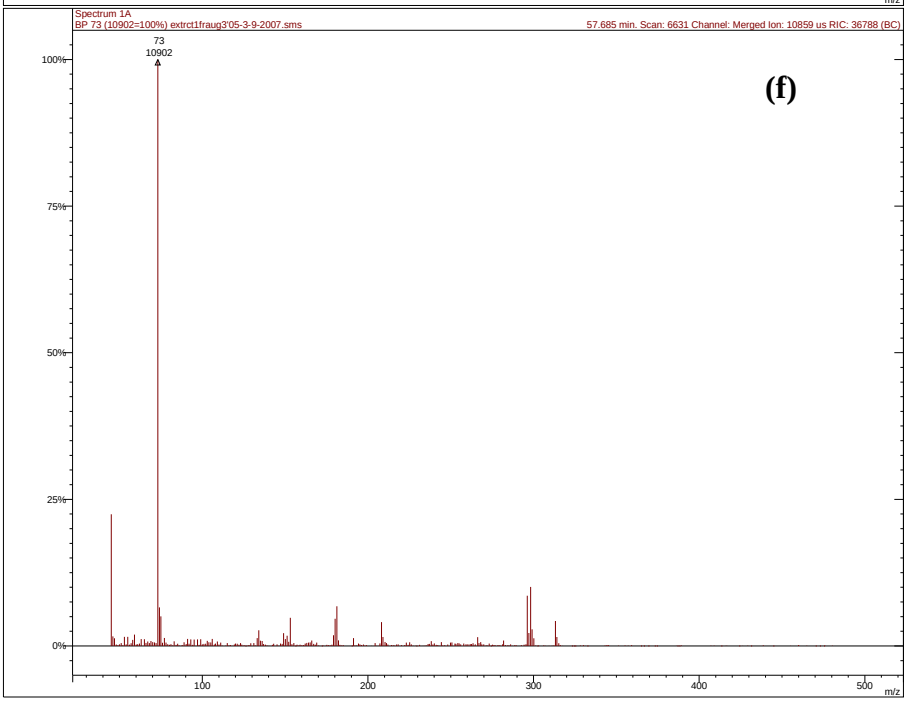

Appendix C. Continued: (e), Product Peak 5 and (f) Product Peak 6.

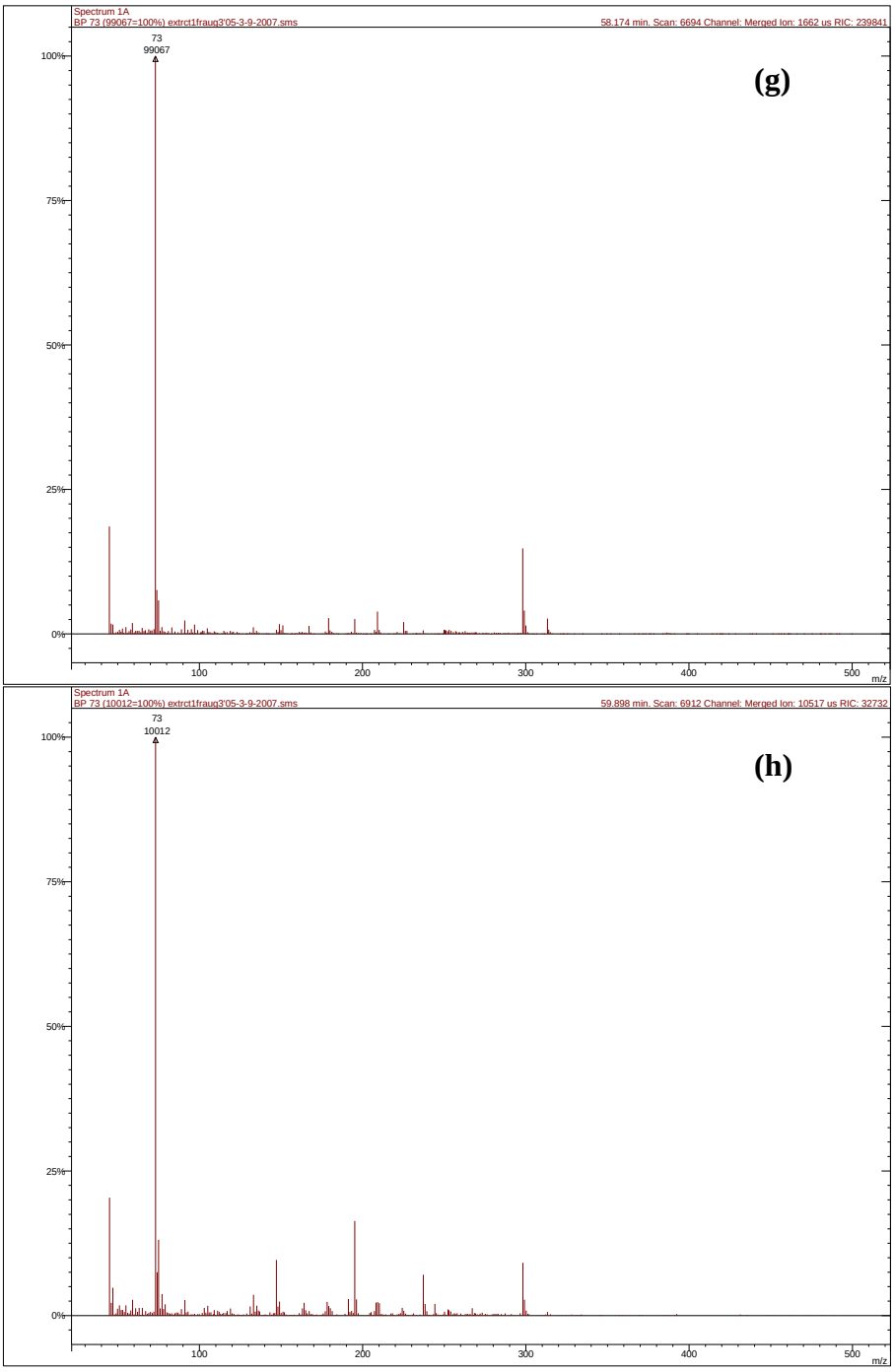

Appendix C. Continued: (g) Product Peak 7 and (h), Product Peak 8.